

SI

Regularization Techniques in System Identification  
for Damage Assessment of Structures

2002 2

# 구조물 손상진단을 위한 SI에서의 정규화 기법






## Regularization Techniques in System Identification for Damage Assessment of Structures

지도교수 이 해 성

이 논문을 공학박사 학위논문으로 제출함.  
2001년 10월

서울대학교 대학원  
토목공학과 토목공학전공  
박 현 우

박현우의 공학박사 학문논문을 인준함.  
2001년 12월

위원장	張 丞 弼	
부위원장	李 海 成	
위원	高 鉉 武	
위원	尹 楨 邦	
위원	申 修 奉	

## 학위논문 원문제공 서비스에 대한 동의서

본인은 본인의 연구결과인 학위논문이 앞으로 우리나라의 학문발전에 조금이나마 기여 할 수 있도록, 서울대학교 중앙도서관을 통한 "학위논문 원문제공 서비스"에서 다음과 같은 방법 및 조건하에 논문을 제공함에 동의합니다.

1. 인터넷을 통한 온라인 서비스와 보존을 위하여 저작물의 내용을 변경하지 않는 범위 내에서의 복제를 허용함.
2. 저작물을 이미지DB(PDF)로 구축하여 인터넷을 포함한 정보통신망에서 공개하여 논문 일부 또는 전부의 복제·배포 및 전송에 동의함.
3. 해당 저작물의 저작권을 타인에게 양도하거나 또는 출판허락을 하였을 경우 1개월 이내에 서울대학교 중앙도서관에 알림.
4. 배포, 전송된 학위논문은 이용자가 다시 복제 및 전송할 수 없으며 이용자가 연구목적 아닌 상업적 용도로 사용하는 것을 금함에 동의함.

---

논문제목 : 구조물의 손상진단을 위한 SI에서의 정규화 기법

학위수여 : **박사**

학 과 : 토목공학과 토목공학전공

학 번 : 97415-807

연 락 처 : 011-227-4396

제 출 일 : 2002년 2 월 일

저 작 자 : 박 현 우



## ABSTRACT

Regularization techniques in system identification (SI) for damage assessment of structures are proposed. This study adopts an SI scheme based on the minimization of the least squared error between measured and calculated responses, which is a nonlinear inverse problem.

A general concept of the regularity condition of the system property is presented. By imposing a proper regularity condition, inherent ill-posedness of the SI scheme is alleviated satisfactorily. It is shown that the regularity condition for elastic continua is defined by the  $L_2$ -norm of the system properties. Tikhonov regularization technique is employed to impose the regularity condition on the error function. The characteristics of nonlinear inverse problems and the role of the regularization are investigated by the singular value decomposition of a sensitivity matrix of responses. It is shown that the regularization results in a solution of a generalized average between the a priori estimates and the a posteriori solution. Based on this observation, a geometric mean scheme (GMS) is proposed. In the GMS, the optimal regularization factor is defined as the geometric mean between the maximum singular value and the minimum singular value of the sensitivity matrix of responses. The validity of the GMS is demonstrated through numerical examples with measurement errors and modeling errors.

It is shown that a solution space defined by the  $L_2$ -norm of system property is not appropriate for framed structures unlike elastic continua. The  $L_1$ -norm of the system property is introduced as a new regularization function for framed structures. The truncated singular value decomposition (TSVD) is employed to filter out noise-polluted solution

components in quadratic sub-problems of the error function. The discretized regularity condition defined by the  $L_1$ -norm of the stiffness parameter vector is imposed as a separate optimization problem in each quadratic sub-problem. The optimization of the  $L_1$ -norm is performed by the simplex method. The optimal truncation number is determined by the cross validation. The final damage status of a framed structure is assessed by the statistical approach based on the data perturbation and the hypothesis test. The validity of the proposed regularity condition for framed structures is presented by detecting damage of a two-span continuous truss with different damage cases with measurement errors.

Key Words : system identification, regularization technique, damage assessment, ill-posedness, regularity condition, geometric mean scheme

**Student Number : 97415-807**

## Table of Contents

### CHAPTER

1. Introduction .....	1
1.1 System Identification as an Inverse Problem .....	2
1.2 A Damage Assessment Algorithm Using System Identification.....	4
1.3 Objective and Scope .....	6
1.4 Notations.....	9
2. System Identification for Elastic Continua.....	16
2.1 Output Error Estimator in the SI Scheme for Structural Systems.....	17
2.2 Ill-posedness of the Output Error Estimator .....	22
2.2.1 SVD of the Output Error Estimator .....	23
2.2.2 Non-Uniqueness of the Solution .....	25
2.2.3 Discontinuity of the Solution .....	27
2.3 Regularization – Preserving Regularity of the Solution of SI.....	30
2.4 Numerical Remedies for Output Error Estimator .....	35
2.4.1 Truncated Singular Value Decomposition (TSVD) .....	36
2.4.2 Tikhonov Regularization .....	38
2.5 Determination of an Optimal Regularization Factor .....	42
2.5.1 Geometric Mean Scheme (GMS) .....	42
2.5.2 The L-Curve Method (LCM) .....	44

2.5.3 Variable Regularization Factor Scheme (VRFS) .....	47
2.5.2 Generalized Cross Validation (GCV) .....	48
2.6 Numerical Examples .....	49
2.6.1 Measurement Error - Identification of a Foreign Inclusion in a Square Plate.....	49
2.6.2 Modeling Error - Identification of Three Internal Cracks in a Thick Pipe .....	62
3. System Identification for Damage Assessment of Framed Structures....	71
3.1 Previous SI-Based Damage Assessment Algorithms.....	71
3.1.1 Grouping Technique - Resolving Sparseness of Measurements.....	71
3.1.2 Measurement Perturbation - Considering Measurement Noise.....	74
3.2 SI with $L_1$ -Regularization for Framed Structures .....	75
3.2.1 A Regularity Condition of the System Property in SI for a Framed Structure.....	75
3.2.2 TSVD solution for $L_1$ -regularity condition .....	80
3.2.3 Optimal Truncation Number by the Cross Validation.....	84
3.3 Damage Assessment .....	86
3.3.1 Measurement Perturbation.....	86
3.3.2 Hypothesis Test, Damage Index, and Damage Severity .....	88
3.4 Numerical Examples – Damage Assessment of a Two-Span Continuous Truss.....	94
3.4.1 Damage Case I.....	97
3.4.2 Damage Case II.....	99
3.4.3 Damage Case III.....	102

4. Conclusions and Recommendations for Further studies.....	108
References .....	113



## List of Figures

1.1	Engineering problems .....	3
2.1	Problem definition and element groups .....	18
2.2	System property, displacement field, forward mapping and inverse mapping.....	31
2.3	Inverse mapping with regularization.....	33
2.4	Alleviation of the non-uniqueness of the solution by regularization .....	33
2.5	Alleviation of the discontinuity of the solution by regularization .....	34
2.6	Schematic drawing for an optimal regularization factor in the GMS .....	43
2.7	Basic concept of the L-curve method .....	45
2.8	Schematic drawing – Oscillating results of the LCM .....	47
2.9	Geometry and boundary conditions of a square plate .....	50
2.10	Observation points and element group configuration of a square plate .....	51
2.11	Estimated Young's moduli by different regularization schemes (Soft inclusion - measurement case I) .....	52
2.12	Estimated Young's moduli by different regularization schemes (Hard inclusion - measurement case I).....	53
2.13	Regularization factors by different regularization schemes (measurement case I).....	53
2.14	Two oscillating solutions by the LCM and the solution by the GMS (Hard inclusion - measurement case I) .....	54
2.15	Distribution of singular values and weighting factors by GMS at the 1st iteration (Hard inclusion - measurement case I).....	55

2.16	Solution of the unconstrained sub-problem by the noise-free measurement at the 1st iteration (Hard inclusion - measurement case I).....	57
2.17	Solution of the unconstrained sub-problem by noise components in measurements at the 1st iteration (Hard inclusion - measurement case I) .....	57
2.18	Singular value, Fourier coefficient and solution of the unconstrained sub-problem at the converged iteration without regularization (Hard inclusion - measurement case I) .....	58
2.19	Solution of the unconstrained sub-problem at the converged iteration by the GMS (Hard inclusion - measurement case I) .....	58
2.20	Mean values and standard deviations of estimated Young's moduli by Monte-Carlo simulation (Hard inclusion - measurement case I) .....	60
2.21	Estimated Young's moduli by different regularization schemes (Soft inclusion - measurement case II) .....	61
2.22	Estimated Young's modulus by different regularization schemes (Hard inclusion - measurement case II) .....	61
2.23	Geometry and boundary conditions of a thick pipe .....	63
2.24	Element group configuration of a thick pipe.....	63
2.25	Estimated Young's Moduli by different regularization schemes (Thick pipe with three internal cracks).....	65
2.26	Distribution of singular values and weighting factors by GMS at the 1st iteration (Thick pipe with three internal cracks).....	66
2.27	Singular value, Fourier coefficient and solution of the unconstrained sub-problem at the 60th iteration without regularization (Thick pipe with three internal cracks).....	67
2.28	Mean values and standard deviations of estimated Young's moduli by Monte-Carlo simulation for noise-polluted measurements using GMS. (Thick pipe with three internal cracks).....	68
2.29	Comparison of singular value distribution and regularization factor at the 1'st iteration.....	69
2.30	Comparison of identified Young's moduli.....	70

3.1	Idealization of a framed structure .....	76
3.2	Optimal truncation number by the discrepancy principle .....	87
3.3	Two typical types of statistical distribution of system parameters using $L_1$ -TSVD .....	91
3.4	Geometry, cross sectional areas and measured dofs of a two-span continuous truss.....	94
3.5	Member ID numbers and load cases of a two-span continuous truss.....	95
3.6	Distribution of singular values for the two-span continuous truss.....	96
3.7	Case I – the 16 <sup>th</sup> bottom member and the 21 <sup>st</sup> bottom member are damaged.....	97
3.8	Variation of the error function with truncation numbers and estimated noise level for damage case I.....	98
3.9	Mean values and standard deviations of estimated system parameters for damage case I.....	98
3.10	Identified damage severity for damage case I.....	99
3.11	Case II – the 22 <sup>nd</sup> bottom member and the 48 <sup>th</sup> inclined member are damaged.....	99
3.12	Variation of the error function with truncation numbers and estimated noise level for damage case II.....	100
3.13	Mean values and standard deviations of estimated system parameters for damage case II.....	100
3.14	Identified damage severity for damage case II.....	101
3.15	Case III – the 17th bottom member, the 33rd vertical member, and the 39th inclined member are damaged.....	102
3.16	Variation of the error function with truncation numbers and estimated noise level for damage case III.....	103

3.17	Mean values and standard deviations of estimated system parameters for damage case III.....	103
3.18	Identified damage severity for damage case III.....	104
3.19	Variations of estimated noise level and truncation number for damage case III with the noise amplitude.....	104
3.20	Identified system parameters for noise-free data versus the truncation number.....	105
3.21	Identified damage severity of damage case III for 1% and 3% noise amplitude.....	106

## **Chapter 1**

### **Introduction**

Civil infrastructures suffer from damages due to unexpected disasters such as earthquake, fire, and blast. As the traffic volume increases rapidly, structures such as bridges are exposed to continuous overloads that may lead to fatigue failures. A proper design enables structures endure unexpected events that may result in damages. However, it cannot be always guaranteed that no damage occurs in the structure after unexpected events. Once damage occurs in a structure, timely and proper actions should be taken to prevent an irreparable catastrophe. Therefore, systematic and regular inspections are required to clarify the existence of damage in structures.

Non-destructive testing (NDT) methods for the existing structures have been used to assess damage. Visual inspection, ultrasonic techniques, magnetic flux leakage techniques, radiographic techniques, penetrant techniques, eddy current techniques can be categorized as the local NDT methods [Bra89]. Since not only these methods are time-consuming and expensive but also the vicinity of damage should be known a priori, they are used for the inspection of local parts that are accessible easily.

Recently, structural health monitoring is an emerging area of civil engineering as the number of large and complex infrastructures increases rapidly. Structural health monitoring can be defined as the science of inferring the health and safety of an engineered system by monitoring its status [Akt00, Doe96]. Innovative developments of sensor, computer, and information technologies enable engineers to design a well-established structural monitoring system. These technologies have made it possible to resolve the complexity of

relevant physical phenomena through detailed computer simulations and their signatures in the measured data through innovative data acquisition and system identification methods. Especially, the damage assessment based on the system identification (SI) is a beneficiary of these innovations of the technologies since the SI requires both measurements with a high precision and a large amount of numerical calculations.

### **1.1 System Identification as an Inverse Problem**

In general, engineering problems can be categorized into three different ones as shown in Fig.1.1. The first problem is the forward problem that is usually referred to as analysis. In the forward problem, the unknown output is obtained using the known input and model. Most engineering problems belong to the forward problems. The second problem is the reconstruction problem in which the unknown input is obtained using the known model and output. The third problem is the system identification (SI) in which the unknown model is obtained using the known input and output. The reconstruction problem and system identification are usually referred to as inverse problems.

Applications of inverse problems to engineering areas go way back to the 1970's in aerospace engineering [Ali75, Bec84, Bec85]. Estimation of heat-flux generated on the surface of the space shuttle is an important issue for successful navigation of the space shuttle. Image enhancing technique of blurred images in the medical imaging and the astronomy is popular areas of inverse problems [Car94, Fes94, Han96a, Fra00].

As far as the engineering mechanics is concerned, shape identification [Sch92, Lee99, Lee00], estimation of material properties [Gio80, Nor89, Hon94, Mah96, Par01], reconstruction of traction boundaries [Man89, Sch90], tomography [Bui94], and defect identifi-

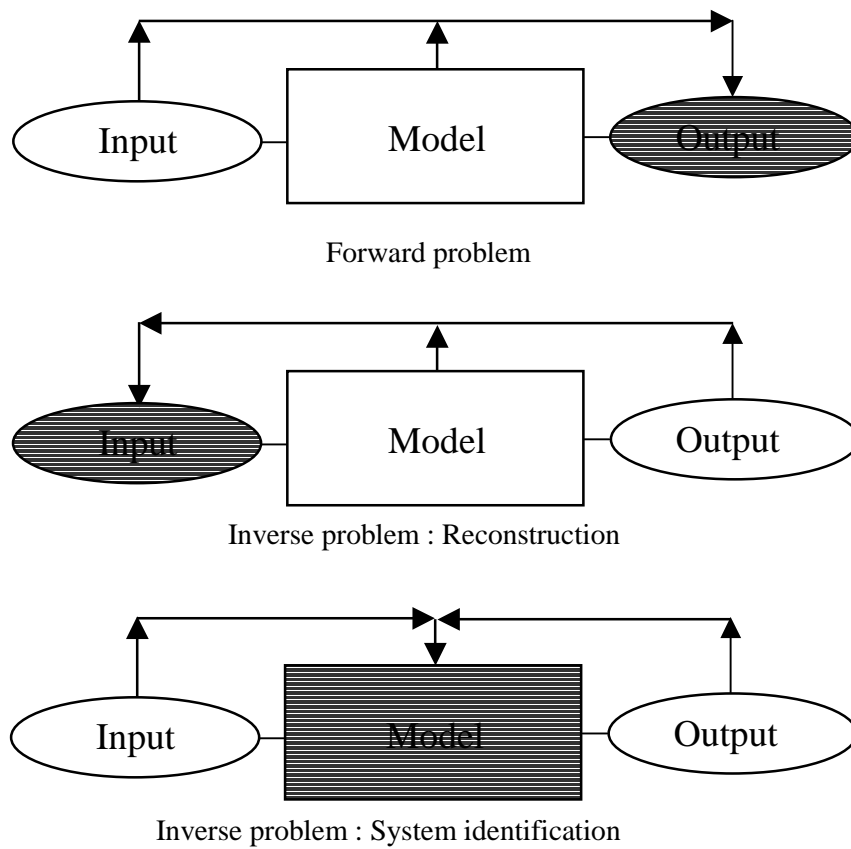


Fig.1.1 Engineering problems

cation [Tan89, Bez93, Mel95] are categorized as inverse problems.

It is well-known that inverse problems suffer from ill-posedness unlike the forward problems that are usually well-posed. The solution of an inverse problem may suffer from non-existence, non-uniqueness, and discontinuity unlike that of the forward problem, which are referred as ill-posedness [Tik77, Gro84, Mor93, Bui94, Han98].

A. N. Tikhonov, a famous mathematician of the USSR, concentrated on this issue and established a regularization theory to alleviate ill-posedness of an inverse problem [Tik77, Gro84, Mor93]. Numerous researches on inverse problems in the engineering field that

are mentioned above have adopted regularization technique and obtained satisfactory results [Ali75, Bec84, Bec85, Man89, Sch90, Sch92, Lee99, Lee00, Yeo00, Par91]. There are various kinds of schemes that can realize the regularization.

However, a common idea of several regularization techniques is to preserve the regularity of solution by defining a proper function space in which the solution must exist [Tik77, Joh87, Bui94].

## **1.2 A Damage Assessment Algorithm Using System Identification**

SI for the structural systems can be defined as the parametric correlation of structural response characteristics predicted by a mathematical model and analogous quantities derived from experimental measurements [Doe99]. Many SI methods using various measured responses have been developed for damage assessment in the last few decades.

From the 1970's to the 1980's, an offshore oil platform was the first target structure of SI-based damage assessment as a civil structure [Doe96, Doe99]. Several researches were performed for damage assessment of an oil platform. Unfortunately, there were many practical problems to produce satisfactory results in SI of the offshore oil platform. Environmental and structural uncertainties such as measurement noise caused by the machinery, hostile environments for instrumentation, and the change of foundation with time were main enemies. In addition, the natural frequencies representing the measured response were not sensitive enough to indicate the several types of damage to be identified.

Researchers have paid attention to the SI-based damage assessment for the bridge and roadways. Bridge failure may result in irreparable catastrophe like the collapse of the Sungsoo bridge. Since the number of large scale complex bridges increases, the auto-



mated health monitoring system is necessary to prevent the catastrophes. The SI-based damage assessment plays an important role in the health monitoring system of the existing structures. Earlier works focused on the changes of the natural frequencies to detect the damage. It becomes generally known that only the natural frequencies are not sufficient to obtain both damage location and severity. More recently, mode shapes and modal frequencies are used simultaneously to find the damage location and severity of damages [Doe99]. Extensive and detailed literature reviews of almost every damage assessment method using vibration responses are available in the technical report published by Los Alamos laboratory in 1996 [Doe96]. Static data such as strain and displacement can be used for the SI-based damage assessment in addition to the modal data [San91, Shi94, Yeo00].

Whatever a target structure is, an important assumption of the SI-based damage assessment is that the measured response of the structures changes if the structure experiences damage and the change of measured response can lead to quantitative or qualitative properties of damage [Doe96]. The purpose of the SI-based damage assessment is not only to identify the existence of damage but also to predict the location and the severity of damage.

The most embarrassing difficulties of the SI-based damage assessment are sparseness of measurements and measurement noise [Shi94, Yeo00]. To obtain satisfactory results by using the SI-based damage assessment, inevitable ill-posedness of SI due to sparseness and noise of measurements should be resolved properly [Bui94, Yeo00, Par01]. Sparseness of measurements is unavoidable since the civil structures are usually large and complex. Measurement noise is also inevitable due to the uncertain environment of sensor

instrumentation. Various SI-based damage assessment algorithms have adopted intuitive remedies to alleviate the difficulties without theoretical insight into an inherent ill-posedness of SI. With a strong theoretical background of SI, a rigorous SI scheme for a damage assessment algorithm can be established and a reliable damage assessment is possible.

Recently, Ge and Soong presented a damage identification scheme based on the minimization of cost functional using the regularization method [Ge98a, Ge98b]. The SI-based damage assessment algorithm proposed by Yeo adopted regularization technique and yielded satisfactory results for damage assessment of framed structures [Yeo99, Yeo00]. In his work, conceptual explanations with schematic drawings about the SI are presented to explain ill-posedness of a SI problem.

### **1.3 Objective and scope**

The current study presents regularization techniques in SI for damage assessment of structures. SI is based on the minimization of the least squared error between measured and calculated responses, which is a nonlinear inverse problem. SI based on the minimization of the least squared error between measured and calculated responses suffers from inherent instabilities caused by ill-posedness of inverse problems.

In chapter 2, a general concept of regularity condition with respect to the system property for SI is presented. By imposing a proper regularity condition, inherent ill-posedness of SI can be relieved satisfactorily. A regularity condition of the system property for elastic continua is presented. Based on the proposed regularity condition, a regularization function based on the  $L_2$ -norm with respect to the system property is proposed. A regular-

ity condition of the system property is discretized in terms of system parameters. Two different approaches to impose the discretized regularity condition on minimization of error function were presented; the truncated singular value decomposition (TSVD) and the Tikhonov regularization.

In Tikhonov regularization, the most important issue is to keep consistent regularization effect through the parameter estimation, which is controlled by a regularization factor. Therefore, it is crucial to determine a well-balanced regularization factor in order to obtain a physically meaningful and numerically stable solution of an inverse problem with the regularization technique.

This study illustrates that the minimization of the error function with the Tikhonov regularization function results in a solution of a generalized average between the a priori estimates and the a posteriori solution. Here, the a priori estimates represent known baseline properties of system parameters, and the a posteriori solution denotes the solution obtained by given measured data. A new idea of the geometric mean scheme (GMS) is presented to select optimal regularization factors in nonlinear inverse problems [Par01]. In the GMS, the optimal regularization factor is defined as the geometric mean between the maximum and minimum singular value for balancing the maximum and minimum effect of the a priori estimates and the a posteriori solution in a generalized average sense. Detailed discussions on the behaviors of the GMS are presented and compared with identification results from other schemes in the numerical examples. The numerical examples are to estimate Young's modulus of a foreign inclusion in a finite body from a given measurements polluted with random noise and modeling error.

In chapter 3, it is shown that a solution space defined by Tikhonov regularization func-

tion is inadequate to SI for framed structures unlike elastic continua. To establish SI adequate for framed structures, a new regularity condition of the system property for framed structures is proposed. Based on the proposed regularity condition, a regularization function based on the  $L_1$ -norm with respect to the system parameters is proposed.

Minimization of error function with  $L_1$ -based regularization function is performed using the TSVD and  $L_1$ -optimization iteratively since the error function with  $L_1$ -based regularization function is usually nonlinear and non-differentiable with respect to the system parameters. The cross validation method is utilized to determine an optimal truncation number in each quadratic sub-problem. Also, a simplified method based on the discrepancy principle is proposed to reduce computational effort in the final damage assessment [Mor84, Mor93].

The statistical approach proposed by Yeo et al is adopted to assess the damage status of a framed structure using identification results of SI [Yeo00]. Data perturbation is used to obtain samples of system parameters [Shi94], and the damage status of each member is determined by applying a hypothesis test for the interval estimation of the mean value.

The validity of the proposed damage assessment algorithm is presented by detecting damage of a two-span continuous truss with different damage cases with measurement errors

## 1.4 Notations

The symbols used in this study are defined where they first appear in the text and whenever clarification is necessary. The most frequently used symbols are listed below.

Boldfaced characters represent vectors.

$A_N$	Noise amplitude
$b_i$	Body force vector
$\mathbf{b}^r$	Displacement residual considering the axis transformation. ( $= \mathbf{S}(\boldsymbol{\xi} - \mathbf{1}) - \mathbf{U}^r$ )
$c$	Critical value in the hypothesis test
$C_{ijkl}$	Elasticity tensor
$\mathbf{e}$	Noise vector in the measurement data
$H^1(V)$	Sobolev space of degree one on $V$
$H_0$	Null hypothesis
$H_1$	Alternative hypothesis
$\mathbf{H}_{k-1}$	Gauss Newton Hessian at the $k-1$ 'th optimization iteration ( $= \mathbf{S}^T \mathbf{S}$ )
$I_D$	Damage index
$\mathbf{I}_n$	Identity matrix of order $n$
$k$	Iteration count for the nonlinear optimization
$\mathbf{K}$	Stiffness matrix
$l_i$	Length of member $i$ in a framed structure
$L_2(V)$	$L_2$ space on $V$
$n_G$	Size of system parameter group vector

$N(a, b^2)$	Normal distribution with mean $a$ and standard deviation $b$
$p$	Numerical rank of sensitivity matrix
$\mathbf{P}_i$	Nodal force vector of $i$ 'th load case
$\mathbf{q}$	A linear combination of truncated RSVs [See Eq.(3.14)]
$\mathbf{q}_{\text{opt}}$	Optimal solution obtained by the linear programming [See Eq.(3.16)]
$R$	Constraint for the system property
$R_s$	Size of the function space
$\mathbf{R}$	Constraint vector for the system parameters
$\hat{r}_t^i$	Predicted displacement residual for truncation number $t$ in the cross validation [See Eq.(3.20)]
$\mathbf{s}_i$	$i$ -th row of the original sensitivity matrix at the $k-1$ 'th optimization iteration in the cross validation
$S_D$	Damage severity
$\mathbf{S}_{k-1}$	Sensitivity matrix of calculated displacements with respect to the system parameters at the $k-1$ 'th optimization iteration
$\mathbf{S}^\#$	Regularized inverse of the sensitivity matrix ( $= \mathbf{V} \text{diag}(1 - \alpha_j) \text{diag}(\frac{1}{\omega_j}) \mathbf{Z}^T$ )
$\mathbf{S}^{-i}$	Reduced sensitivity matrix in which the $i$ -th row is omitted at the $k-1$ 'th optimization iteration in the cross validation
$\bar{T}_i$	Traction vector
$u$	Displacement field
$u^*$	Admissible displacement field
$u_A$	Element of $u^*$
$u_i$	Displacement vector

$u_{i,j}$	Derivative of the displacement vector with respect to $j$ 'th material coordinate
$\hat{u}_i$	Virtual displacement vector
$\hat{u}_{i,j}$	Derivative of the virtual displacement with respect to $j$ 'th material coordinate
$u_i^m$	Measured displacement vector
$\mathbf{u}_i$	Nodal displacement vector of $i$ 'th load case
$\mathbf{u}_i^c$	Calculated displacement vector of $i$ 'th load case obtained by the finite element method
$\mathbf{u}_i^m$	Measured displacement vector of $i$ 'th load case at the discrete observation points
$(\mathbf{U}_{k-1}^r)_i$	$i$ -th row of the original displacement residual vector at the $k-1$ 'th optimization iteration in the cross validation
$\mathbf{U}^c$	Vectors obtained by arranging the vectors of the computed displacements for each load case in a row
$\mathbf{U}^m$	Vectors obtained by arranging the vectors of the measured displacements for each load case in a row
$\tilde{\mathbf{U}}$	Normalized calculated displacement vector ( $\mathbf{U}^c$ )
$\bar{\mathbf{U}}$	Normalized measured displacement vector ( $\mathbf{U}^m$ )
$\bar{\mathbf{U}}^f$	Noise-free measurement vector
$\mathbf{U}_{k-1}^r$	Displacement residual at the $k-1$ 'th optimization iteration ( $= \bar{\mathbf{U}} - \tilde{\mathbf{U}}_{k-1}$ )
$(\mathbf{U}_{k-1}^r)^{-i}$	Reduced displacement residual vector in which the $i$ -th row is omitted at the $k-1$ 'th optimization iteration in the cross validation
$\mathbf{v}_j$	$j$ 'th column vector of $\mathbf{V}$
$V$	Material configuration; Structural volume

$V_i^e$	Volume of member $i$ in a framed structure
$\mathbf{V}$	Right singular matrix of the sensitivity matrix in the SVD
$x$	System property
$x^*$	Admissible system property
$x^R$	Subspace of $x^*$ determined by the regularization technique
$x_A$	Element of $x^R$
$x_I$	Element not in $x^R$
$\mathbf{x}$	System parameter vector
$X_i$	System parameter of member $i$ in a framed structure
$(X_i)_0$	Baseline value of system parameter of member $i$ in a framed structure
$\mathbf{z}_j$	$j$ 'th column vector of $\mathbf{Z}$
$z$	Standardized probabilistic variable
$z_\mu$	Standardized critical value in the hypothesis test
$\mathbf{Z}$	Left singular matrix of the sensitivity matrix in the SVD
$\alpha_j$	Weighting factor corresponding to $j$ 'th singular value $(= \lambda^2 / (\omega_j^2 + \lambda^2))$
$\alpha_{\max}$	Weighting factor corresponding to the largest singular value
$\alpha_{\min}$	Weighting factor corresponding to the smallest singular value
$\beta$	Step length for the line search in the direction of the solution increment
$\beta_{\text{opt}}$	Optimal step length for the line search in the direction of the solution increment at the current iteration
$\Delta\chi$	Transformed regularized solution [See Eq.(2.42)]



$\gamma_j$	Arbitrary real number [See Eq. (2.17)]
$\Gamma_t$	Traction boundary
$\Gamma_u$	Displacement boundary
$\delta$	Dirac delta function
$\delta_m$	Tolerance based on the machine precision
$\varepsilon_p$	Threshold value to determine the numerical rank of the sensitivity matrix
$\Phi$	CDF of the standardized normal distribution
$\eta(\lambda)$	Log of $\pi_R$ in the LCM
$\eta_x^i, \eta_y^i, \eta_z^i$	A local coordinate system for member $i$ of a framed structure
$\kappa(\lambda)$	Curvature of L-curve with respect to $\lambda$ in the LCM
$\lambda$	Regularization factor
$\lambda_{opt}$	Optimal regularization factor
$\mu$	Significance level in the hypothesis test
$\pi_R$	Normalized regularization function
$\pi_E$	Normalized error function ( $\Pi_E$ )
$\pi_E^l$	Linearized error function in the LCM [See Eq. (2.43)]
$\pi_P$	Penalty function of $\pi_{SME}$
$\pi_{SME}$	Squared model error [See Eq. (3.1)]
$\Pi_E$	Least squared error between the measured responses and the calculated responses; Error function

$\Pi_R$	Regularization function
$\rho(\lambda)$	Log of $\pi_E^l$ in the LCM
$\sigma$	Standard deviation of each system parameter obtained by data perturbation
$\sigma_{ij}$	Stress tensor
$\bar{\sigma}^2$	Prior estimate of the averaged random noise variance
$\mathcal{U}_u$	Function space for the displacement
$\mathcal{U}_i$	Function space for the virtual displacement
$\tau$	Decreasing rate of Fourier coefficients [See Eq. (2.19)]
$\omega_j$	$j$ 'th diagonal component value of $\mathbf{V}$ ; $j$ 'th singular value
$\mathbf{\Omega}$	Diagonal matrix with singular values of the sensitivity matrix
$\xi$	Normalized system parameter vector ( $\mathbf{x}$ )
$\xi_G$	System parameter group vector in parameter group updating scheme
$\xi_{k-1}$	Normalized system parameter vector at the $k-1$ 'th optimization iteration
$\xi_u^R$	Regularized solution of unconstrained nonlinear optimization problem at the current iteration
$\xi_t^*$	Converged solution obtained by the $L_1$ -TSVD for a fixed truncation number $t$
$\xi_{\text{opt}}^{L_1\text{-TSVD}}$	Converged solution by the $L_1$ -TSVD with the truncation number determined by the cross validation
$\Delta\xi$	Solution increment of constrained nonlinear optimization problem at the current iteration without regularization
$\Delta\xi_u$	Solution increment of unconstrained nonlinear optimization problem at the current iteration without regularization
$\Delta\xi_u^f$	Solution increments contributed by the noise-free displacement residual

$\Delta \xi_u^e$	Solution increments contributed by the noise in measurement
$\Delta \xi_t^{TSVD}$	Solution increment by the TSVD at the current optimization iteration with truncation number $t$
$\Delta \xi_t^{L_1-TSVD}$	Optimal solution increment by the $L_1$ -TSVD at the current iteration
$\Xi$	Unknown actual value of each system parameter in the hypothesis test
$\Delta \xi_{\text{opt}}^{-i}$	Solution increment by the $L_1$ -TSVD for truncation number $t$ in the cross validation
$\kappa_e$	Noise level
$\mathfrak{S}_{\text{max}}$	Maximum perturbation amplitude
$\ \cdot\ _1$	$L_1$ -norm of a function or a vector
$\ \cdot\ _2$	$L_2$ -norm of a function or a vector
$\ \cdot\ _\infty$	$L_\infty$ -norm of a function or a vector

## Chapter 2

### System Identification for Elastic Continua

System identification (SI) algorithms have been widely used for the last few decades in the area of structural engineering to identify mechanical systems [Bui94] and to detect damage in structures [Hje96a, Shi99, Yeo00]. It is currently recognized that two different approaches to SI exist, i.e. a model based one and a non-model based one [Lju87]. In a model based approach, the system parameters are estimated by least square methods in which the difference between calculated and measured response is minimized. The calculated response is obtained from mathematical model simulating real physical phenomena and the measured ones are obtained from real physical phenomena. In a non-model based approach, the system parameters are obtained from a black box which can accommodate a variety of systems without looking into the internal structures of the physical phenomena. Neural network [Bis94, Sim99], and genetic algorithms [Gol89] are well-known non-model based approaches.

Each approach has its own merits and drawbacks. In model based approaches, the physical and mathematical theories are clearly defined for development of the SI algorithm while appropriate remedies such as regularization techniques are required to resolve the numerical instabilities. In non-model based approaches, algorithms are very robust and easy to adapt to complex physical phenomena while they cannot yield good results without a lot of well-refined information about the phenomenon.

No matter which approach is used in SI for structural systems, it should be noted that two inherent problems are inevitable, i.e. *sparseness* and *noise* in measurements. [Shi94,

Yeo00] Sparseness of measurements grows severe as the ratio of measured data to the unknown system parameters decreases. Noise in measurements occurs due to sensitivity of measuring instruments and uncertainty in experimental environments. Especially, problems of both sparseness and noise in measurements are very serious in complex structures like bridges because the number of measurable responses is much smaller than that of the system parameters and uncertainty in experimental environments is very serious.

In this study, minimization of the least squared error between measured and calculated response is adopted in SI for structural systems. Minimization of the least squared error is referred to as the output error estimator hereafter. In many previous researches based on the output error estimator for structural systems, however, inherent ill-posedness due to sparseness and noise in measurements has not been fully recognized. A detailed investigation of the instabilities is also rarely available.

Ill-posedness of SI based on the output error estimator is investigated in the context of the inverse problems. Regularization technique is adopted to reduce the instabilities of the output error estimator.

## **2.1 Output Error Estimator in the SI Scheme for Structural Systems**

In structural systems, there are various measurable physical responses such as static displacements, acceleration, natural frequencies, and mode shapes. Mass, damping, and stiffness of the structural system may be identified in SI using these responses. In this study, it is assumed that structural system is time-invariant and linear. Two-dimensional finite body with static response will be dealt with as a target structure for the simplicity of further discussion. This simplification causes no loss of generality when it comes to the

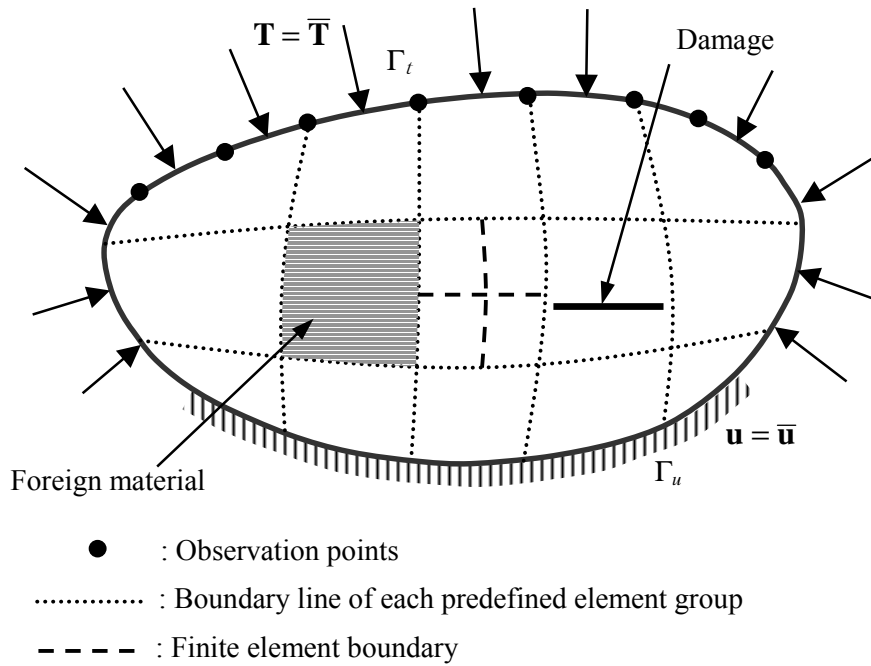


Fig 2.1 Problem definition and element groups

type of structural system, measured responses, and system parameters to be estimated because any type of measured response and system parameters can be used in this formulation.

Fig. 2.1 shows a two-dimensional finite body, for which the geometry and the boundary conditions of the exterior boundary are known. Prescribed traction is applied on  $\Gamma_t$ , and displacement is specified on  $\Gamma_u$ . It is assumed that only small parts of a given body have different material properties from the original, known material properties, which are referred to as baseline properties hereafter. The variation in the material properties may be caused by either an inclusion of a foreign material or degradation of material. Damage such as a crack can be also approximately represented by reducing the elastic material properties around damage without modifying the finite element model [Shi99].

A variational statement of the equilibrium equation for a finite body can be represented as the following equation.

$$\int_V \hat{u}_{i,j} \sigma_{ij} dV = \int_V \hat{u}_i b_i dV + \int_{\Gamma_t} \hat{u}_i \bar{T}_i d\Gamma \quad \text{for } \forall \hat{u}_i \in \mathfrak{v}_{\hat{u}} \quad (2.1)$$

$$\mathfrak{v}_{\hat{u}} \equiv \{ \hat{u}_i \in H^1(V) \mid \hat{u}_i = 0 \text{ on } \Gamma_u \} \quad (2.2)$$

where,  $V$ ,  $\hat{u}_i$ ,  $\hat{u}_{i,j}$ ,  $\sigma_{ij}$ , and  $b_i$  are a material configuration, a virtual displacement vector, a derivative of the virtual displacement with respect to  $j$ 'th material coordinate, a stress tensor, a body force vector, and respectively.  $H^1(V)$  denotes the Sobolev space of degree one on  $V$  [Str73, Hug87]. The stress tensor can be represented as the following equation using the Hooke's law and the strain-displacement relationship.

$$\sigma_{ij} = C_{ijkl} u_{k,l} \quad (2.3)$$

where,  $C_{ijkl}$ ,  $u_i$  and  $u_{i,j}$  are a elasticity tensor, a displacement vector, and a derivative of the displacement vector with respect to  $j$ 'th material coordinate, respectively. The displacement vector  $u_i$  belongs to the function space  $\mathfrak{v}_u$  defined as the following equation.

$$\mathfrak{v}_u \equiv \{ u_i \in H^1(V) \mid u_i = 0 \text{ on } \Gamma_u \} \quad (2.4)$$

Eq.(2.1) can be rewritten as the following equation by using Eq.(2.3) and considering the symmetry of  $C_{ijkl}$ .

$$\int_V \hat{u}_{i,j} C_{ijkl} u_{k,l} dV = \int_V \hat{u}_i b_i dV + \int_{\Gamma_t} \hat{u}_i \bar{T}_i d\Gamma \quad \text{for } \forall \hat{u}_i \in \mathfrak{v}_{\hat{u}} \quad (2.5)$$

The unknown system parameters of the finite body can be identified by minimizing a

least squared error between displacements satisfying Eq.(2.5) and measured displacements at some part of traction boundary  $\Gamma_o$ .

$$\text{Minimize}_{\mathbf{x}} \Pi_E = \frac{1}{2} \int_{\Gamma_o} (u_i(\mathbf{x}) - u_i^m)(u_i(\mathbf{x}) - u_i^m) d\Gamma \quad \text{subject to } R(\mathbf{x}) \leq 0 \quad (2.6)$$

where  $\mathbf{x}$ ,  $u_i^m$ ,  $R$  are unknown system property representing Young's modulus or Poisson ratio, the measured displacement vector at traction boundary  $\Gamma_o$ , a constraint for the system property, respectively.

To represent stiffness properties of the body, the given domain is divided into a finite number of subdomains as shown in Fig. 2.1, and the Young's moduli of the subdomains are selected as the system parameters. The Poisson's ratios of all the subdomains are fixed at the baseline property. Each subdomain may consist of a finite element or a predefined element group, which contains several finite elements of the same system parameter. For the simplicity of discussion, it is assumed that an element group for each subdomain is predefined.

Since the displacement vector satisfying Eq.(2.5) is not available analytically in general cases, the displacement vector is obtained by applying finite element method to Eq.(2.5).

$$\mathbf{K}(\mathbf{x})\mathbf{u}_i = \mathbf{P}_i \quad (2.7)$$

where  $\mathbf{K}$ ,  $\mathbf{x}$ ,  $\mathbf{u}_i$  and  $\mathbf{P}_i$  are the stiffness matrix, system parameter vector, nodal displacement vector of the structure, and the equivalent nodal load vector of the  $i$ -th load case, respectively.

Instead of minimizing Eq.(2.6), a point-collocation method is applied to identify the



unknown system parameters of the finite body since the measured displacements are obtained at some discrete observation points located on  $\Gamma_i$  as shown in Fig. 2.1.

$$\text{Minimize}_{\mathbf{x}} \Pi_E = \frac{1}{2} \sum_{i=1}^{nlc} \|\mathbf{u}_i^c(\mathbf{x}) - \mathbf{u}_i^m\|_2^2 \quad \text{subject to } \mathbf{R}(\mathbf{x}) \leq 0 \quad (2.8)$$

where,  $\mathbf{u}_i^c$ ,  $\mathbf{u}_i^m$ , and  $\|\cdot\|_2$  denote calculated displacement vector obtained by the finite element method, measured displacement vector of  $i$ 'th load case at the discrete observation points, and the  $L_2$ -norm of a vector [Wat80]. Linear constraints are used to set physically significant upper and lower bounds of the system parameters [Hje96]. The minimization problem defined in Eq. (2.8) is a constrained nonlinear optimization problem because the displacement vector  $\mathbf{u}_i^c$  is a nonlinear implicit function of the system parameters  $\mathbf{x}$ .

The error function defined in Eq. (2.8) is rewritten in a single vector form as

$$\Pi_E = \frac{1}{2} \|\mathbf{U}^c(\mathbf{x}) - \mathbf{U}^m\|_2^2 \quad (2.9)$$

where  $\mathbf{U}^c$  and  $\mathbf{U}^m$  are vectors obtained by arranging the vectors of the computed displacements and the measured displacements for each load case in a row. The error function is normalized by the square of the Euclidean norm of the measured displacement vector, while system parameters are normalized with respect to the corresponding baseline properties. The normalized quantities corresponding to  $\Pi_E$ ,  $\mathbf{U}^c$ ,  $\mathbf{U}^m$  and  $\mathbf{x}$  are denoted as  $\pi_E$ ,  $\tilde{\mathbf{U}}$ ,  $\bar{\mathbf{U}}$  and  $\xi$  respectively. The normalized minimization problem is written in the following form.

$$\begin{aligned} \text{Minimize}_{\xi} \pi_E &= \frac{1}{2} \frac{\|\mathbf{U}^c(\mathbf{x}) - \mathbf{U}^m\|_2^2}{\|\mathbf{U}^m\|_2^2} = \frac{1}{2} \|\tilde{\mathbf{U}}(\xi) - \bar{\mathbf{U}}\|_2^2 \\ \text{subject to } &\mathbf{R}(\xi) \leq 0 \end{aligned} \quad (2.10)$$

## 2.2 Ill-posedness of the Output Error Estimator

Ill-posedness of the output error estimator are characterized by non-uniqueness of solution and discontinuity of solutions [Han98, Yeo00, Par01]. In particular, when measured data are polluted with noise or when a finite element model used for SI does not represent actual situations, the instabilities become very severe [Bui94, Par01].

Since the output error estimator of Eq. (2.10) is nonlinear optimization problem, it should be solved iteratively by linearizing Eq. (2.10) with respect to the system parameters. Therefore, inherent ill-posedness of Eq. (2.10) should be investigated by using the solution of the linearized form of Eq. (2.10).

Sparseness of measurements cause rank deficiency in the sensitivity matrix under which no unique solution is guaranteed [Han98]. Noise in measurements violates the discrete Picard condition which ensures both continuity and convergence of the solution [Gro84, Han98]. In short, numerical instabilities of the output error estimator are caused by rank-deficiency of the sensitivity matrix and violation of discrete Picard.

Numerical instabilities of linearized output error estimator will be investigated by singular value decomposition (SVD) [Gol96]. Two important kinds of ill-posedness, non-uniqueness and discontinuity of solution of the output error estimator will be investigated by the SVD because it can be verified through the SVD whether either rank-deficiency or violation of Picard condition occurs.

### 2.2.1 SVD of the Output Error Estimator

The solution of the minimization problem Eq. (2.10) is obtained by solving the following quadratic sub-problem iteratively.

$$\begin{aligned} & \text{Minimize}_{\Delta \boldsymbol{\xi}} \left[ \frac{1}{2} \Delta \boldsymbol{\xi}^T \mathbf{H}_{k-1} \Delta \boldsymbol{\xi} - \Delta \boldsymbol{\xi}^T \mathbf{S}_{k-1}^T \mathbf{U}_{k-1}^r \right] \\ & \text{subject to } \mathbf{R}(\boldsymbol{\xi}_{k-1} + \Delta \boldsymbol{\xi}) \leq 0 \end{aligned} \quad (2.11)$$

where the subscript  $k$  denotes the iteration count, and  $\mathbf{S}_{k-1}$  and  $\mathbf{H}_{k-1}$  are the sensitivity matrix of  $\tilde{\mathbf{U}}_{k-1}$  and the Hessian matrix of the error function, respectively. The displacement residual  $\mathbf{U}_{k-1}^r$  is defined as  $\mathbf{U}_{k-1}^r = \bar{\mathbf{U}} - \tilde{\mathbf{U}}_{k-1}$ , and  $\Delta \boldsymbol{\xi}$  is the increment of normalized system parameters at the current iteration step. The Hessian matrix in Eq. (2.11) is approximated by the Gauss-Newton Hessian to avoid the computational complexity of calculating the second order sensitivities of displacements.

$$\mathbf{H}_{k-1} \approx \mathbf{S}_{k-1}^T \mathbf{S}_{k-1} \quad (2.12)$$

To simplify the expressions, the subscript  $(k-1)$  of all the variables in the incremental formulation presented hereafter is omitted.

The linear constraints of Eq. (2.11) on the upper and lower bounds of system parameters can alleviate ill-posedness of the output error estimator to some extent. However, the inherent instabilities of the output error estimator cannot be suppressed in general by imposing linear constraints on the upper and lower bounds of system parameters, which has been reported by several researchers [Neu73, Neu75, Neu79, Yeo00]. This is because the instabilities of the output error estimator arise from the characteristics of the

Hessian and the errors in measurements. Therefore, the instabilities of the SI algorithm should be investigated before the constraints are imposed, and thus the constraints are not considered for discussions on the stability of the SI algorithm hereafter. In other words, the instabilities of the SI algorithm are presented in the original solution space, not in the solution space reduced by the constraints for the remaining parts of this chapter.

The first-order necessary optimality condition for Eq. (2.11) without the constraints is given by the following linear equation.

$$\mathbf{S}^T \mathbf{S} \Delta \xi_u - \mathbf{S}^T \mathbf{U}^r = 0 \quad (2.13)$$

here,  $\Delta \xi_u$  denotes the solution of the unconstrained quadratic sub-problem of Eq. (2.11).

By the singular value decomposition (SVD) [Gol96], the  $m \times n$  sensitivity matrix  $\mathbf{S}$  can be written as a product of an  $m \times n$  matrix  $\mathbf{Z}$ , an  $n \times n$  diagonal matrix  $\mathbf{\Omega}$ , and the transpose of an  $n \times n$   $\mathbf{V}$  as expressed in Eq. (2.14). In the definition,  $m$  is the total number of measured degrees of freedom for all the applied loads and  $n$  is the number of system parameters.

$$\mathbf{S} = \mathbf{Z} \mathbf{\Omega} \mathbf{V}^T \quad (2.14)$$

where

$$\begin{aligned} \mathbf{Z}^T \mathbf{Z} &= \mathbf{I}_n \\ \mathbf{V}^T \mathbf{V} &= \mathbf{V} \mathbf{V}^T = \mathbf{I}_n \\ \mathbf{\Omega} &= \text{diag}(\omega_j) \end{aligned} \quad (2.15)$$

in which  $\mathbf{I}_n$  is the identity matrix of order  $n$ , and  $\omega_j$  is a singular value of  $\mathbf{S}$  which has the descending order of  $\omega_1 = \omega_{\max} \geq \dots \geq \omega_p \geq \varepsilon_p \geq \omega_{p+1} \geq \dots \geq \omega_n = \omega_{\min} \geq 0$ .  $\varepsilon_p$  and  $p$  denotes

a threshold value to determine the rank and the rank of  $\mathbf{S}$ , respectively [Gol96].

From the mathematical points of view, the threshold value  $\epsilon_p$  is exact 0. However, the threshold value,  $\epsilon_p$  cannot be 0 if the numerical calculations are used to obtain the singular values because it should be consistent with the machine precision used in the numerical calculations [Gol96]. In this study, the threshold value is determined considering the machine precision by the following equation because the singular values can be obtained by numerical calculations.

$$\hat{\epsilon}_p = \delta_m \|\mathbf{S}\|_\infty \quad (2.16)$$

where  $\hat{\epsilon}_p$  and  $\delta_m$  are a threshold value to determine the *numerical rank*  $p$  and the tolerance based on the machine precision, respectively.  $\|\cdot\|_\infty$  denotes the  $L_\infty$ -norm of the matrix [Wat80].

If  $p=n$ , the sensitivity matrix is called rank-sufficient while it is called rank-deficient if  $p<n$ . More detailed discussions about rank-deficiency will be treated in section 2.2.2. The columns of  $\mathbf{Z}$  are referred to as the left singular vectors (LSV) while the columns of  $\mathbf{V}$  are referred to as the right singular vectors (RSV).

### 2.2.2 Non-Uniqueness of the Solution

Sparseness of measurements occurs when the ratio of the number of measurements to the unknown system parameters is very small. Because of sparseness of measurements, minimization problem of the output error estimator becomes an underdetermined one in which there is infinite number of solutions. As far as the linear algebra is concerned, an

underdetermined problem has rank-deficiency. Therefore, sparseness of the measurement data in SI problems based on the output error estimator causes rank-deficiency of the sensitivity matrix mentioned in section 2.2.1. The sparseness of the measured response occur very often in the area of SI for structural systems. However, many remedies for the sparseness depend on ad-hoc method that enforces a simple condition that the number of measured responses should be always larger than that of the system parameters. It should be noted that rank-deficiency may occur under even this condition unless independency of the measurements is provided sufficiently. The most appropriate method which can measure the degree of the rank-deficiency, is singular value decomposition of the sensitivity matrix. Once the sensitivity matrix is decomposed as Eq. (2.14), existence and degree of the rank-deficiency is revealed. Rank-deficiency in the rank-deficient problems arises when the numerical rank of the sensitivity matrix  $r$  is smaller than  $n$  as mentioned in section 2.1.2.

Using the properties of Eq. (2.15), the solution of the rank-deficient case can be represented as the following equation [Gol96, Han98].

$$\Delta \xi_u = \sum_{j=1}^p \mathbf{v}_j \omega_j^{-1} \mathbf{z}_j^T \mathbf{U}^r + \sum_{j=p+1}^n \gamma_j \mathbf{v}_j \quad (2.17)$$

where  $\mathbf{v}_j$  and  $\mathbf{z}_j$  are column vectors which consist of the RSV and LSV corresponding to the  $j$ 'th singular value  $\omega_j$ , and  $\gamma_j$  is an arbitrary real value. The arbitrariness of the coefficient  $\gamma_j$  causes the number of the solution infinite, which is ill-posedness as the *non-uniqueness* of the solution. The first term of Eq. (2.17) is a constant solution part which is affected by the  $\mathbf{U}^r$  directly while the second term is an arbitrary solution part which is not affected by

$\mathbf{U}^r$  and makes the number of the solution infinite. In other words, the solution parts combined linearly with RSVs from  $\mathbf{v}_{r+1}$  to  $\mathbf{v}_n$  has no influence on the residual  $\mathbf{U}^r$  because they lie in the null space of the sensitivity matrix.

### 2.2.3 Discontinuity of the Solution

Noise in measurements is the main source which results in discontinuity of the solution in Eq. (2.13). With noise in the measurements, the degree of discontinuity increases as the number of system parameters increases regardless of rank-deficiency. This phenomenon can be easily verified if SVD is applied to Eq. (2.13). For the simplicity of explanation, Eq.(2.13) is assumed rank-sufficient.

Using similar manipulation as in Eq. (2.17), the solution of the rank-sufficient problem is represented as the following equation.

$$\Delta \xi_u = \mathbf{V} \text{diag}\left(\frac{1}{\omega_j}\right) \mathbf{Z}^T \mathbf{U}^r = \sum_{j=1}^n \mathbf{v}_j \omega_j^{-1} \mathbf{z}_j^T \mathbf{U}^r \quad (2.18)$$

Eq. (2.18) is defined as the a posteriori solution increment because it is determined purely by the measured displacements and the analytical model of a given structure without utilizing the a priori information on the system. The term  $\mathbf{Z}^T \mathbf{U}^r$  in Eq. (2.18) is often referred to as the Fourier coefficients [Han92a, Han98].

The displacement residual  $\mathbf{U}^r$  cannot converge to zero for noise-polluted measurements because noisy displacements usually contain incompatible components that cannot be obtained just by adjusting the system parameters of a mathematical model. In that case, in order to make  $\Delta \xi_u$  converge to zero, each column  $\mathbf{z}_j$  should become

orthogonal to  $\mathbf{U}_r$  in an absolute sense through the minimization iterations. Even so, the optimization iteration may diverge if some of the singular values become smaller than the corresponding Fourier coefficients during iterations. In other words, the ratio of the singular value to the corresponding Fourier coefficients must converge to zero to guarantee the convergence of the nonlinear optimization. Therefore, Fourier coefficients must converge faster than the corresponding singular value so that the optimization iteration can converge. This condition is called *discrete Picard condition*. The discrete Picard condition can be represented with respect to a certain tolerance as the following equation.

$$\omega_j^{-1} \mathbf{z}_j^T \mathbf{U}^r = \tau^j, j = 1, \dots, n \quad (2.19)$$

where  $\tau$  is some number between 0 and 1. Eq. (2.19) indicates that the Fourier coefficient must decay to zero more rapidly than the corresponding singular value as the  $j$  increases. Picard condition will be easily violated if either sensitivity matrix or measurements are polluted with noise components. Especially, if the measurements are polluted with severe noise, the Picard condition may be violated because the Fourier coefficient corresponding to the smaller singular values will level off at the noise level while the corresponding singular value decay to zero [Han98].

There are two sources of noise when applying an SI algorithm; i.e. measurement errors and modeling errors. The former represents noise caused by sensitivity of sensors or misreading of test equipment during actual measurements. The latter occurs due to the discrepancy between a real structure and its mathematical model employed in the SI. For example, in case the a priori information is not available on internal flaws like cracks in a structure, such flaws cannot be taken into account in the finite element model used for SI.



The modeling errors cannot be reduced in the minimization with a predefined finite element model. The measurement errors are probabilistic while the modeling errors are systematic in nature.

The measured displacement can be theoretically decomposed into the noise-free displacement  $\bar{\mathbf{U}}^f$  and the noise vector  $\mathbf{e}$  as follows.

$$\bar{\mathbf{U}} = \bar{\mathbf{U}}^f + \mathbf{e} \quad (2.20)$$

The modeling errors, which lead to errors in the stiffness matrix, result in noise in the computed displacements, but not in measured displacements. However, it is still possible to employ Eq. (2.20) by defining the noise-free displacements as the best-fitting displacements with measured ones obtainable by adjusting predefined system parameters in the mathematical model. This decomposition of displacement cannot be achieved explicitly, and is purely conceptual.

Substitution of Eq. (2.20) into Eq. (2.18) leads to the following expression.

$$\Delta \xi_u = \mathbf{V} \text{diag} \left( \frac{1}{\omega_j} \right) \mathbf{Z}^T (\bar{\mathbf{U}}^f - \tilde{\mathbf{U}}) + \mathbf{V} \text{diag} \left( \frac{1}{\omega_j} \right) \mathbf{Z}^T \mathbf{e} = \Delta \xi_u^f + \Delta \xi_u^e \quad (2.21)$$

where  $\Delta \xi_u^f$  and  $\Delta \xi_u^e$  represent the solution increments contributed by the noise-free displacement residual and by the noise in measurement, respectively. Unless noise in measurement data is negligible or the noise vector is nearly orthogonal to the LSV, the solution increment for the noisy measurement deviates from the noise-free solution mainly due to the second term of Eq. (2.21). In particular, the components of  $\mathbf{Z}^T \mathbf{e}$  associated with small singular values amplify the deviation more severely. Under this circumstances, the

discrete Picard condition in Eq.(2.19) is easily violated. The solution is likely to lose physical significance due to the accumulation of solution components amplified by physically meaningless noise during optimization iterations. A small change in noise may yield a totally different solution because small singular values amplify the change in measurements, which is a source of discontinuity characteristics in SI problems. It can be concluded that the discontinuity of the solution increment also occur during the optimization iteration when the discrete Picard condition is violated.

### **2.3 Regularization – Preserving Regularity of the Solution of SI**

There are several kinds of complex methodologies and techniques that can realize the regularization. However, the main idea of the regularization is to preserve the regularity of the solution that defines a proper function space where the solution must exist [Tik77, Joh87, Bui94]. Since a proper function space for the solution is usually provided in a forward problem either explicitly or implicitly, the regularity of the solution is guaranteed and the forward problem is well-posed.

To explain the regularity of the solution easily, the function spaces representing the system property and the displacement field, and mapping between the system property and displacement field are shown in Fig. 2.2.  $x$ ,  $x^*$ ,  $u$ , and  $u^*$  represent the system property, an *admissible* system property, the displacement field, and an *admissible* displacement field, respectively. In this study, the term ‘*admissible*’ implies that a function space representing a physical property should be regular so that it has both physical and mathematical significance. Whether a function space is regular is judged by the regularity (integrability) of the function space [Joh83].

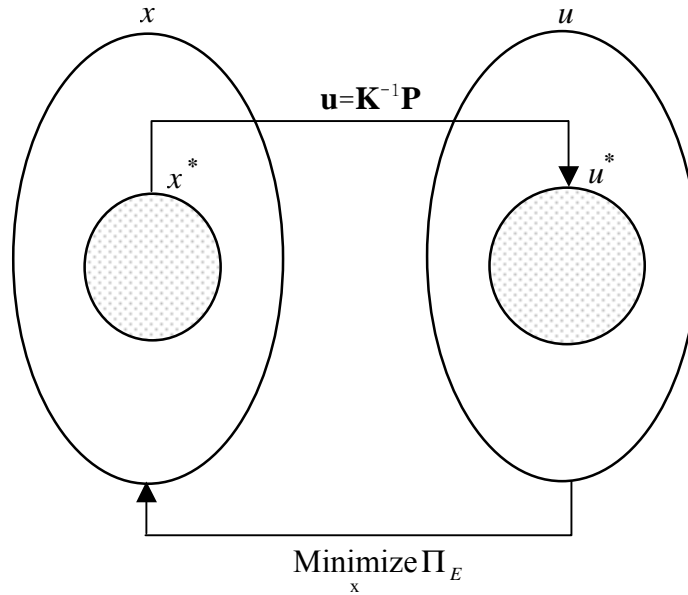


Fig. 2.2 System property, displacement field, forward mapping and inverse mapping

In general, the forward mapping represented by a structural stiffness equation is performed from an admissible system property onto an admissible displacement field as shown in Fig. 2.2 since the stiffness equation is derived from the variational formulations. However, it is not guaranteed that the inverse mapping represented by the output error estimator between measured and calculated response is performed from the admissible. This is because a proper solution space of the system property is not defined by the output error estimator and the measurements inevitably contain random and modeling errors. In other words, ill-posedness of the inverse mapping represented only by the output error estimator occurs since there is no proper regularity condition of the system property. Therefore a proper regularity condition should be adopted to alleviate ill-posedness of the inverse mapping.

In general, a strong form of the regularity conditions with respect to the model space is

represented by the integrability of the model space [Joh83, Ode79].

$$\left( \int_V |x - x_0|^r dV \right)^{1/r} < \infty, \quad 1 \leq r \leq \infty \quad (2.22)$$

where,  $x_0$  is the center of the function space given *a priori*. The system property satisfying Eq.(2.22) is an admissible system property,  $x^*$  in Fig. 2.2. The topology of the system property depends on  $r$ .

The weak form of the regularity is usually imposed in practice since it is impossible to employ the strong form of regularity condition directly.

$$\int_V |x - x_0|^r dV < R_s^r \quad (2.23)$$

where,  $R_s$  denotes the size of the function space.  $r$  and  $R_s$  is determined properly by the regularization technique by considering the physical and the mathematical characteristics of the system property as known *a priori*. For example, standard Tikhonov regularization  $r=2$ , which means the original system property should be square-integrable in the vicinity of  $x_0$ . In other words, the system property defined by Tikhonov regularization is a subspace of the  $L_2$ -space that consists of piecewise continuous functions [Joh87].

$$\int_V |x - x_0|^2 dV < R_s^2 \quad (2.24)$$

A subspace of function space  $x^*$  satisfying Eq.(2.24) is also an admissible system property,  $x^R$  determined by the regularization technique in Fig. 2.3.

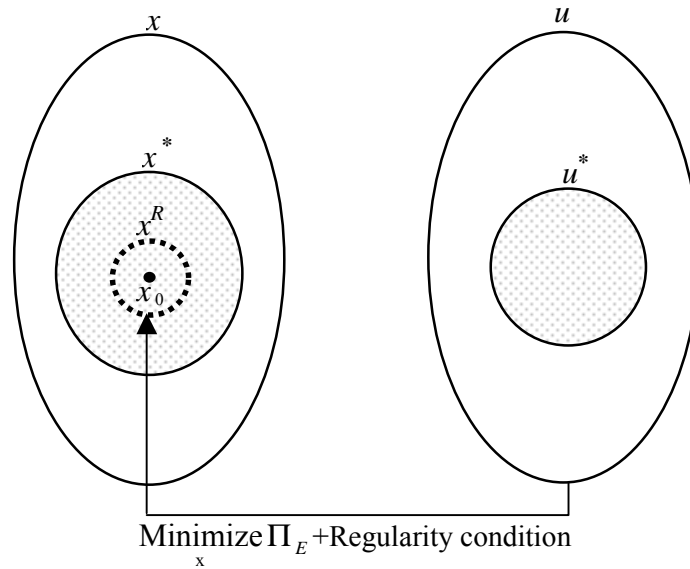


Fig. 2.3 Inverse mapping with regularization

Fig. 2.4 and Fig. 2.5 present the effect of the regularization that alleviate the typical ill-posedness, non-uniqueness and the discontinuity of the solution.  $x_A$ ,  $x_I$ , and  $u_A$ , denote elements that satisfy the following condition.

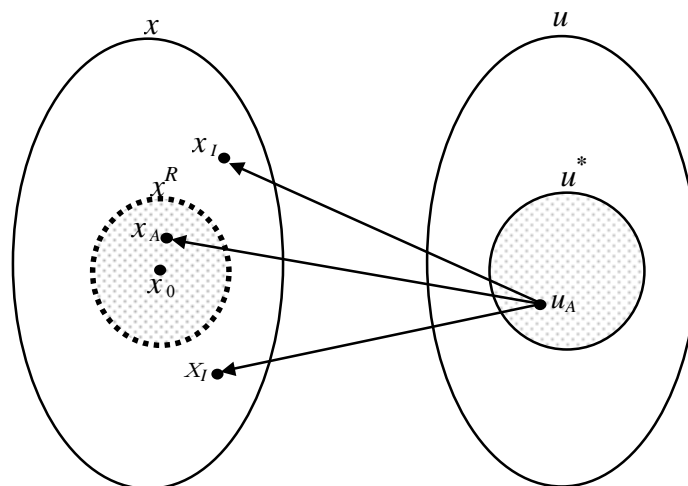


Fig. 2.4 Alleviation of the non-uniqueness of the solution by regularization

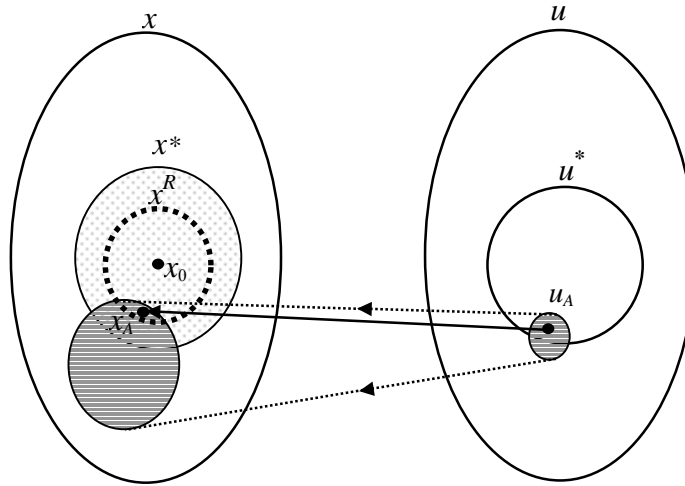


Fig. 2.5 Alleviation of the discontinuity of the solution by regularization

$$\begin{aligned}
 x_A &\in x^R \\
 x_I &\notin x^* \\
 u_A &\in u^*
 \end{aligned}
 \tag{2.25}$$

The non-uniqueness of the solution may occur when the solution corresponding to the displacement  $u_A$  is not unique. Solutions obtained from the inverse mapping corresponding to  $u_A$  may include those in the admissible and inadmissible system property as shown in Fig.2.4. If the regularity condition is enforced by the regularization technique, only the solution that belongs to an admissible system property can be obtained.

The discontinuity of the solution occurs when the inverse mapping from the displacement field in the vicinity of  $u_A$  to the system property yields large deviations depicted as the darkly shadowed region in the vicinity of  $x_A$ . The darkly shadowed region includes solutions of admissible and inadmissible system property. In general, most of the darkly shadowed region lies in the inadmissible system property as shown in Fig. 2.5.

Therefore, if the regularity condition is enforced by the regularization technique, solutions continuous with respect to the small perturbation of the output can be obtained, which lies in the admissible system property.

## **2.4 Numerical Remedies for Output Error Estimator**

There are two major numerical remedies to reduce ill-posedness of the inverse problems. One is truncated singular value decomposition (TSVD) [Go196, Han98] which resolves the non-uniqueness of the solution, and the other is Tikhonov regularization technique [Tik77, Gro84, Bui94, Han98] which enhances both convergence and continuity of the solution. However, both are equivalent each other because they convert ill-posed problem into well-posed one by imposing the positive definiteness on original ill-posed problems. The degree of smoothness is proportional to that of positive definiteness which is determined by a truncation number of TSVD and a regularization factor in the regularization technique.

In these numerical remedies, the most important issue is to keep consistent regularization effect on the parameter estimation, which is controlled by truncation number of TSVD [Vog86] and a regularization factor [Bui94, Han98, Par01] in the regularization technique. Therefore, it is crucial to determine a well-balanced truncation number and regularization factor in order to obtain a physically meaningful and numerically stable solution of an inverse problem. This section presents detailed description on the TSVD and regularization technique. Various schemes to determine an optimal truncation number and regularization factor are also presented.

### 2.4.1 Truncated Singular Value Decomposition

As mentioned in section 2.2.2, there is an infinite number of solutions in the rank-deficient problem. Truncated singular value decomposition(TSVD) is motivated from the simple idea that feasible solutions are smooth rather than oscillatory among an infinite number of solutions if the a priori estimates of the solution is smooth. The degree of the smoothness of the solution can be measured by the  $L_2$ -norm of the solution vector. In the TSVD, the solution with the least  $L_2$ -norm is defined as the most feasible one [Gol96, Han98]. Using this definition, the solution in Eq.(2.11) can be determined uniquely.

$$\text{Min}_{\xi} \|\xi - \mathbf{1}\|_2^2 = \text{Min}_{\Delta \xi_u} \|\Delta \xi_u - (\mathbf{1} - \xi_k)\|_2^2 \quad (2.26)$$

Substituting Eq. (2.17) into Eq. (2.26), Eq. (2.26) can be converted into the minimization problem with respect to the coefficient  $\gamma_j$ .

$$\begin{aligned} & \text{Min}_{\Delta \xi_u} \left\| \sum_{j=r+1}^n \gamma_j \mathbf{v}_j + \left\{ \sum_{j=1}^r \mathbf{v}_j \omega_j^{-1} \mathbf{z}_j^T \mathbf{U}^r + (\mathbf{1} - \xi_k) \right\} \right\|_2^2 \\ &= \text{Min}_{\Delta \xi_u} \left[ \underbrace{\left\| \sum_{j=1}^r \mathbf{v}_j \omega_j^{-1} \mathbf{z}_j^T \mathbf{U}^r - (\mathbf{1} - \xi_k) \right\|_2^2}_{\text{constant}} + 2 \underbrace{\left( \sum_{j=1}^r \mathbf{v}_j \omega_j^{-1} \mathbf{z}_j^T \mathbf{U}^r \right)^T \left( \sum_{j=r+1}^n \gamma_j \mathbf{v}_j \right)}_0 \right. \\ & \quad \left. + 2 \left( \sum_{i=r+1}^n \gamma_i \mathbf{v}_i \right)^T (\mathbf{1} - \xi_k) + \left\| \sum_{j=r+1}^n \gamma_j \mathbf{v}_j \right\|_2^2 \right] \quad (2.27) \end{aligned}$$

The minimization problem of Eq.(2.17) can be rewritten as the following equation because the first term is constant, the second term is 0 due to the orthogonality of the RSV in Eq. (2.27).



$$\text{Min}_{\gamma_k} \left[ \left\| \sum_{j=r+1}^n \gamma_j \mathbf{v}_j \right\|_2^2 + 2 \left( \sum_{i=r+1}^n \gamma_i \mathbf{v}_i \right)^T (1 - \boldsymbol{\xi}_k) \right] \quad (2.28)$$

The solution  $\gamma_j$  to Eq. (2.28) can be obtained easily by differentiating Eq.(2.28) with respect to  $\gamma_j$  and making the differential equations equal to zero for all  $\gamma_j$ .

$$\frac{\partial}{\partial \gamma_j} \left[ \left\| \sum_{i=r+1}^n \gamma_i \mathbf{v}_i \right\|_2^2 + 2 \left( \sum_{i=r+1}^n \gamma_i \mathbf{v}_i \right)^T (1 - \boldsymbol{\xi}_k) \right] = 2 \mathbf{v}_j^T \mathbf{v}_j \gamma_j + 2 \mathbf{v}_j^T (1 - \boldsymbol{\xi}_k) = 0 \quad (2.29)$$

The solution  $\gamma_j$  is determined as the following equation from Eq.(2.29) with  $\mathbf{v}_j^T \mathbf{v}_j$  equaling to 1.

$$\gamma_j = \frac{(1 - \boldsymbol{\xi}_k)^T \mathbf{v}_j}{\mathbf{v}_j^T \mathbf{v}_j} = \mathbf{v}_j^T (1 - \boldsymbol{\xi}_k) \quad (2.30)$$

Thus an arbitrary solution in Eq. (2.17) can be determined uniquely incorporated with Eq. (2.30) as the following equation.

$$\Delta \boldsymbol{\xi}_r^{TSVD} = \sum_{j=1}^r \mathbf{v}_j \omega_j^{-1} \mathbf{z}_j^T \mathbf{U}^r + \sum_{j=r+1}^n \mathbf{v}_j \mathbf{v}_j^T (1 - \boldsymbol{\xi}_k) \quad (2.31)$$

where the solution is denoted as  $\Delta \boldsymbol{\xi}_r^{TSVD}$  since it can be obtained by the truncated singular value decomposition (TSVD) of the sensitivity matrix if  $r$ , the rank of the sensitivity matrix, is less than  $n$  [Han98].

### 2.4.2 Tikhonov Regularization

The concept of the Tikhonov regularization has been adopted to overcome ill-posedness of inverse problems, and successfully applied to various types of inverse problems [Bec84, Sch92, Lee99, Lee00, Par01]. However, little attention has been paid to the regularization technique in the realm of structural engineering. Recently, some regularization techniques have been tested for system identification and damage detection in structures [Bec84, Sch92, Lee99, Lee00, Par01].

The regularization can be interpreted as a process of mixing the a priori estimates of system parameters and the a posteriori solution [Bui94, Par01]. The baseline properties are selected as the a priori estimates of the system parameters in this paper. The a priori estimates are taken into account in the problem statement of inverse problems by adding a regularization function with the a priori estimates of the system parameters to the error function. The regularization function should be defined differently for different problems since each problem has different regularity condition that defines the feasible solution space as mentioned in section 2.3. Focusing on the estimation of foreign material properties of elastic continua, the solution space should be defined as a subspace of  $L_2(V)$ , square-integrable with respect to the system property since the physical distribution of the system property is piecewise continuous. The regularity condition of the solution space can be weakly imposed by adding the following regularization function to the output error estimator of Eq.(2.6). [Tik77, Gro84, Mor93].

$$\Pi_R = \frac{1}{2} \lambda^2 \int_V (x - x_0)^2 dV \quad (2.32)$$

where,  $\lambda$  usually referred as the regularization factor that controls the degree of the regularity of the solution space [Tik77, Gro84, Mor93, Bui94, Par01]. Eq.(2.32) is referred as the standard Tikhonov regularization function.

Since the group configuration of material properties are predefined as shown in Fig.2.1, Eq.(2.32) is converted into the discrete form.

$$\Pi_R = \frac{1}{2} \lambda^2 \|\mathbf{x} - \mathbf{x}_0\|_2^2 \quad (2.33)$$

where  $\mathbf{x}_0$  denote the a priori estimates of system parameters. By adding the regularization function normalized by the a priori estimates to the minimization problem of Eq. (2.10), a regularized system identification problem is written in the following form.

$$\text{Minimize}_{\xi} \pi = \frac{1}{2} \|\tilde{\mathbf{U}}(\xi) - \bar{\mathbf{U}}\|_2^2 + \frac{1}{2} \lambda^2 \|\xi - \mathbf{1}\|_2^2 \quad \text{subject to } \mathbf{R}(\xi) \leq 0 \quad (2.34)$$

where  $\mathbf{1}$  denotes a column vector which has unit values in all the components. The objective function in Eq. (2.34) is referred to as the regularized error function or regularized output error estimator. The regularization factor determines the degree of regularization in the system identification; i.e. the influence of the a priori estimates on the solution of Eq. (2.34). The quadratic sub-problem of Eq. (2.34) is defined as

$$\text{Minimize}_{\Delta\xi} \left[ \frac{1}{2} \Delta\xi^T \mathbf{S}^T \mathbf{S} \Delta\xi - \Delta\xi^T \mathbf{S}^T \mathbf{U}^r \right] + \lambda^2 \left[ \frac{1}{2} \Delta\xi^T \Delta\xi - \Delta\xi^T (\mathbf{1} - \xi) \right] \quad (2.35)$$

subject to  $\mathbf{R}(\xi + \Delta\xi) \leq 0$

The stability of Eq. (2.35) is investigated under the unconstrained condition to clearly present the effect of the regularization. Furthermore, the regularization factor should be

determined for the unconstrained problems so that it can overcome the original sources of instabilities explained in the previous section 2.2.1. Once the regularization factor is obtained for the unconstrained problem, the quadratic sub-problem with the active constraints defined in Eq. (2.35) can be solved.

The regularized solution of the unconstrained problem of Eq. (2.35) is obtained by use of the SVD.

$$\Delta \xi_u^R = \mathbf{V} \text{diag}(1 - \alpha_j) \text{diag}\left(\frac{1}{\omega_j}\right) \mathbf{Z}^T \mathbf{U}^r + \mathbf{V} \text{diag}(\alpha_j) \mathbf{V}^T (\mathbf{1} - \xi) \quad (2.36)$$

where  $\alpha_j = \lambda^2 / (\omega_j^2 + \lambda^2)$ . With some mathematical manipulation of Eq. (2.36) by use of the orthogonal properties of  $\mathbf{V}$  and  $\mathbf{Z}$ , an intuitive expression is derived as follows.

$$\mathbf{V}^T \xi_u^R = \text{diag}(\alpha_j) \mathbf{V}^T \mathbf{1} + \text{diag}(1 - \alpha_j) \mathbf{V}^T \xi_u \quad (2.37)$$

where

$$\xi_u^R = \xi + \Delta \xi_u^R, \quad \xi_u = \xi + \Delta \xi_u \quad (2.38)$$

In Eq. (2.37),  $\xi_u^R$  and  $\xi_u$  represent the regularized solution and the a posteriori solution of the unconstrained problem at the current iteration, respectively. The expression in Eq. (2.37) implies that the projection of the regularized solution onto  $\mathbf{V}$  is a generalized average between the projections of the a priori estimates and the a posteriori solution onto  $\mathbf{V}$ .

The weighting factor  $\alpha_j$ , which varies with the regularization factor  $\lambda$  from 0 to 1, adjusts the relative magnitude between the a posteriori solution and the a priori estimates in

the regularized solution. The weighing factor approaches zero as the regularization factor becomes smaller, and one as the regularization factor becomes larger. Therefore, the solution converges to the a priori estimates for a large regularization factor while the solution converges to the a posteriori solution for a small regularization factor. In case the regularization factor is fixed, the weighting factors become larger for smaller singular values. This fact implies that the stronger effect of the a priori estimates is included in a solution component corresponding to the smaller singular value, and vice versa.

Unlike Eq. (2.18), the orthogonality of the displacement residual  $\mathbf{U}^r$  to each LSV is not required for the convergence of Eq. (2.36) because non-vanishing components in the first term can be cancelled out by the second term. By decomposing the a posteriori solution increment into the noise-free components and error components using Eq. (2.14), the following expression is obtained.

$$\begin{aligned} \mathbf{V}^T \boldsymbol{\xi}_u^R = & \{ \text{diag}(\alpha_j) \mathbf{V}^T \mathbf{1} + \text{diag}(1 - \alpha_j) \mathbf{V}^T \boldsymbol{\xi}_u^f \} \\ & + \text{diag}(1 - \alpha_j) \text{diag}\left(\frac{1}{\omega_j}\right) \mathbf{Z}^T \mathbf{e} \end{aligned} \quad (2.39)$$

where  $\boldsymbol{\xi}_u^f$  denotes the noise-free a posteriori solution. Since the weighting factors range from 0 to 1 for all singular values, the effect of noise on the solution can be reduced. In particular, the components of  $\mathbf{Z}^T \mathbf{e}$  associated with small singular values, which are responsible for the discontinuity and deviation from the noise-free solution, are mostly suppressed in the regularized solution by the regularization effect. This is because the weighting factors corresponding to smaller singular values become almost one for a properly selected regularization factor.

## **2.5 Determination of an Optimal Regularization Factor**

Several well-defined methods have been proposed to determine an optimal regularization factor in linear inverse problems. The L-curve method (LCM) proposed by Hansen [Han92a] and the generalized cross validation (GCV) method proposed by Golub *et al.* [Gol78] are well-known schemes. Kaller and M. Bertrant utilized the GCV for medical image enhancing problems [Kal96]. While the aforementioned schemes have been proven to be effective in linear inverse problems, no rigorous schemes for nonlinear inverse analysis have been proposed yet. Regularization factors of nonlinear inverse problems can be determined by applying the LCM and the GCV at each minimization iteration, where a linearized quadratic sub-problem is solved. Eriksson *et al.* reported that the LCM yields non-convergent results for a nonlinear inverse problem with an explicit nonlinear function model [Eri96], which is also observed in the current research. It has also been found through our extensive numerical experiments that the GCV often yields too small regularization factors, and is unable to effectively control the instabilities of the SI algorithms.

A new scheme, defined as a geometric mean scheme (GMS) proposed Park *et al.*, is successfully utilized to overcome drawbacks of existing schemes in the determination of the regularization factor for SI in elastic continua [Par01]. In this section several determination schemes including GMS will be presented.

### **2.5.1 Geometric Mean Scheme (GMS)**

A new scheme of a geometric mean scheme (GMS) proposed by Park *et al.*(2001) determines the optimal regularization factor. In this method, an optimal regularization

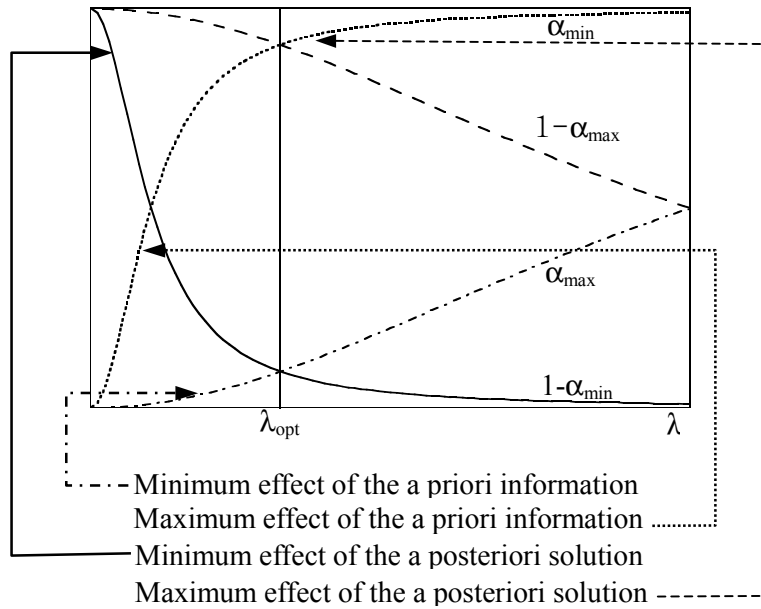


Fig. 2.6. Schematic drawing for an optimal regularization factor in the GMS

factor is defined as the geometric average between the maximum and the minimum singular value of the sensitivity matrix. As shown in Eq. (2.37), the regularization effect on each component of the solution depends on the magnitude of the corresponding singular value. Fig.2.6 illustrates the variation of weighting factors for the maximum and the minimum singular values with the regularization factor. In the regularized solution, the maximum effect of the a priori information and the a posteriori solution occurs with the smallest singular value and the largest singular value, respectively. On the other hand, the minimum effect of the a priori information and the a posteriori solution occurs for the largest singular value and the smallest singular value, respectively. Based on this observation, the optimal regularization factor is defined as the one that yields the same maximum and minimum effect of the a priori information and the a posteriori solution,

which can be stated as

$$1 - \alpha_{\max} = \alpha_{\min}, \quad 1 - \alpha_{\min} = \alpha_{\max} \quad (2.40)$$

where  $\alpha_{\max}$  and  $\alpha_{\min}$  are the weighting factors corresponding to the maximum singular value and the minimum singular value, respectively. The first and the second equation in Eq. (2.40) represent the balancing conditions on the maximum and the minimum effect, respectively as shown in Fig. 2.6. An interesting point is that the two equations are identical and yield the geometric average between the smallest and the largest singular value for the optimal solution of  $\lambda$ .

$$\lambda_{opt} = \sqrt{\omega_{\max} \omega_{\min}} \quad (2.41)$$

If zero singular values exist, the smallest non-zero singular value may be used for  $\omega_{\min}$ .

### 2.5.2 The L-Curve Method (LCM)

The L-curve is a log-log plot of the regularization function versus the error function for various regularization factors. Hansen showed for linear inverse problems that the plot always formed a ‘L’ shaped curve as shown in Fig. 2.7, and that the optimal regularization factor corresponds to the sharp edge of the curve where the curvature of the curve becomes maximal [Han92a]. For nonlinear inverse problems, the L-curve is defined at each iteration for the linearized error function.

To apply the LCM directly at each iteration, the following transformation between  $\Delta \xi_u$  and  $\Delta \chi$  is necessary.

$$\Delta \chi^R = \xi + \Delta \xi_u^R - \mathbf{1} \quad (2.42)$$



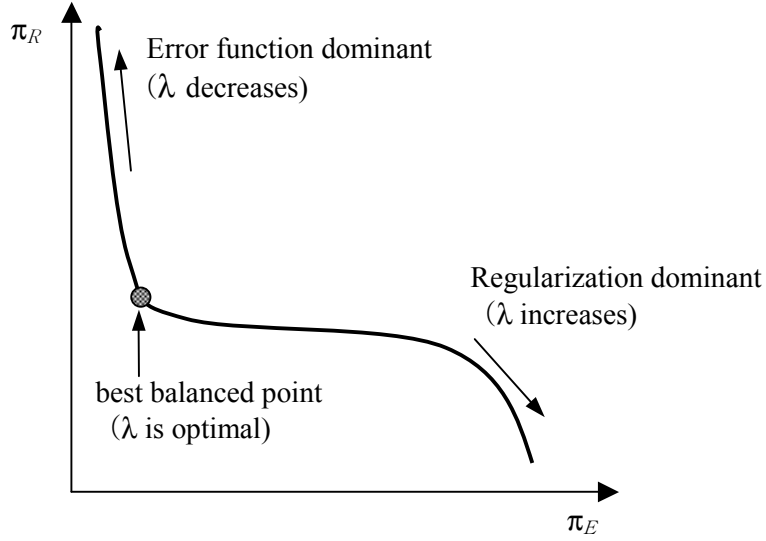


Fig. 2.7. Basic concept of the L-curve method

where  $\Delta\boldsymbol{\chi}$  is transformed regularized solution of Eq. (2.23).

The regularization function  $\pi_R$  and the linearized error function  $\pi_E^l$  are expressed in terms of the weighting factor, which is a function of the regularization factor as follows.

$$\pi_R = \left\| \boldsymbol{\xi} + \Delta\boldsymbol{\xi}^R - \mathbf{1} \right\|_2^2 = \left\| \Delta\boldsymbol{\chi}^R \right\|_2^2 = \left\| \text{diag} \left( \frac{1 - \alpha_i}{\omega_i} \right) \mathbf{Z}^T \mathbf{b}^r \right\|_2^2 \quad (2.43)$$

$$\begin{aligned} \pi_E^l &= \left\| \tilde{\mathbf{U}} - \bar{\mathbf{U}} + \mathbf{S}\Delta\boldsymbol{\xi}^R \right\|_2^2 = \left\| \mathbf{S}\Delta\boldsymbol{\chi}^R - \mathbf{b}^r \right\|_2^2 \\ &= \left\| (\mathbf{I} - \mathbf{Z}\mathbf{Z}^T) \mathbf{b}^r \right\|_2^2 + \left\| \text{diag}(\alpha_i) \mathbf{U}^T \mathbf{b}^r \right\|_2^2 \end{aligned}$$

where  $\mathbf{b}^r = \mathbf{S}(\boldsymbol{\xi} - \mathbf{1}) - \mathbf{U}^r$ . The parametric form of the L-curve for the current iteration step is given by the following expression.

$$(\rho(\lambda), \eta(\lambda)) = (\log(\pi_E^l), \log(\pi_R)) \quad (2.44)$$

The elimination of  $\lambda$  from Eq. (2.43) leads to the L-curve for the current iteration. Since the regularization function and the linearized error function given in Eq. (2.42) are monotonically decreasing and monotonically increasing with respect to  $\lambda$ , respectively, Eq. (2.43) forms a ‘L’ shaped curve. Since all the variables in Eq. (2.42) are calculated from the previous iteration, only one SVD for the sensitivity matrix is required to construct the L-curve.

The curvature of the L-curve is given as

$$\kappa(\lambda) = \frac{\rho' \eta'' - \rho'' \eta'}{((\rho')^2 + (\eta')^2)^{1.5}} \quad (2.45)$$

where the superscript ‘ $\prime$ ’ denotes the differentiation of a variable with respect to  $\lambda$ . Since  $\rho$  and  $\eta$  are continuous functions of  $\lambda$  and expressed explicitly for  $\lambda$ , the derivatives in Eq. (2.44) are obtained analytically. The optimal regularization factor that yields the maximum curvature of the L-curve is calculated precisely by a one-dimensional line search.

However, for some nonlinear inverse problems, the solutions by the LCM do not converge but oscillate between two L-curves as schematically drawn in Fig. 2.8. In view of the regularization factor, two optimal regularization factors are repeatedly obtained with a large and a small value. The L-curve with a large regularization factor corresponds to the nonlinear problem more affected by the solution error in addition to the measurement noise. On the other hand, the L-curve with a smaller regularization factor is affected by the measurement noise.

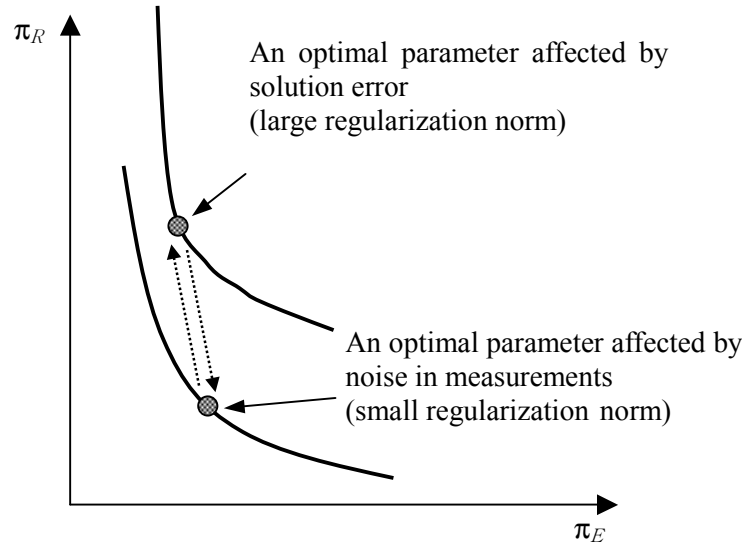


Fig. 2.8. Schematic drawing – Oscillating results of the LCM

### 2.5.3 Variable Regularization Factor Scheme (VRFS)

Recently, the variable regularization factor scheme (VRFS) is proposed by Lee *et al.* for nonlinear inverse problems to identify shapes of inclusions in finite bodies [Lee99, Lee00, Yeo00]. The VRFS is based on an argument that the regularization function should be smaller than the error function to prevent the regularization function from dominating the optimization process.

In the VRFS, the regularization factor is defined as the inequality between the error function and the regularization function as follows.

$$\|\tilde{\mathbf{U}}(\boldsymbol{\xi}) - \bar{\mathbf{U}}\|_2^2 \geq \lambda^2 \|\boldsymbol{\xi} - \mathbf{1}\|_2^2 \quad (2.46)$$

When the regularization function becomes larger than the error function by the solution of the current iteration, the regularization factor is reduced by multiplying a

prescribed reduction factor  $\beta$  ranging from 0 to 1. Lee *et al.* demonstrated that identification results are relatively insensitive to moderate values of the reduction factor around 0.1. The VRFS with  $\beta = 0.1$  has been successfully applied to shape identification problems and damage detection in framed structures [Lee99, Lee00, Yeo00]. However, the VRFS fails to converge for some nonlinear problems with modeling errors as demonstrated by simulation studies. One of the advantages of the VRFS is that the VRFS method can be easily applied to any type of regularization functions.

#### 2.5.4 Generalized Cross Validation (GCV)

Generalized cross validation (GCV) has been a popular method not only for determining the regularization factor but for estimating the noise amplitude of measurements [Gol78, Han98]. GCV is based on the statistical idea that an appropriate regularization factor should predict missing measurements. That is, if an arbitrary component of the measurement vector is left out, the corresponding regularization factor should predict this component of the measurement well. The optimal regularization factor by GCV can be obtained from the minimization of GCV function with respect to the regularization factor [Gol78, Han98].

$$\text{Min}_{\lambda} \frac{\|\mathbf{S}\Delta\boldsymbol{\chi}^R - \mathbf{b}^r\|_2^2}{\text{Trace}(\mathbf{I}_m - \mathbf{S}\mathbf{S}^\#)^2} \quad (2.47)$$

where  $\Delta\boldsymbol{\chi}^R$ ,  $\mathbf{I}_m$ , and  $\mathbf{S}^\#$  are transformed regularized solution as Eq.(2.42), an identity matrix of order  $m$ , and regularized inverse, say,  $\mathbf{V}\text{diag}(1-\alpha_j)\text{diag}(\frac{1}{\omega_j})\mathbf{Z}^T$  in Eq.(2.46), respectively.  $\text{Trace}(\cdot)$  denotes summation of diagonals of a squared matrix.

## 2.6 Numerical Examples

The effectiveness of the regularization is investigated through numerical simulation studies. Noise caused by measurement error is simulated by adding random noise generated from a uniform probability function to displacements calculated by a finite element model [Shi94, Yeo99]. The uniform probability function is selected because it generates more widely distributed errors than the normal distribution for given amplitude of error. The Monte Carlo simulation is carried out to illustrate the enhancement of continuity of the solution by regularization for both examples.

The Young's modulus of each element group is taken as the system parameter. Element groups are predefined to limit discussions to the regularization technique. The convergence criterion,  $\|\Delta\xi\|/\|\xi\| \leq 10^{-3}$ , is used to terminate optimization iterations unless otherwise stated. The baseline properties are assumed to be the Young's modulus of steel. The initial values of the system parameters are taken to be the same as the baseline properties for the optimization. The following upper and lower bounds are used for each system parameter.

$$0.1 \text{ GPa} \leq x_0 \leq 630 \text{ GPa} \quad (2.48)$$

The reduction factor of the VRFS,  $\beta=0.1$ , is used throughout the numerical study [Lee99]. The recursive quadratic programming with the active set algorithm [Lue89] is utilized for optimization.

### 2.6.1 Measurement error – Identification of a Foreign Inclusion in a Square Plate

To investigate the effects of measurement errors on the identification, a simulated

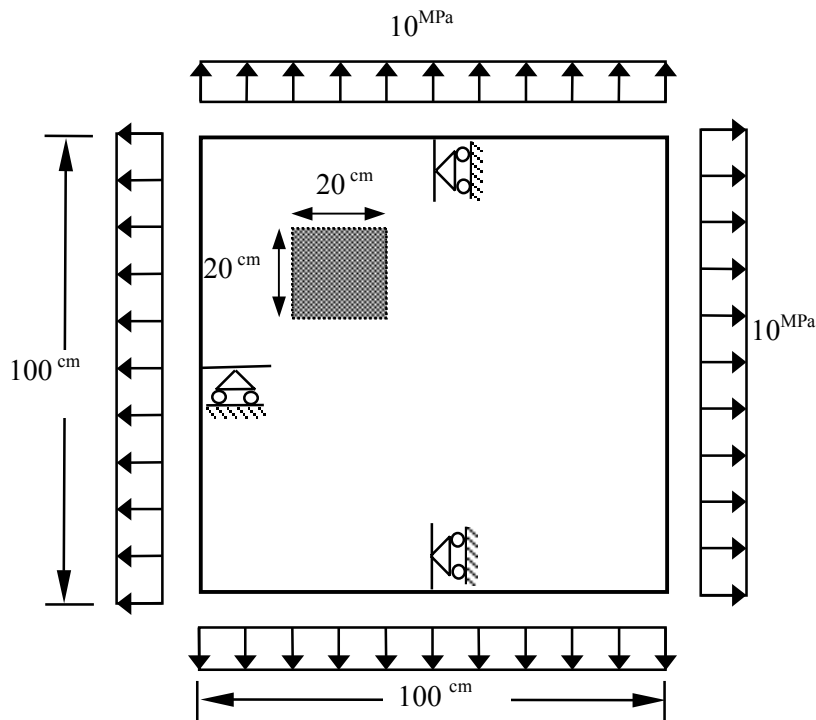


Fig. 2.9 Geometry and boundary conditions of a square plate

study is carried out with an inclusion in a square plate under the plane stress condition. Fig. 2.9 illustrates the geometry, boundary conditions and applied traction. The shadowed region in the figure denotes the inclusion. Young's modulus of the square plate is 210 GPa, which is representative of steel. Two types of inclusions – a soft inclusion of aluminum ( $E = 70$  GPa) and a hard inclusion of tungsten ( $E = 380$  GPa) – are considered.

Displacements are measured at the observation points located on the outer boundary of the square plate. Two different measurement cases are considered. The observation points are depicted as solid circles and open squares in Fig. 2.10 for measurement cases I and II, respectively. It is assumed that measurements are performed independently for two load cases,  $t_x$  and  $t_y$ . Both  $x$ - and  $y$ -component of displacements are measured at each

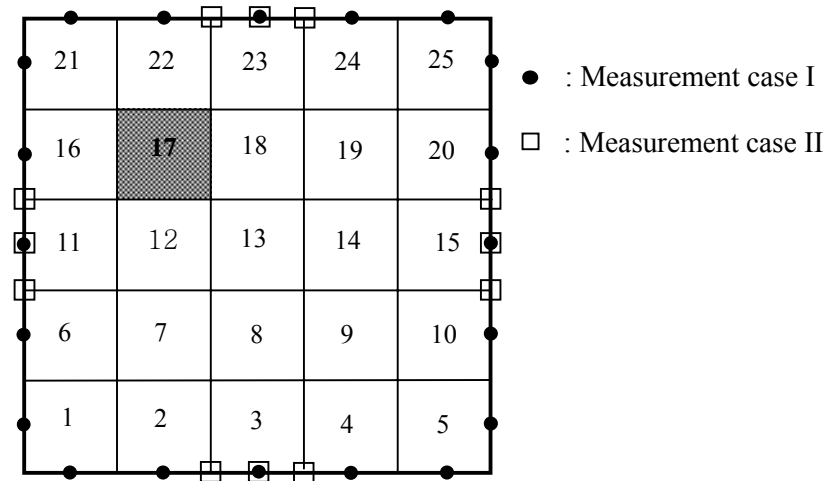


Fig. 2.10 Observation points and element group configuration of a square plate

observation point. The noise amplitudes of 5% and 1 % are applied for measurement cases I and II, respectively.

The finite element model employed in the parameter estimation is identical to the model used for obtaining the measured displacement, which consists of 100 8-node quadratic elements and 384 nodes. The predefined element groups are shown in Fig. 2.10, and each element group contains 4 elements.

***Measurement Case I***

Identified results for the soft inclusion by different regularization techniques are compared in Fig. 2.11. Identification without regularization yields results that oscillate severely. It is difficult to determine the existence of the inclusion from the identified results without regularization because the reduction in the Young’s modulus of element group 17 may be caused by either an actual inclusion or the oscillating results. When a regularization technique is employed, however, the amplitude of oscillation is reduced for

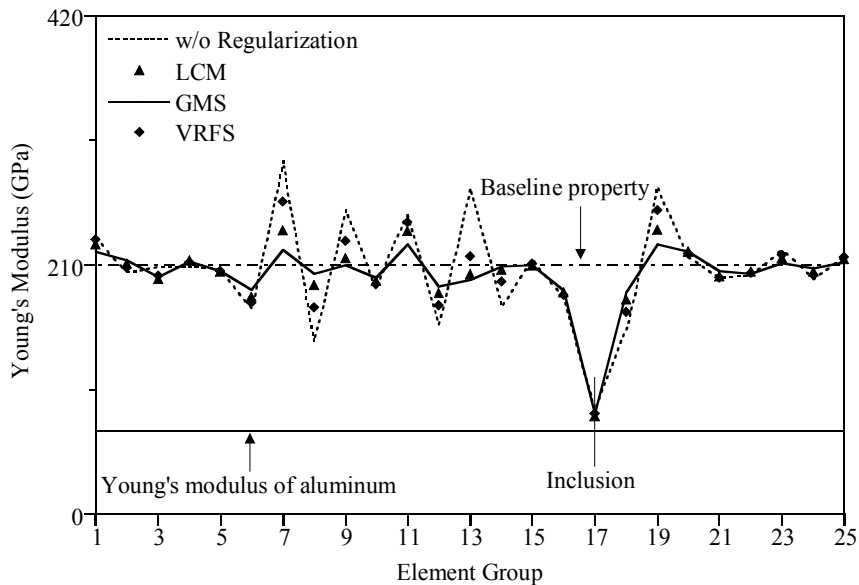


Fig. 2.11 Estimated Young's moduli by different regularization schemes (Soft inclusion - measurement case I)

the element groups in the matrix material. From the figure, it is seen clearly that the GMS controls the oscillation of the identified results most effectively among the other schemes. Although the LCM and VRFS alleviate the oscillation magnitudes to some extent, they yield rather large oscillation magnitudes compared to the GMS. Since Young's modulus of the soft inclusion reduces prominently compared with the oscillation magnitude of the other element groups by the GMS, the existence of a soft inclusion is clearly assured.

Fig. 2.12 illustrates the identification results for the hard inclusion with the measurements of case I. The results by SI without the regularization severely oscillate as in the soft inclusion. The identified results by the LCM are not drawn in the figure because optimization by the LCM does not converge as reported by Eriksson [Eri96]. Both the GMS and VRFS converge to almost the same results for the element groups in the matrix material. However, the GMS yields higher Young's modulus of the inclusion than



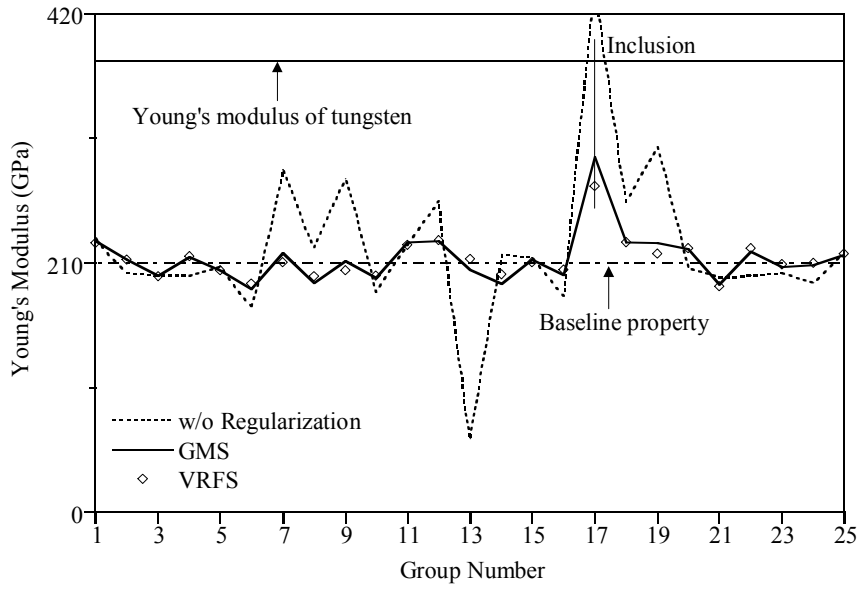


Fig. 2.12 Estimated Young's moduli by different regularization schemes (Hard inclusion - measurement case I)

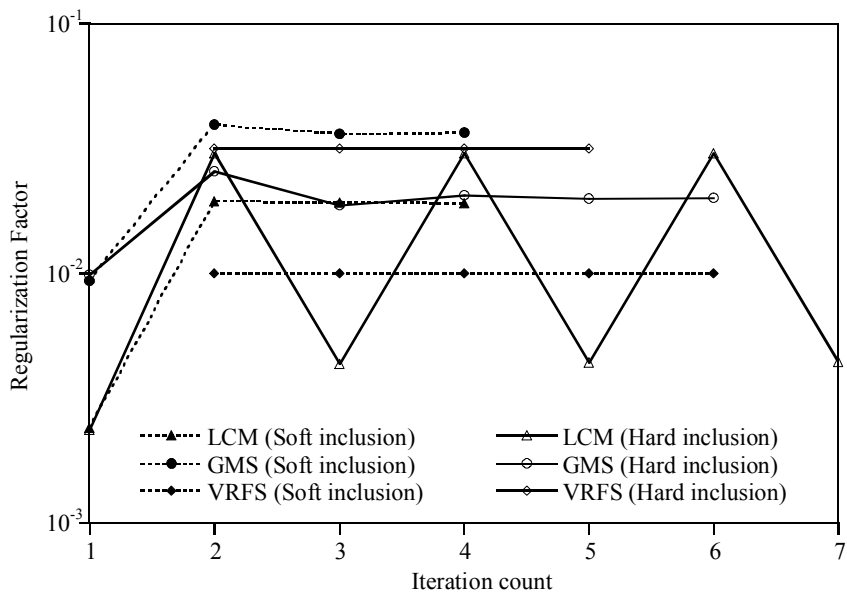


Fig. 2.13 Regularization factors by different regularization schemes (measurement case I)

VRFS. Although Young's modulus of the inclusion is estimated somewhat lower than the actual value, the identification results by the GMS are good enough to point out the existence of a stiff material at element group 17.

Fig. 2.13 shows regularization factors at each iteration step obtained by the different schemes for the hard and soft inclusions, respectively. By relating regularization factors shown in Fig. 2.13 to the identified results in Fig. 2.11 and Fig. 2.12, it is easily observed that a larger regularization factor yields less oscillating results. For the hard inclusion case, the LCM yields periodically oscillating regularization factors between the two values, which causes non-convergent optimization iterations. Fig. 2.14 shows the solutions corresponding to the lower and upper regularization factor during oscillations by the LCM together with the converged solution by the GMS. In the LCM, the lower regularization factor yields more oscillating results with sharp resolution at the hard inclusion while the

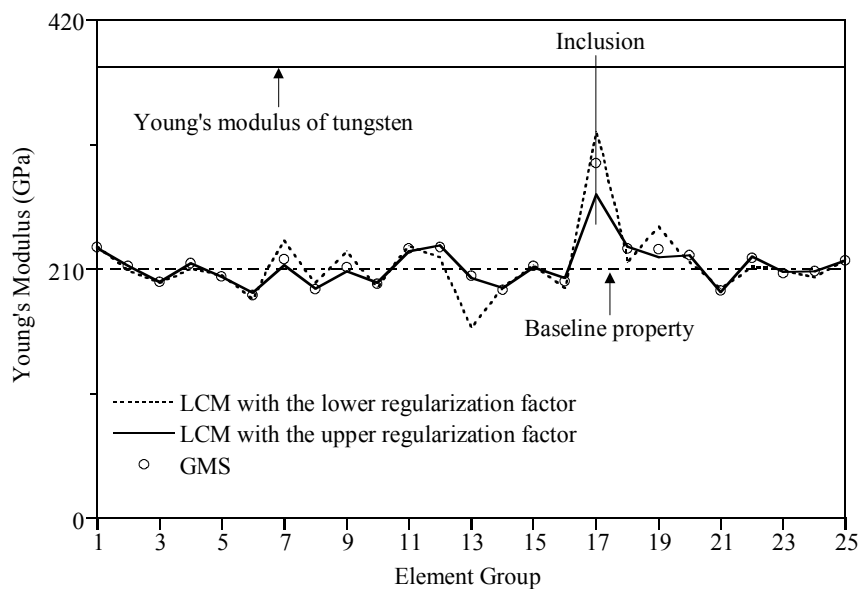


Fig. 2.14 Two oscillating solutions by the LCM and the solution by the GMS (Hard inclusion - measurement case I)

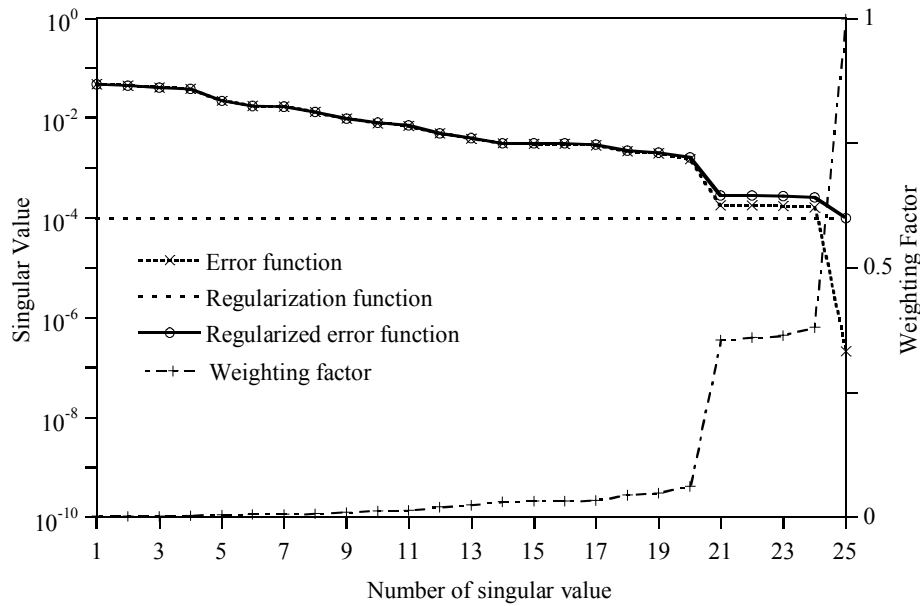


Fig. 2.15 Distribution of singular values and weighting factors by GMS at the 1st iteration (Hard inclusion - measurement case I)

upper regularization factor yields less oscillating results with smeared resolution at the hard inclusion. The solution by the GMS seems to be a mixture of favorable aspects of the two solutions by the LCM, i.e., a less oscillating solution with sharper resolution at the hard inclusion.

Fig. 2.15 shows distributions of singular values of three different Hessian matrices, the error function, the regularization function and the regularized error function of Eq. (2.34) at the first iteration step for the hard inclusion problem. In the same figure, the weighting factors  $\alpha_j$  associated with the singular values are also drawn. For drawing the weighting factors, the right vertical axis is used as the reference. In the figure, it is observed that the lowest singular value of the error function is very small compared with the other singular values, which caused the oscillations in the identification without the regularization as

shown in Fig. 2.12. The singular values of the Hessian matrix of the regularized error function are shifted by the singular value of the regularization function. However, the regularization function does not affect the distribution of the singular values of the regularized error function from the sixth singular value. Therefore, the a priori estimates have a strong influence on the solution components corresponding to the smaller singular values, and the influence of the a priori estimates decrease drastically for larger singular values. This phenomenon can be clearly observed by the distribution of the weighting factors in the same figure.

Fig. 2.16 and Fig. 2.17 illustrate the solution of the unconstrained quadratic subproblem in the RSV direction and in the system parameter direction at the first iteration corresponding to the noise-free and noise components in the measured displacements, respectively. The SI algorithms with the GMS and without the regularization yield almost identical solution increments for the noise-free components, even though the GMS causes a little smeared increments corresponding to lower singular values. However, for the noise components, the regularization develops surprising differences in the solution increments as demonstrated in Fig. 2.17. Without regularization, the noise components of the measurements are amplified by the lowest singular value. The solution increment caused by the noise components corresponding to the lowest singular value is about 30 times larger than the maximum solution increments caused by the noise-free components in the RSV direction. The amplified noise component contaminates the whole solution increments with the noise in the system parameter direction. Since the weighting factor for the lowest singular values in the GMS is almost 1 as shown in Fig. 2.15, most of the noise components corresponding to the lowest singular value in Eq. (2.37) are suppressed.

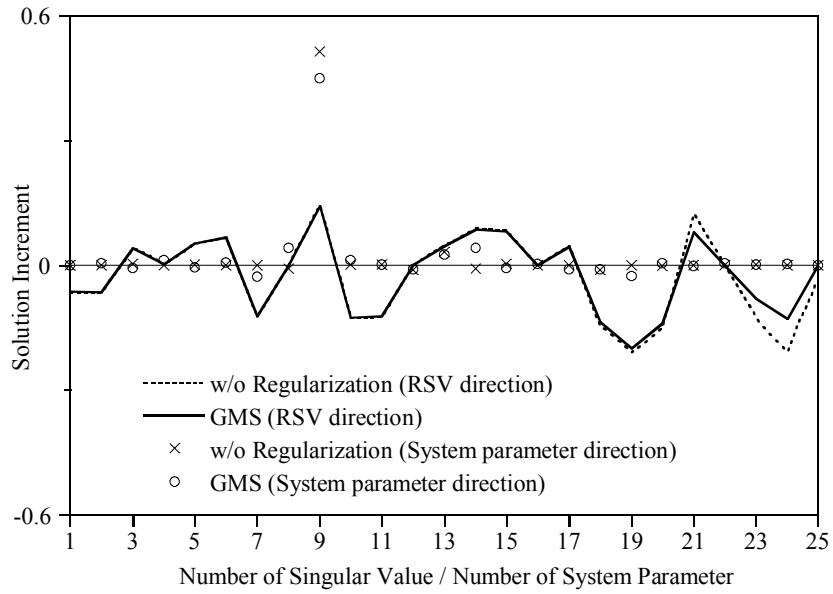


Fig. 2.16 Solution of the unconstrained sub-problem by the noise-free measurement at the 1st iteration (Hard inclusion - measurement case I)

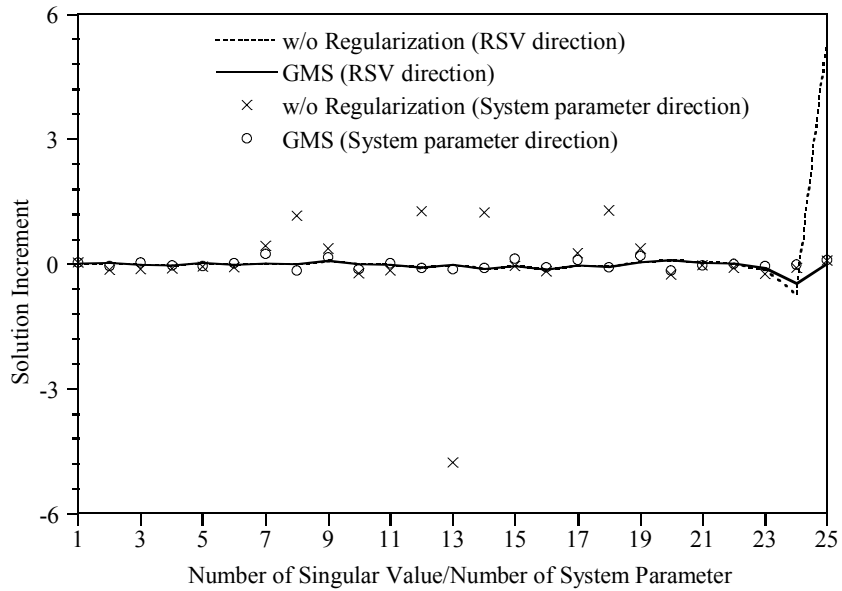


Fig. 2.17 Solution of the unconstrained sub-problem by noise components in measurements at the 1st iteration (Hard inclusion - measurement case I)

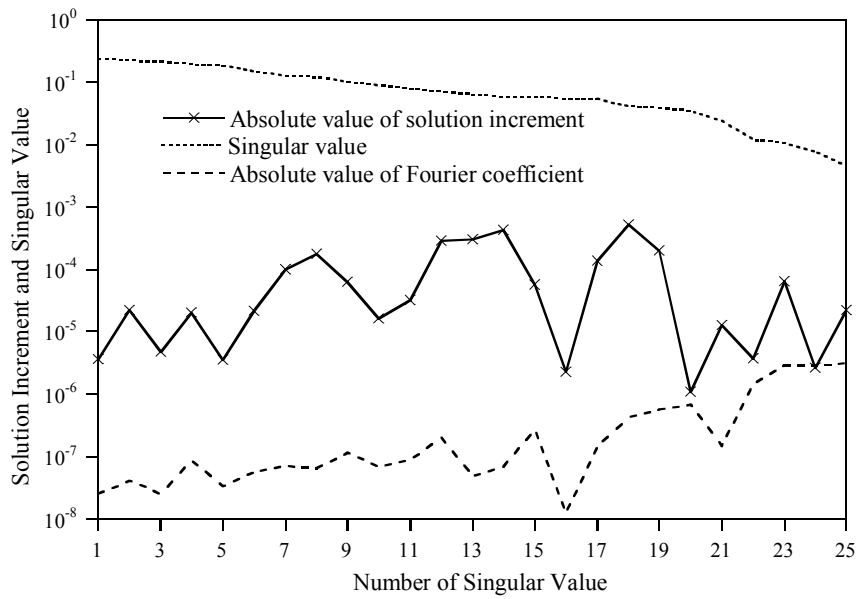


Fig. 2.18 Singular value, Fourier coefficient and solution of the unconstrained sub-problem at the converged iteration without regularization (Hard inclusion - measurement case I)

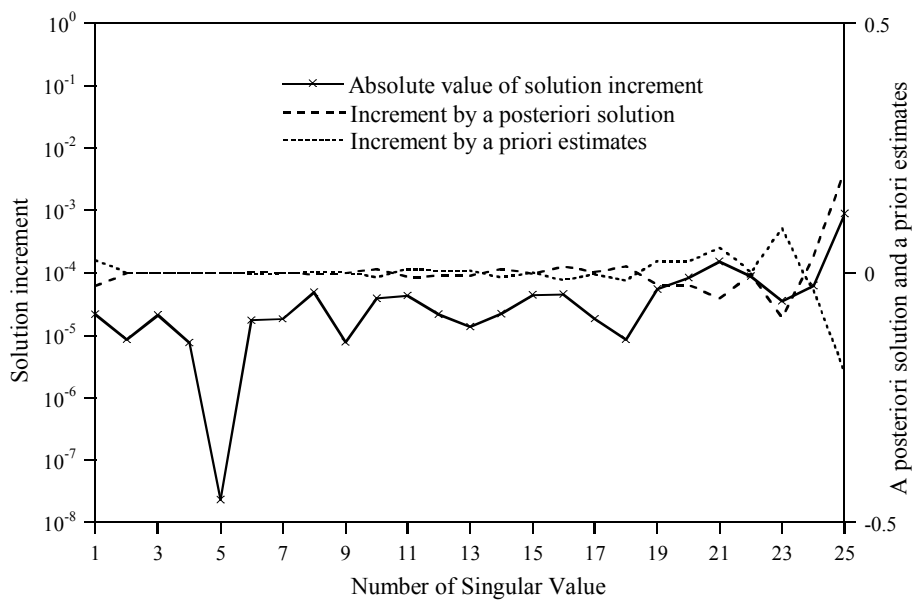


Fig. 2.19 Solution of the unconstrained sub-problem at the converged iteration by the GMS (Hard inclusion - measurement case I)

Consequently, the solution increments caused by the noise components are very small in the SI with the GMS compared to those in SI without the regularization.

Fig. 2.18 and Fig. 2.19 show the solution of the unconstrained quadratic sub-problem in the RSV direction at the converged stage for SI with the GMS and without regularization, respectively. In Fig. 2.19, the absolute values of regularized solution increments are plotted in logarithmic scale for the left vertical axis while the increments associated with the a posteriori solution and a priori estimates are plotted in a linear scale for the right vertical axis. Both the SI algorithms yield almost zero increments in the RSV direction at the converged state. However, two schemes exhibit different patterns in reducing solution increments. The norm of the displacement residual reduces only by 0.033 in the SI algorithm without regularization. Nevertheless, the norm of the solution increments is converged to the specified criterion because the Fourier coefficients are reduced to below  $10^{-5}$  order and the singular values maintain relatively larger values than the Fourier coefficients. On the other hand, the SI algorithm with the GMS reduces the solution increments by balancing the increments associated with the a priori estimates and a posteriori solution as shown in Fig. 2.19.

To investigate continuity of solutions in various SI algorithms to measurement errors, a Monte-Carlo simulation with 30 trials at 5% noise amplitude is carried out. A different set of measured data is used for each trial by generating different random noise from the uniform probability density function [Hje96]. The relative magnitude of the standard deviation to the mean value of each system parameter obtained by the Monte-Carlo simulation is a good indicator of the continuity of solutions because the standard deviation represents the degree of scatter of a statistical variable. The computed mean and standard

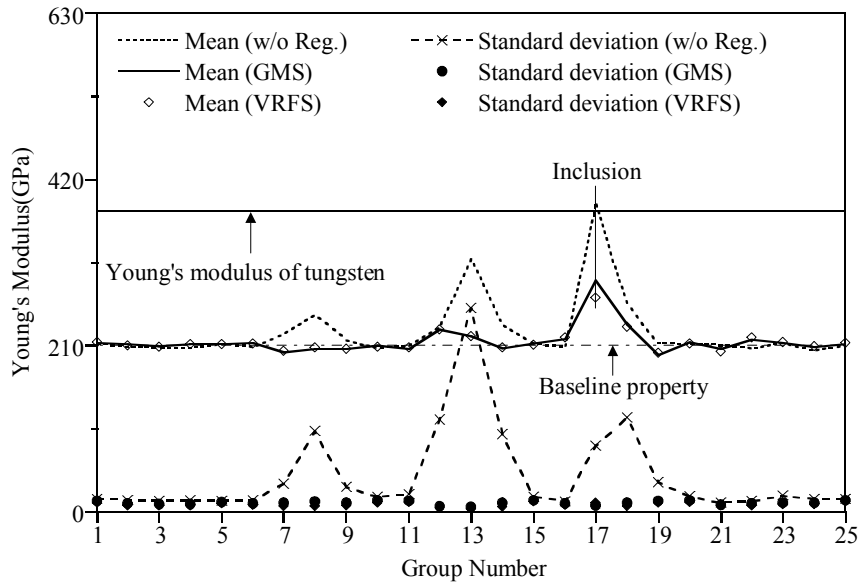


Fig. 2.20 Mean values and standard deviations of estimated Young's moduli by Monte-Carlo simulation (Hard inclusion - measurement case I)

deviation of each system parameter from the Monte Carlo simulations are compared in Fig. 2.20 for different regularization schemes. Results by the LCM are not presented since the LCM fails to converge in 15 out of 30 trials. When the regularization is not employed in the SI algorithm, large standard deviations usually occur at the element groups of which estimated moduli are larger than the baseline property. Meanwhile, SI with a regularization technique yields small and consistent standard deviations for all system parameters, which illustrates an enhancement of the continuity of solutions with a regularization technique. Both the VRFS and GMS yield almost identical results and smaller elastic modulus of the inclusion than the actual value in an average sense. Despite the underestimation, the existence of an inclusion with a stiffer material at element group 17 is clearly distinguishable in general because oscillations in the other element gro-



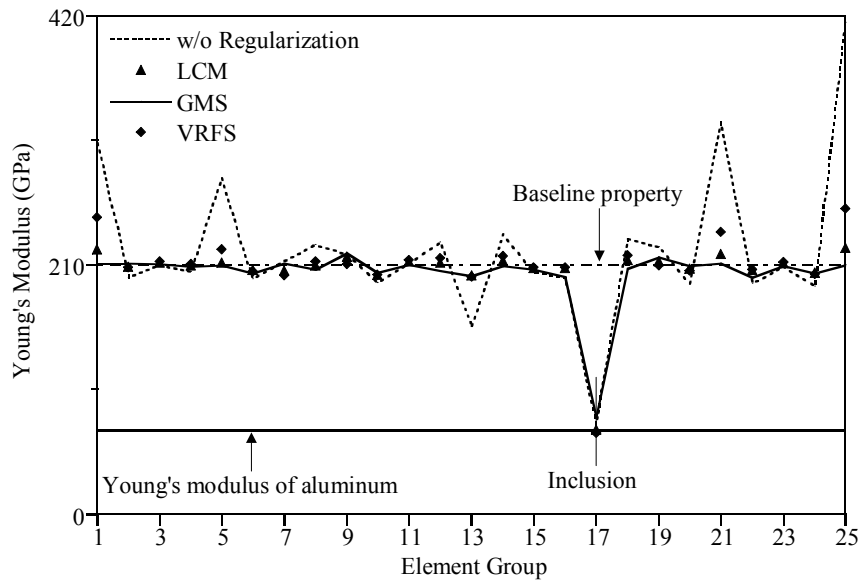


Fig. 2.21 Estimated Young's moduli by different regularization schemes (Soft inclusion - measurement case II)

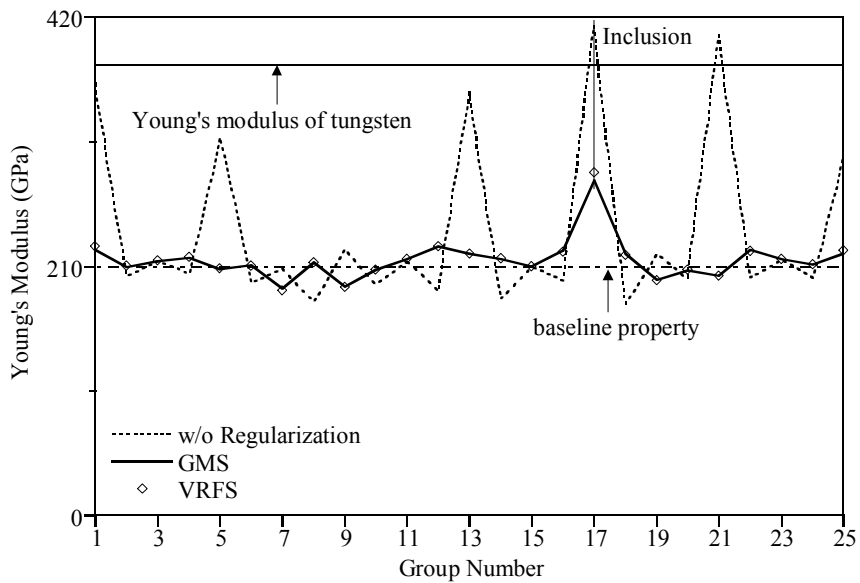


Fig 2.22 Estimated Young's modulus by different regularization schemes (Hard inclusion - measurement case II)

-ups are negligible.

### ***Measurement Case II***

The influence of sparseness of measured data on estimated results is studied in Fig. 2.21 and Fig. 2.22. The sparseness of measured data is simulated by reducing the number of the observation points and by locating some of the observation points close to each other as shown in Fig 2.10. Since the three observation points on each side of the square plate are closely placed, the independence of information supplied by those observation points is reduced, which deteriorates the quality of information.

Fig. 2.21 and Fig 2.22 show the estimated Young's modulus for the soft and hard inclusion case with 1% noise amplitude, respectively. Although the noise amplitude of this measurement case is much smaller than that of measurement case I, the solutions by SI without the regularization oscillate more severely. This is because the lowest singular value of the sensitivity matrix becomes much smaller in this measurement case than in the previous one due to the poor quality of information.

All three regularization techniques yield very stable and accurate results for the soft inclusion. However, the LCM fails to converge for the hard inclusion due to the oscillations of the regularization factor as explained in measurement case I. The VRFS and GMS yield almost identical results, but underestimates the Young's modulus of the hard inclusion as in measurement case I.

### **2.6.2 Modeling Error – Identification of Three Internal Cracks in a Thick Pipe**

Behaviors of SI algorithms with respect to modeling errors are investigated in this example. A thick pipe with three cracks is subjected to internal pressure as shown in

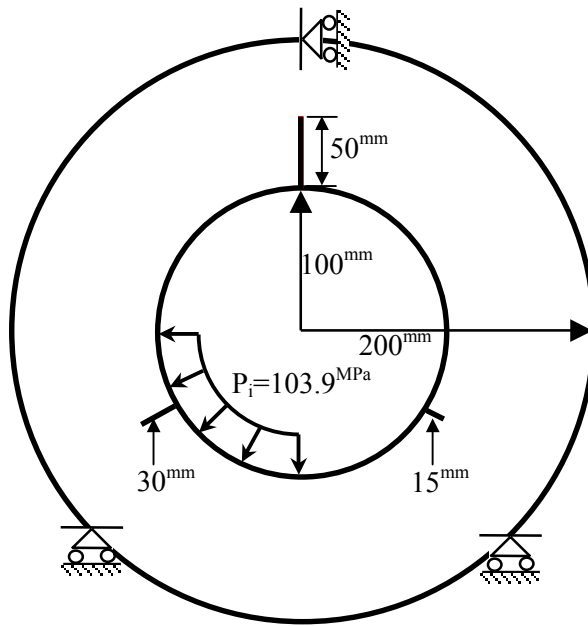


Fig. 2.23 Geometry and boundary conditions of a thick pipe

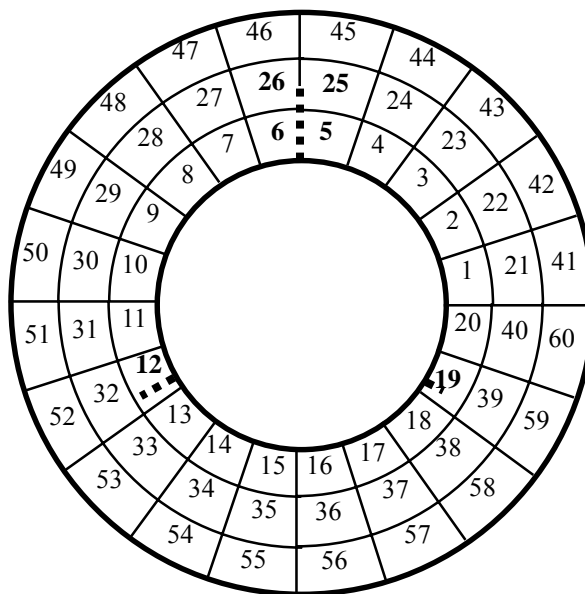


Fig. 2.24 Element group configuration of a thick pipe

Fig. 2.23. Measured displacements at equally spaced 80 observation points on the outer surface of the pipe are obtained by a finite element model with 6400 8-node quadratic elements and 19608 nodes. Both  $x$ - and  $y$ -components of displacements are measured at each observation point. To simulate actual behaviors of structures realistically, elastic-perfect-plastic response of the pipe is considered with the von-Mises yield condition. For the SI, the pipe is discretized by 480 8-node quadratic elements and 1520 nodes, and only the elastic behaviors are considered. The element groups used in this example are illustrated in Fig. 2.24. A total of 60 element groups are used, and each element group contains 8 elements. The finite element model for the identification does not include the cracks while the model used for calculating displacements contains the cracks. Therefore, this example contains modeling errors in the boundary conditions in addition to errors in the constitutive law.

Identified results are shown in Fig. 2.25, in which arrows indicate the element groups with a real crack. The SI algorithms without regularization and with the VRFS cannot yield converged solutions within 60 iterations, and thus only the solutions by the LCM and GMS are presented in the figure. The GMS and LCM yield converged solutions at 30 and 53 iterations, respectively, which demonstrates the stability of the GMS over the LCM.

As shown in Fig. 2.25, both the LCM and GMS yield physically meaningful solutions in an overall sense. The Young's moduli of the element groups with a crack exhibit significant drops from the baseline property compared with the oscillation amplitudes at the other element groups. However, the LCM predicts a large reduction in the Young's modulus at element group 7, which is located beside element group 6 and does not contain an actual crack. Both methods estimate a smaller Young's modulus at element group 19

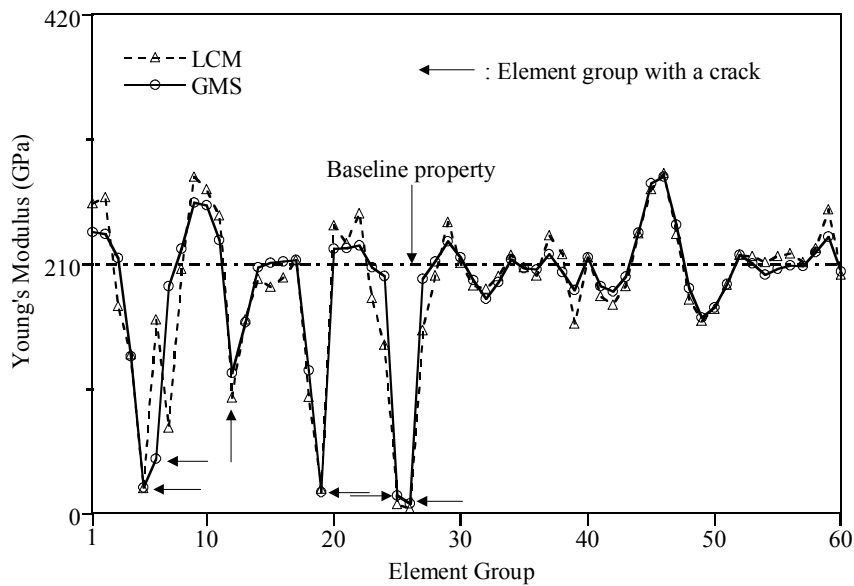


Fig. 2.25 Estimated Young's Moduli by different regularization schemes (Thick pipe with three internal cracks)

than that of element group 12. From the physical point of view, this result may not represent the real situation of damage in the pipe properly because the length of the crack in element group 12 is longer than that in element group 19. Despite such an inaccuracy in the assessment of actual damage, the existence of damage at three different locations in the pipe can be clearly identified by the SI algorithms with the LCM and GMS.

Fig. 2.26 shows a singular value distribution of each Hessian matrix and the distribution of weighting factors at the first iteration step when the GMS is applied. By comparing with Fig. 2.15, it is easily observed that this example is much more ill-posed than the hard inclusion case presented in the previous example since the 22 singular values are smaller than the regularization factor obtained by the GMS. Severe ill-posedness of this problem is caused by the axis-symmetry of the observed points that are equally spaced on the outer boundary of the pipe. The solution components contributed by the a

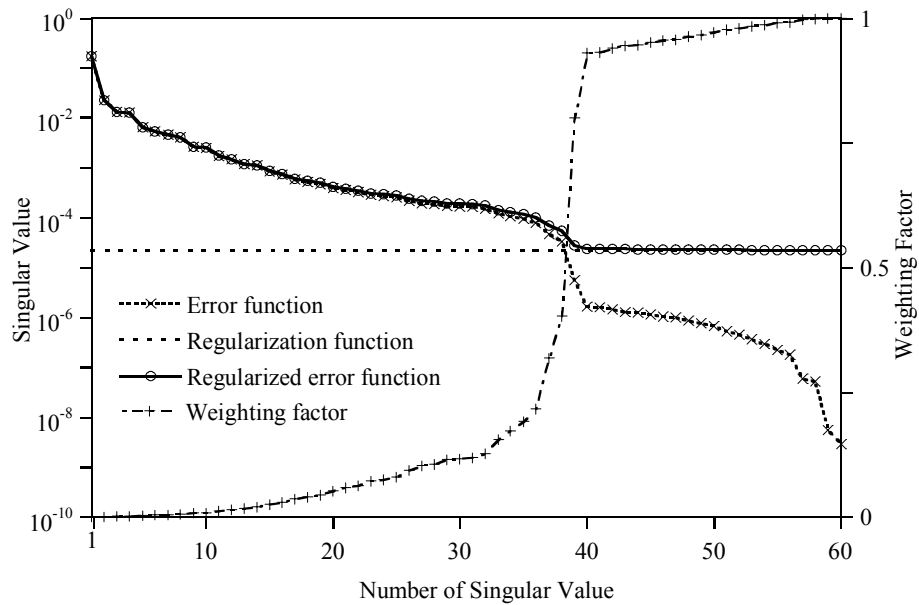


Fig. 2.26 Distribution of singular values and weighting factors by GMS at the 1st iteration (Thick pipe with three internal cracks)

posteriori solution corresponding to the 22 singular values are mostly suppressed, and the a priori estimates are dominant in the solution. The contribution of the a priori estimates to the solution rapidly increases for singular values larger than the 39<sup>th</sup> singular value, and most parts of the regularized solution consist of the a posteriori solution. The distribution of the weighting factors represents the relative magnitude of regularization corresponding to each singular value.

The non-convergence of the SI algorithm without regularization can be clearly explained by Fig. 2.27, which shows the solution of the unconstrained quadratic subproblem in the RSV direction at the 60<sup>th</sup> iteration. The Fourier coefficients are reduced to some extent in the figure. However, since some of the singular values marked by solid circles in Fig. 2.27 become smaller than the corresponding Fourier coefficients, the

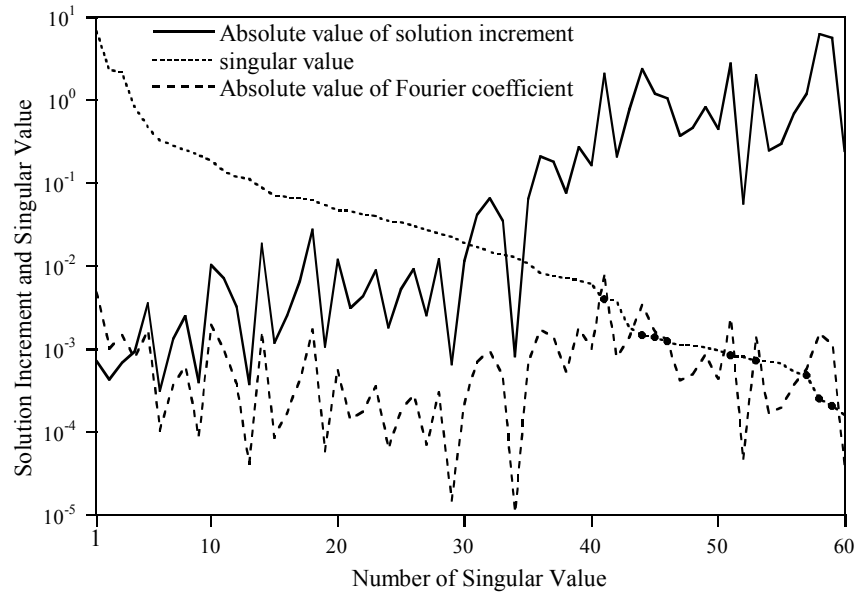


Fig. 2.27 Singular value, Fourier coefficient and solution of the unconstrained sub-problem at the 60th iteration without regularization (Thick pipe with three internal cracks)

solution increments are amplified and non-convergence of the optimization iterations is caused. Meanwhile, SI with the GMS reduces the solution increments very effectively by balancing the a posteriori solution and the a priori estimates as in the previous example.

To consider measurement error as well as the modeling error, 30 different sets of random noise of 5% magnitude are added to the measured displacements, and Monte Carlo trials are carried out for the 30 sets of simulated measurements. Since the convergence criterion,  $10^{-3}$ , is too tight for 30 trials with modeling errors as well as measurement errors, a new convergence criterion of  $10^{-2}$  is used for the Monte-Carlo simulation. The average number of iterations for the new criterion is 10 for the GMS and 26 for the LCM, respectively, when 10 Monte-Carlo trials are carried out. As the GMS and LCM yield almost identical results for 10 trials, and the LCM requires much more iterations than the

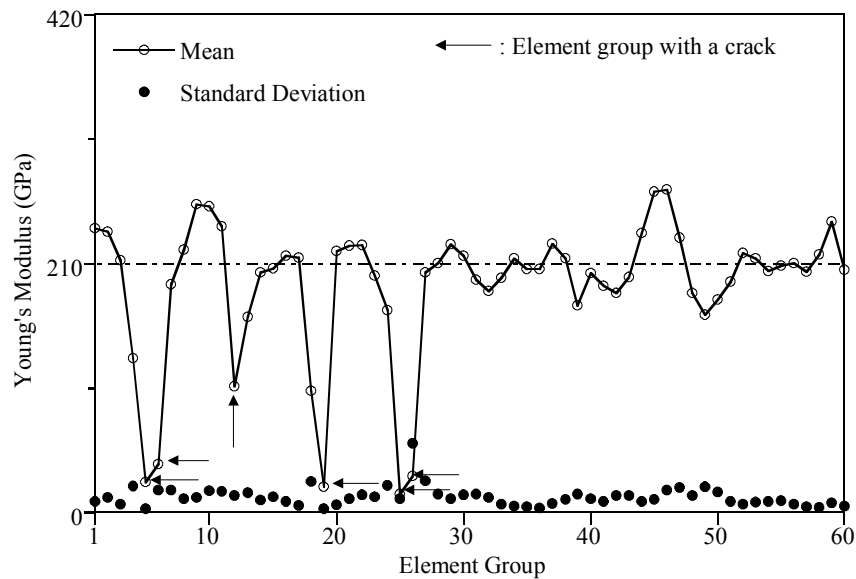


Fig. 2.28 Mean values and standard deviations of estimated Young's moduli by Monte-Carlo simulation for noise-polluted measurements using GMS. (Thick pipe with three internal cracks)

GMS, the Monte-Carlo simulation with 30 trials are performed only for the GMS.

The computed mean and standard deviation of the Young's modulus of each group by the GMS from 30 Monte Carlo trials are drawn in Fig. 2.28. In the Monte Carlo trials, the GMS successfully converges 29 out of 30 trials. The mean values are almost identical with the estimated Young's moduli from measurement data without measurement errors. Since the standard deviations are negligibly small, it can be concluded that the GMS is insensitive to different noise components in the measurements, and enhances the continuity of solution very effectively.

To investigate

The influence of sparseness of measured data on estimated results is also investigated. The sparseness of measured data is simulated by reducing the number of the observation



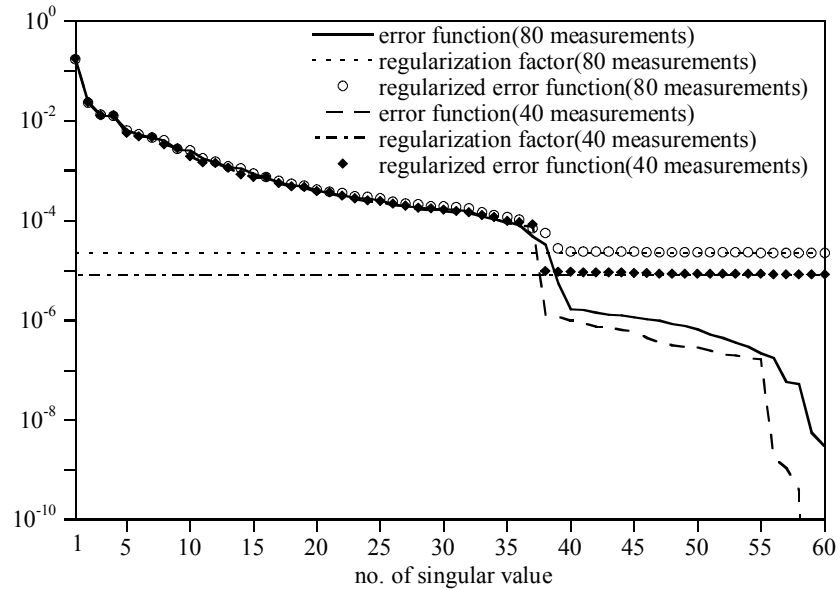


Fig. 2.29 Comparison of singular value distribution and regularization factor at the 1<sup>st</sup> iteration

points from 80 to 40 by eliminating the observations points one after the other. Singular value distributions of Hessian matrix and the regularization factor determined by the GMS at the 1<sup>st</sup> iteration are drawn in Fig. 2.29. Though the number of measurements is reduced in half, the singular value distribution of 40 measurements above the regularization factor is almost same as that of 80 measurements except the 38<sup>th</sup> singular value. Singular value distribution of 40 measurements below the regularization factor shows faster decreasing rate to zero than that of 80 measurements. Identified results of 40 measurements are compared with those of 80 measurements in Fig. 2.30. Though Young's modulus of element group 7 is identified lower than that of element group 6, the other identified Young's moduli of 40 measurements are almost same as those of 80 measurements. The GMS successfully identifies the location of the internal cracks by reducing the Young's

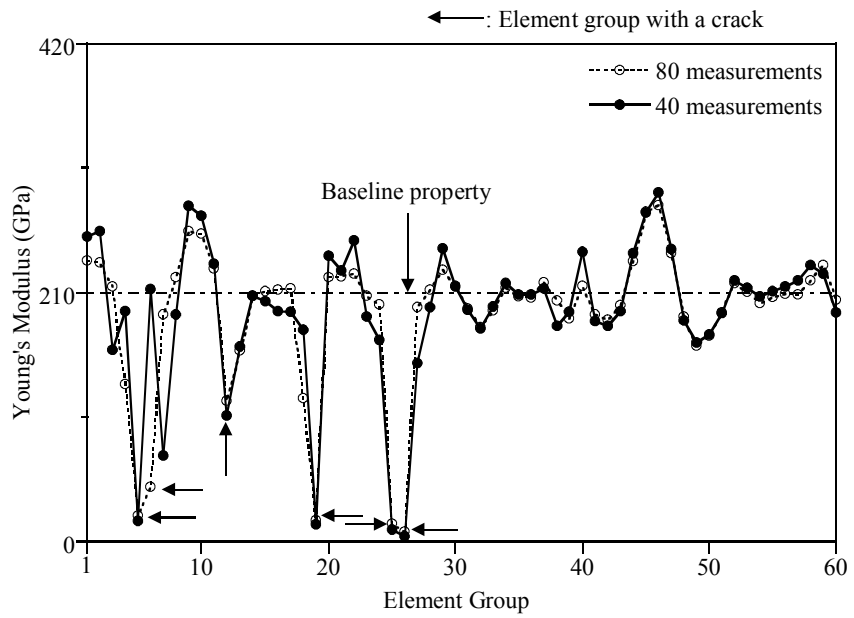


Fig. 2.30 Comparison of identified Young's moduli

moduli of the element groups associated with three cracks even though measurement data are severely sparse.

## Chapter 3

### System Identification for Damage Assessment of Framed Structures

Many SI-based damage assessment algorithms have been proposed to detect damages of structures in a global sense [San91, Doe96, Hje96, Yeo00]. Though each method has its own advantages over the others on a specific target problem, a clear discussion on the applicability to different problems and the limitations of the method are not always presented. To the author's opinion, the previous remedies are too problem-dependent since they are developed without full consideration of the proper regularity condition of the solution mentioned in chapter 2.

In this chapter a regularity condition of SI for framed structures is proposed. It is shown that the solution space of SI for a framed structure is properly defined by the  $L_1$ -norm of the system property, which is referred to as the  $L_1$ -regularization. Data perturbation and statistical approaches are incorporated with the  $L_1$ -TSVD to assess the damage status of a framed structure.

#### 3.1 Previous SI-Based Damage Assessment Algorithms

Previous studies to overcome difficulties caused by sparseness of measurements and measurement noise in SI-based damage assessment algorithms are presented. Though each method is different from the others, a basic concept to treat the problem can be summarized as shown in the following subsections.

##### 3.1.1 Grouping technique – Resolving Sparseness of Measurement

An SI-based damage assessment algorithm ignoring the sparseness of measurements

yields unreliable results since SI results in an infinite number of solutions due to the rank-deficiency as mentioned in chapter 2. Two different types of techniques are proposed in the previous studies to overcome the difficulties caused by the sparseness of measurements; a measurement expansion technique and grouping technique.

The responses corresponding to unmeasured degrees of freedom are approximated by interpolating measured responses in the measurement expansion technique. An advantage of the measurement expansion algorithm is that the number of measurements can be increased to a certain degree. However, the approximated responses suffer from an inevitable error caused by both approximation error and measurement noise. An instability caused by the inevitable error may be more severe than that caused by the sparseness of measurements. The measurement expansion technique is useful when both an approximation method and measurements are very accurate.

The idea of grouping technique is to reduce the total number of unknown system parameters used in SI by grouping similar parameters together without modifying the finite element model. Grouping the system parameters corresponding to undamaged members together, the number of system parameters can be reduced considerably since the number of the system parameters associated with the damaged members is very small. Grouping technique is more promising than the measurement expansion technique since no modification is required in either the measured responses or the finite element model.

The parameter group updating scheme proposed by Shin [Shi94, Hje96] performs damage localization in a systematic manner. At the first stage, predefined system parameter groups with the baseline values are determined, which is referred as a baseline grouping. If a certain system parameter group contains damage, it is subdivided to separate damaged

members from undamaged ones by consecutive updates of the parameter groups. At the last stage of the parameter group updating, a parameter group case is reached by clearly identifying all the damaged members.

The most important issue in the parameter group updating scheme to determine is the most appropriate measure for subdivision of the system parameter groups to isolate all the damaged members. The squared model error (SME) was proposed as the measure for subdivision of system parameter groups [Shi94].

$$\underset{\xi_G}{\text{Minimize}} \pi_{SME} = 2\pi_E(\xi_G) + \pi_P(n_G, \bar{\sigma}^2) \text{ subject to } \mathbf{R}(\xi_G) \leq 0 \quad (3.1)$$

where,  $\pi_E$ ,  $\xi_G$ ,  $\pi_P$ ,  $n_G$ , and  $\bar{\sigma}^2$  are error function, the system parameter group vector, a penalty function, size of system parameter group vector, and the prior estimate of the averaged random noise variance.

From the viewpoints of optimization, the ultimate purpose of the parameter group updating scheme is to find the global minimum of the SME with respect to the system parameter groups and the number of system parameter groups. The configuration of system parameter groups associated with the global minimum of SME is an optimal one for damage separation. Parameter group updating scheme solves this optimization problem by consecutive subdivision of system parameter groups. The final group configuration is not unique unless the subdivision process used in the parameter group updating scheme is unique. For example, same system parameter group may be subdivided into either halves or quarters. As the number of individual system parameters consisting of a specific system parameter group increases, the combinations of subdivision also increase. Whether

all the damaged members can be separated or not highly depends on which path the consecutive subdivisions follow. This is referred as the path-dependency of the subdivision process in this study. To avoid the path-dependency of subdivision, a specific system parameter group should be subdivided into individual system parameters, which conflicts with the original concept of the damage localization. Therefore, the path-dependency of the parameter group updating scheme is inevitable as the number of system parameters increases.

### **3.1.2 Data perturbation – Considering Measurement Noise**

If a lot of measurement sets are available, it is possible to obtain meaningful statistical properties with respect to estimated system parameters from these measurement sets. However, if a few measurement sets are available in practice, it is almost impossible to obtain satisfactory statistical properties. In this case, data perturbation proposed by Shin [Shi94, Hje96] can be used to obtain a statistical distribution in the vicinity of a specific measurement set. If the noise magnitude of a specific measurement set is estimated, data perturbation generates artificial sets of measurements around the specific measurement [Shi94, Hje96].

The representative statistical properties of estimated system parameters obtained from the perturbed measurements are the mean and the standard deviation of the estimated system parameters. Using these properties, the damage indices that classify damaged members from undamaged ones are determined. Shin proposed two damage indices that consist of the bias of the mean with respect to the baseline value (*bias\_cx*) and the bias of the mean from the baseline property with respect to the standard deviation (*bias\_sd*) [Shi94].

The  $bias_{cx}$  indicates the damage severity of the corresponding member while the  $bias_{sd}$  represents variation of the estimated results. Whether a member is actually damaged highly depends on the  $bias_{sd}$  rather than  $bias_{cx}$ .

Yeo proposed damage indices based on the hypothesis test [Yeo99, Yeo00]. In his study, estimated system parameters follows normal distribution by virtue of the regularization scheme. Damaged members are identified by a hypothesis test of the interval estimation of a mean value. Damage index is determined based on the results of the hypothesis test. If the null hypothesis that a member is undamaged is rejected in the hypothesis test, the damage index of the member is 1. If the null hypothesis is accepted, the damage index of the member is 0. The damage severity of a member is 0 if the damage index is 0 while it is the bias of the mean with respect to the baseline value if the damage index is 1.

## 3.2. SI with $L_1$ -Regularization for Framed Structures

### 3.2.1 A Regularity Condition of the System Property in SI for a Framed Structure

In modeling a framed structure such as a truss or a frame, each member is idealized by a line representing the centroid of the member [McC96]. As a result of this idealization, the mechanical properties of a member are considered to be concentrated at the centroid of the member as shown in Fig. 3.1, in which  $\eta_x^i, \eta_y^i, \eta_z^i$  represent a local coordinate system for member  $i$ , and  $V_i^e$  denotes the volume of member  $i$ . The centroid of the cross section at one end of a member is taken as the origin of the local coordinate system, and the trajectory of the centroid of each member is taken as the  $\eta_x^i$ -axis. The mechanical properties include material properties and cross-sectional properties of a member. The

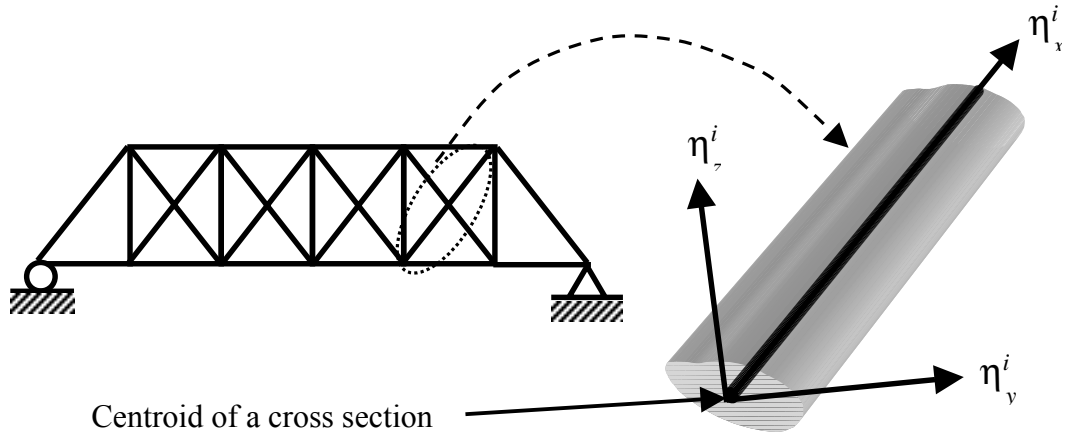


Fig.3.1 Idealization of a framed structure

structural volume  $V$  is the union of the member volumes, i.e.,  $V = \bigcup_i V_i^e$ .

The system property of a framed structure is defined in the structural volume as the collection of the mechanical properties of all members that are expressed in terms of the two-dimensional Dirac delta functions.

$$x = \sum_{i=1}^n X_i \delta(\eta_y^i) \delta(\eta_z^i) \quad \text{in } V \quad (3.2)$$

where  $x$ ,  $n$ ,  $X_i$ ,  $l_i$ , and  $\delta$  are the system property, the number of members in a structure, the system parameter, the length of member  $i$ , and the Dirac delta function, respectively. The system parameters represent the stiffness characteristics of members such as the axial rigidities and/or the flexural rigidities. The assumption on the system property given in (3.2) leads to one dimensional integration expression along the  $\eta_x^i$ -axis for a member stiffness equation, in which the mechanical behaviors at the centroid represent those of a whole cross section.



The baseline value of system parameters of each member represents the original, undamaged system parameter of the member. The baseline system property is obtained by replacing  $X_i$  with  $(X_i)_0$  in (3.2). Here,  $(X_i)_0$  represents the baseline value of system parameter of member  $i$ .

To avoid the instabilities of SI caused by the aforementioned fact, a proper function space for the system property of the SI problems should be supplied along with the minimization problem (2.10). The solution space of the SI problems can be defined by the regularity condition that represents the integrability condition of the system property. In case the solution of Eq. (2.10) is a square integrable function, the following regularity condition defined by the  $L_2$ -norm around the baseline value is appropriate.

$$\Pi_R = \|x - x_0\|_{L_2(V)}^2 = \int_V (x - x_0)^2 dV < \infty \quad (3.3)$$

Here,  $V$  denotes the structural volume. The regularity condition (3.3) are widely used for the identification of piecewise continuous functions in conjunction with various regularization schemes. The TSVD and the Tikhonov regularization presented in chapter 2 are weak statements of Eq.(3.3).

The function space defined by Eq.(3.3) is too stringent for SI of the system property of a framed structure since the Dirac delta functions in Eq.(3.2) are not square-integrable.

$$\begin{aligned}
\Pi_R = \|x - x_0\|_{L_2(V)}^2 &= \sum_e \int_{V^e} (x - x_0)^2 dV \\
&= \sum_e \int_{V^e} (X_i - (X_i)_0)^2 \delta(\eta_x - \chi_x)^2 \delta(\eta_y - \chi_y)^2 dV \\
&= \sum_e \int_{V^e} (X_i - (X_i)_0)^2 \delta(\eta_x - \chi_x)^2 \delta(\eta_y - \chi_y)^2 d\eta_x d\eta_y d\eta_z \\
&= \sum_{i=1}^{nm} (X_i - (X_i)_0)^2 l_i \times \delta(0) \times \delta(0) \rightarrow \infty
\end{aligned} \tag{3.4}$$

Therefore, the TSVD and Tikhonov regularization may be inadequate to define the proper solution space of SI used in the damage assessment. Either false warning events (FWE) or missing damage events (MDE) are frequently observed in the numerical studies of an SI-based damage assessment with Tikhonov regularization. Undamaged structural members in the vicinity of the severely damaged ones are classified as damaged ones in the FWE while structural members with mild damages are regarded as undamaged ones in the MDE. The FEW and MDE of the SI-based damage assessment may be caused by the smearing effect of the Tikhonov regularization.

When the regularization is used in the SI-based damage assessment, the regularization function should be defined so that the associated solution space can include the exact solution. A proper regularity condition for the function in Eq.(3.2) is defined by the  $L_1$ -norm as follows.

$$\Pi_R = \|x - x_0\|_{L_1(V)} = \int_V |x - x_0| dV < \infty \tag{3.5}$$

The discretized form of Eq.(3.5) is obtained by performing the integral in Eq.(3.5) memberwise.

$$\begin{aligned}
\Pi_R = \|\mathbf{X} - \mathbf{X}_0\|_{L_1(V)} &= \sum_e \int_{V^e} |x - x_0| dV \\
&= \sum_e \int_{V^e} |X_i - (X_i)_0| \delta(\eta_x - \chi_x) \delta(\eta_y - \chi_y) dV \\
&= \sum_e \int_{V^e} |X_i - (X_i)_0| \delta(\eta_x - \chi_x) \delta(\eta_y - \chi_y) d\eta_x d\eta_y d\eta_z \\
&= \sum_{i=1}^{nm} |X_i - (X_i)_0| l_i < \infty
\end{aligned} \tag{3.6}$$

Since the length of each member and the system parameters of a framed structure are finite, the regularity condition (3.6) is defined by the  $L_1$ -norm of the normalized system parameter vector without loss of generality.

$$\Pi_R = \sum_{i=1}^n \left| \frac{X_i - (X_i)_0}{(X_i)_0} \right| = \|\boldsymbol{\xi} - \mathbf{1}\|_1 < \infty \tag{3.7}$$

where  $\|\cdot\|_1$  denotes the  $L_1$ -norm of a vector, respectively. The regularity condition given in (3.7) should be imposed to the minimization problem (2.10) to obtain numerically stable and physically meaningful solutions of the SI problems for framed structures.

It should be noted that even though the  $L_2$ -norm of the system parameter vector itself is definable, it could not represent the actual regularity condition of the system property space of framed structures. In case the  $L_2$ -norm of the system parameter vector is used as a discrete regularization function, it restores piecewise continuous solutions, which are not actual solutions expressed by the Dirac delta functions. In other words, the discrete regularization function based on the  $L_2$ -norm of system parameter vector merely filters out noise-polluted solution components without imposing the actual regularity condition.

Nevertheless, an SI scheme regularized by the  $L_2$  norm of the system parameter vector is referred to as the  $L_2$ -regularization scheme for comparative purpose in this study.

### 3.2.2 TSVD solution for $L_1$ -regularity condition

The regularity condition of a solution space given in Eq.(3.6) is imposed to the original minimization problem (2.10) by the regularization techniques, among which the Tikhonov regularization technique and the TSVD are widely used. In the Tikhonov regularization technique, the regularity condition is added to the original error function defined in Eq.(2.10), and the optimization is performed for the error function with  $L_1$ -regularization as follows.

$$\text{Minimize } \pi = \frac{1}{2} \|\tilde{\mathbf{U}}(\boldsymbol{\xi}) - \bar{\mathbf{U}}\|_2^2 + \lambda \|\boldsymbol{\xi} - \mathbf{1}\|_1 \text{ subject to } \mathbf{R}(\boldsymbol{\xi}) \leq 0 \quad (3.8)$$

where  $\lambda$  is a regularization factor, which adjust the degree of regularization. Eq.(3.8) is a nonlinear optimization problem with respect to the normalized system parameters. However, a Newton type algorithm, which requires the gradient information of  $\Pi$ , cannot be applied to solve Eq.(3.8) since the  $L_1$ -norm is not differentiable with respect to the normalized system parameters.

This study presents a new algorithm, which is referred to as the  $L_1$ -TSVD, to impose the  $L_1$ -regularity condition iteratively in the optimization of the error function using the TSVD. In the proposed method, the incremental solution of the error function is obtained by solving the quadratic sub-problems without the constraints. The noise-polluted solution components are truncated from the incremental solution. Finally, the regularity con-

dition is imposed to restore the truncated solution components and the constraints. The above procedure is defined as follows.

$$\text{Minimize}_{\xi} \|\xi - \mathbf{1}\|_1 \text{ subject to } \text{Minimize}_{\xi} \|\tilde{\mathbf{U}}(\xi) - \bar{\mathbf{U}}\|_2^2 \text{ and } \mathbf{R}(\xi) \leq 0 \quad (3.9)$$

The incremental solution for the minimization of the error function is obtained by solving the following quadratic sub-problem.

$$\text{Minimize}_{\Delta\xi} \|\mathbf{S}\Delta\xi - \mathbf{U}_{k-1}^r\|_2^2 \quad (3.10)$$

where,  $\Delta\xi$  and  $\mathbf{S}$  are the solution increment, the sensitivity matrix of the displacement fields with respect to the normalized system parameters at the observation points, respectively, and the subscript  $k$  denotes the iteration count. The displacement residual  $\mathbf{U}_{k-1}^r$  is defined as  $\mathbf{U}_{k-1}^r = \bar{\mathbf{U}} - \tilde{\mathbf{U}}_{k-1}$ , where  $\tilde{\mathbf{U}}_{k-1}$  is the displacement field calculated by the converged system parameters at the previous iteration.

The first-order necessary optimality condition for Eq.(3.10) is given by the following linear equation.

$$\mathbf{S}^T \mathbf{S} \Delta\xi - \mathbf{S}^T \mathbf{U}_{k-1}^r = 0 \quad (3.11)$$

By the singular value decomposition, the  $m \times n$  sensitivity matrix  $\mathbf{S}$  can be written as a product of an  $m \times n$  matrix  $\mathbf{Z}$ , an  $n \times n$  diagonal matrix  $\mathbf{\Omega}$ , and the transpose of an  $n \times n$  matrix  $\mathbf{V}$  as Eq.(2.14). Here,  $m$  is the total number of measured degrees of freedom for all the applied loads.

Using the orthogonal properties defined in Eq.(2.15), the solution of Eq.(3.11) is

given as shown in Eq.(2.17).

$$\Delta \boldsymbol{\xi} = \sum_{j=1}^p \mathbf{v}_j \omega_j^{-1} \mathbf{z}_j^T \mathbf{U}^r + \sum_{j=p+1}^n \gamma_j \mathbf{v}_j \quad (3.12)$$

where  $p$  is a numerical rank defined in section 2.2.1.

The solution given in Eq.(3.12) satisfies Eq.(3.10) for all real  $\gamma_j$  in rank-deficient problems, which causes the non-uniqueness of solutions. The regularity condition provides additional information to define the undetermined constants  $\gamma_j$ . The solution components corresponding to the smaller singular values are responsible for the discontinuity of the solution because noise components amplified by the smaller singular values pollute a whole solution. To obtain stable solutions, the noise-polluted solution components should be removed from Eq.(3.12) by truncating the solution components associated with the singular values smaller than a critical singular value  $\omega_t$  ( $t \leq p$ ). Here,  $t$  is a truncation number, which plays the crucial role of filtering out noise-polluted components in the incremental solution, Eq.(3.12) [Vog86, Han98]. An algorithm to determine the optimal truncation number is presented in the next section.

The truncated components of the incremental solution in (3.12) are replaced with a linear combination of the truncated RSVs, which increases the number of the undetermined constants.

$$\Delta \boldsymbol{\xi} = \sum_{j=1}^t \frac{\mathbf{z}_j^T \mathbf{U}^r}{\omega_j} \mathbf{v}_j + \sum_{j=t+1}^n \gamma_j \mathbf{v}_j = \Delta \boldsymbol{\xi}_t^{TSVD} + \mathbf{q} \quad (3.13)$$

where

$$\Delta \xi_t^{TSVD} = \sum_{j=1}^t \frac{\mathbf{z}_j^T \mathbf{U}_{k-1}^r}{\omega_j} \mathbf{v}_j, \quad \mathbf{q} = \sum_{j=t+1}^n \gamma_j \mathbf{v}_j \quad (3.14)$$

The incremental form of Eq.(3.9) is expressed with respect to  $\mathbf{q}$  as follows.

$$\begin{aligned} & \text{Minimize}_{\mathbf{q}} \|\mathbf{q} - (\mathbf{1} - \xi_{k-1} - \Delta \xi_t)\|_1 \\ & \text{subject to } \mathbf{V}_t^T \mathbf{q} = 0 \text{ and } \xi_t - \xi_{k-1} - \Delta \xi_t \leq \mathbf{q} \leq \xi_u - \xi_{k-1} - \Delta \xi_t \end{aligned} \quad (3.15)$$

where  $\xi_u$  and  $\xi_t$  are an upper and a lower constraint vector for normalized system parameter, respectively, and  $\mathbf{V}_t = (\mathbf{v}_1, \mathbf{v}_2, \dots, \mathbf{v}_t)$ . The equality constraint of Eq.(3.15) represents that  $\mathbf{q}$  should be a linear combination of the truncated RSVs. Eq.(3.15) is a linear programming with respect to  $\mathbf{q}$  and is solved by the simplex method. In this study, the simplex algorithm developed by Barrondale is employed [Bar73]. Hansen and Mosegaard presented a similar algorithm to identify piecewise continuous functions in linear inverse problems [Han96]. They referred to the algorithm as the piecewise polynomial truncated singular value decomposition (PP-TSVD).

Once the optimal solution  $\mathbf{q}_{\text{opt}}$  is obtained from linear programming, the solution can be obtained by substituting  $\mathbf{q}_{\text{opt}}$  into Eq.(3.13) as the following equation.

$$\Delta \xi_t^{L_1-TSVD} = \Delta \xi_t^{TSVD} + \mathbf{q}_{\text{opt}} \quad (3.16)$$

To guarantee fast convergence, the error function is minimized by a line search method using the solution increment of Eq.(3.16).

$$\text{Minimize}_{\beta} \left\| \tilde{\mathbf{U}}(\xi_{k-1} + \beta \Delta \xi_t^{L_1-TSVD}) - \bar{\mathbf{U}} \right\|^2 \quad (3.17)$$

The solution at the  $k$ 'th iteration is obtained by solution of Eq.(3.17).

$$\xi_k = \xi_{k-1} + \beta_{\text{opt}} \Delta \xi_t^{L_1\text{-TSVD}} \quad (3.18)$$

where,  $\beta_{\text{opt}}$  is an optimal solution of Eq.(3.17).

### 3.2.3 Optimal Truncation Number by the Cross Validation

The determination of a proper truncation number is a keystone in the TSVD. The truncation number plays a similar role to the regularization factor in the Tikhonov regularization technique. In case a truncation number is too small, most of the useful information on a structure is lost while too large a truncation number yields noise-polluted, meaningless solutions [Vog86, Han98]. Therefore, the truncation number should be determined so that as much useful information of a structure can be retained while most of noise-polluted solution components are truncated. The optimal truncation number for each iteration is defined by the cross validation [Gol96].

In the cross validation, a reduced quadratic sub-problem is defined by omitting the  $i$ -th row of the original quadratic sub-problem Eq.(3.10).

$$\text{Minimize}_{\Delta \mathbf{X}^{-i}} \left\| \mathbf{S}^{-i} \Delta \xi^{-i} - (\mathbf{U}_{k-1}^r)^{-i} \right\|_2^2 \quad (3.19)$$

where  $\mathbf{S}^{-i}$  and  $(\mathbf{U}_{k-1}^r)^{-i}$  are the reduced sensitivity matrix and the displacement residual vector in which the  $i$ -th rows of both are omitted, respectively. The  $L_1$ -TSVD is performed for Eq.(3.19) with a truncation number  $t$ , and the following residual is defined.

$$\hat{r}_t^i = (\mathbf{s}_i \Delta \xi_{\text{opt}}^{-i} - (U_{k-1}^r)_i)^2 \quad (3.20)$$



where  $\mathbf{s}_i$  and  $(\mathbf{U}_{k-1}^r)_i$  are the  $i$ -th rows of the original sensitivity matrix and the displacement residual vector, respectively, and  $\Delta \xi_{\text{opt}}^{-i}$  is the  $L_1$ -TSVD solution of Eq.(3.19) for the truncation number  $t$ . The optimal truncation number is defined as the solution of the following minimization problem.

$$\text{Minimize}_t \sum_{i=1}^m \hat{r}_t^i \quad \text{for } 1 \leq t \leq p \quad (3.21)$$

Since it is difficult to solve Eq.(3.21) algorithmically, the objective function in Eq.(3.21) is evaluated for all truncation numbers, and the truncation number that yields the smallest value of the objective function in Eq.(3.21) is selected as the optimal truncation number. It should be noted that there sometimes exists no feasible solution to the  $L_1$ -TSVD for a large truncation number. This is because noise components severely amplified by small singular values are presented in the truncated solution of Eq.(3.19) for a large truncation number. In this case, the  $L_1$ -TSVD is performed up to the truncation number that yields a meaningful solution of Eq.(3.19).

From the statistical point of view, the  $L_2$ -norm of noise in a measurement can be estimated by the converged solution of SI using the optimal truncation number of each iteration defined in Eq.(3.21) as follows [Alt87, Hab00].

$$\|\mathbf{e}\|_2 \approx \|\mathbf{U}(\xi_{\text{opt}}^{L_1\text{-TSVD}}) - \bar{\mathbf{U}}\|_2 \quad (3.22)$$

where  $\mathbf{e}$  is the noise vector in  $\bar{\mathbf{U}}$ , and  $\xi_{\text{opt}}^{L_1\text{-TSVD}}$  is the converged solution by the  $L_1$ -TSVD.

The noise level  $\mathfrak{N}_e$  in the measurements is defined as follows.

$$\mathfrak{K}_e = \frac{\|\mathbf{e}\|_2}{\|\bar{\mathbf{U}}\|_2} \quad (3.23)$$

### 3.3. Damage Assessment

A damage assessment is a step to determine which members in a structure are actually damaged and how seriously they are damaged [Shi96, Yeo00]. Since not only the measurement noise is unavoidable but also the measurements are not provided sufficiently, the estimated results using SI with  $L_1$ -regularity condition is investigated in the statistical sense for a reliable damage assessment.

A hypothesis test is performed to classify the damaged members from undamaged ones using the statistical properties of system parameters obtained from perturbed measurements [Yeo99, Yeo00]. Hypothesis test is accompanied by the fitness test to confirm whether the statistical distribution of estimated system parameters from perturbed measurements actually follows a normal distribution [Yeo99, Yeo00]. The damage index classifying the damage members and undamaged ones is determined using the hypothesis test. After damage index is determined, the damage severity is obtained sequentially.

#### 3.3.1 Data Perturbation

Data perturbation proposed by Shin [Shi94, Shi96] is used to obtain a statistical distribution in the vicinity of a specific measurement set. SI with the  $L_1$ -regularization is adopted to estimate the system parameters for each perturbed measurement set generated by data perturbation. The perturbation bound is determined by the residual of error function at the converged stage using the unperturbed measurements.

The maximum perturbation amplitude,  $\mathfrak{S}_{\max}$ , is defined by the estimated noise level given

in Eq.(3.23).

$$\mathfrak{S}_{\max} = \mathfrak{K}_e = \frac{\|\mathbf{e}\|_2}{\|\bar{\mathbf{U}}\|_2} \quad (3.24)$$

It is very time consuming to determine an optimal truncation number in every iteration for each set of perturbed data by the proposed method in the previous section. It would be more convenient if a fixed optimal truncation number is used in every iteration for each set of perturbed data. For this purpose, the discrepancy principle, which is originally proposed for linear SI problems by Morozov [Mor93, Han98], is employed to choose a fixed truncation number as shown in Fig. 3.2. This principle states the optimal truncation number is the largest one that satisfies the following criterion.

$$\|\tilde{\mathbf{U}}(\xi_i^*) - \bar{\mathbf{U}}\|_2 \geq \|\mathbf{e}\|_2 \quad (3.25)$$

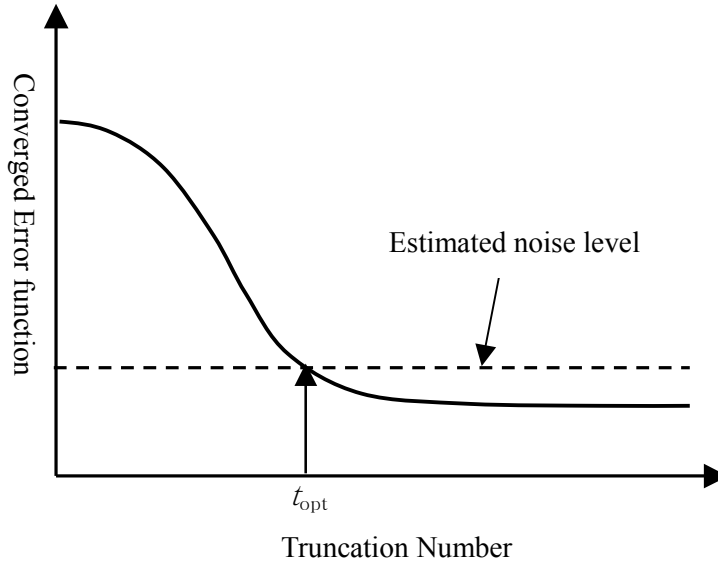


Figure 3.2 Optimal truncation number by the discrepancy principle

where  $\xi_t^*$  is the converged solution obtained by the  $L_1$ -TSVD for a fixed truncation number  $t$ . The TSVD optimization with a varying truncation number proposed in the previous section is performed only once for the original unperturbed data. Once the noise level in the data is estimated by Eq.(3.23), a series of the TSVD optimization with a fixed truncation number is performed by increasing truncation numbers from 1 until the largest truncation number that satisfy Eq.(3.25) is obtained.

### 3.3.2 Hypothesis Test, Damage Index, and Damage Severity

In case normally distributed system parameters are obtained from perturbed measurements, a hypothesis test can be applied to determine damaged members by statistical properties of system parameters. Yeo adopted Kolmogorov-Smirnov goodness-of-fit test to confirm that the error function with Tikhonov regularization usually yields normally distributed system parameters from perturbed measurements [Yeo99, Yeo00]. Since all the system parameters estimated by output error estimator with Tikhonov regularization attain statistical properties sufficient for statistical evaluations using finite number of perturbed measurements, the goodness-of-fit test can be applied to each system parameter. However, all the system parameters estimated by the  $L_1$ -TSVD cannot attain sufficient statistical properties using finite number of perturbed measurements due to the solution characteristics of the  $L_1$ -TSVD. The solution characteristics of the  $L_1$ -TSVD in Eq.(3.15) can be explained by characterization of solution of generalized  $L_1$  approximation problem as the following equation.

$$\underset{\mathbf{a}}{\text{Minimize}} \|\mathbf{A}\mathbf{a} - \mathbf{b}\|_1 = \|\mathbf{r}(\mathbf{a})\|_1 \quad (3.26)$$

Here,  $\mathbf{A}$ ,  $\mathbf{a}$ ,  $\mathbf{b}$ , and  $\mathbf{r}$  are a given  $m$  by  $n$  matrix, an  $n$ -column vector to be sought for solution, a given  $n$ -column vector, a residual vector, respectively. If the matrix  $\mathbf{A}$  has rank  $t$ , there exists at least  $t$  zero's in the residual vector [Wat80]. If this theorem is applied to Eq.(3.15), the solution characteristics of the  $L_1$ -TSVD is revealed. For the simplicity of discussion the upper and lower constraints are not considered. Comparing Eq.(3.15) with Eq.(3.26), the following relationships can be established.

$$\mathbf{A} \equiv (\mathbf{v}_{t+1}, \mathbf{v}_{t+2}, \dots, \mathbf{v}_n) \quad (3.27a)$$

$$\mathbf{a} \equiv (\gamma_{t+1}, \gamma_{t+2}, \dots, \gamma_n)^T \quad (3.27b)$$

$$\mathbf{b} \equiv - \left( \hat{\boldsymbol{\xi}}_{k-1} - \mathbf{1} + \sum_{j=1}^t \mathbf{v}_j \omega_j^{-1} \mathbf{z}_j^T \mathbf{U}_{k-1}^r \right) \quad (3.27c)$$

The rank of in Eq.(3.27) is directly connected with the truncation number  $t$  of Eq.(3.15) and is  $n-t$ . Substituting Eq.(3.27) into Eq.(3.26), the residual vector of Eq.(3.26) has at least  $n-t$  zero components. In other words, the residual vector of Eq.(3.26) has at most  $t$  non-zero components. Combining these results with Eq.(3.14), solution components corresponding to the zero residuals of Eq.(3.26) are determined by only the a priori estimates, not by the a posteriori solutions.

$$\Delta \hat{\boldsymbol{\xi}} = \mathbf{1} - \hat{\boldsymbol{\xi}}_{k-1} \quad (3.28)$$

where,  $\Delta \hat{\boldsymbol{\xi}}$  and  $\hat{\boldsymbol{\xi}}_{k-1}$  are a component of solution increment and a solution at  $k-1$ 'th optimization iteration corresponding to the zero residuals of Eq.(3.26).

It is empirically observed that solution increments associated with undamaged members are determined by the a priori estimates as shown in Eq.(3.28) from the 1'st optimization itera-

tion to the converged stage. Only the solution increments associated with actually damaged members and some members in the vicinity of actually damaged ones are determined by the a priori estimates and the a posteriori information simultaneously. Therefore, the solution increments associated with undamaged members are always zeroes during the optimization iterations if the initial value of each system parameter is assumed as the baseline value. Only the solution increments associated with actually damaged ones and some members in the vicinity of actually damaged ones are non-zeroes throughout the optimization iterations.

Due to these solution characteristics of the  $L_1$ -TSVD, not all system parameters are statistically distributed, but only a few system parameters associated with damaged members and their neighboring members have statistical distributions. Three different classes of distributions of the system parameters are defined in this study for statistical evaluation for damage assessment: a deterministic class, a probabilistic class, and an intermediate class.

The deterministic class consists of only the deterministic samples of system parameters that do not respond to random variations of measurements at all, and stay at the baseline values for a specified number of perturbed data sets. Therefore, the means and standard deviations of system parameters in this class are the baseline values and zero, respectively. A member in the deterministic class is considered to be an undamaged one without any statistical evaluations, and the corresponding damage index  $I_D$  (Yeo et al. 2000) is set to zero for the member.

The probabilistic class consists of only the probabilistic samples of the system parameters that respond to random variations of measurements. A goodness-of-fit test for the

normal distribution and hypothesis test are applied to assess the damage status of the members in this class.

The intermediate class consists of deterministic samples and probabilistic samples simultaneously for a specified number of perturbed data sets. Since it is difficult to treat the intermediate class directly, this class is converted into either a deterministic class or a probabilistic class according to the ratio of deterministic samples to probabilistic ones. It is observed through our numerical experiences that most distributions of system parameters corresponding to the intermediate class consist of very limited probabilistic samples as shown in Fig. 3.3. It is unreasonable to draw statistical meanings for this distribution because most of the samples are deterministic ones. In this study, when more than 90% of the samples of a system parameter are deterministic ones, the intermediate class is consid-

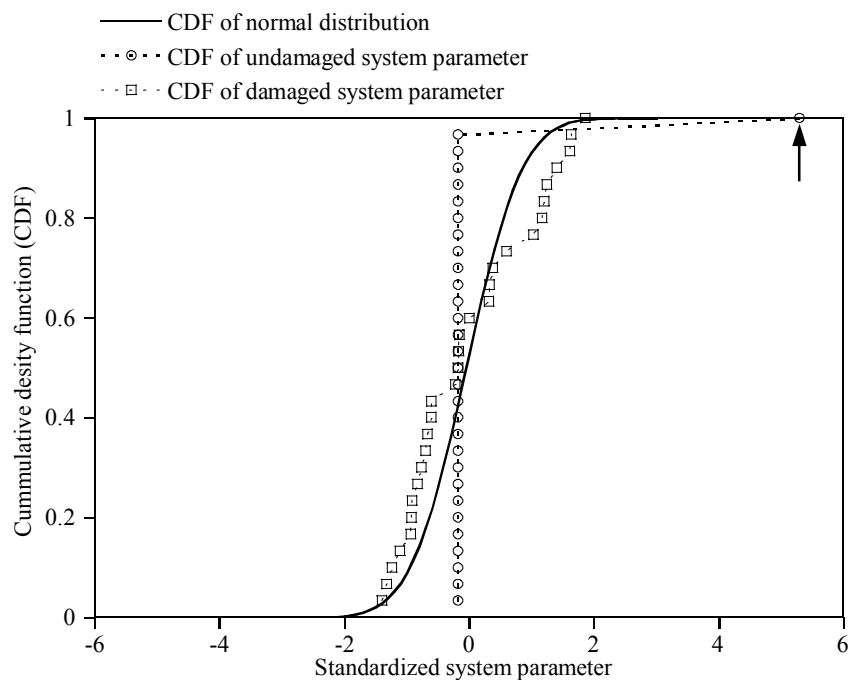


Fig.3.3 Two typical types of statistical distribution of system parameters using  $L_1$ -TSVD

ered as a deterministic one. If less than 90% of the samples of a system parameter are deterministic ones, additional perturbations should be performed to obtain probabilistic samples until the number of probabilistic samples reaches the specified sample size for the system parameter without deterministic samples.

Once system parameters belonging to a probabilistic class pass the fitness test, a hypothesis test is adopted to assess the damage of each member using the statistical properties of system parameters [Yeo99, Yeo00]. In the hypothesis test, a statistical distribution of the baseline structures is assumed to obey the following normal distributions [Yeo00].

$$N(x_0, \sigma^2) \quad (3.29)$$

where,  $x_0$  and  $\sigma$  is baseline value and standard deviation of each system parameter obtained from the perturbed measurements.

Eq.(3.29) is referred as baseline distribution for the system parameters. The damage status of a member in a target structure is determined by applying a hypothesis test for the interval estimation of the mean value on the baseline distribution with a significance level  $\alpha$ . The hypothesis test is defined as the following equation.

$$H_0 : \bar{\Xi} = x_0 \quad (3.30a)$$

$$H_1 : \bar{\Xi} < x_0 \quad (3.30b)$$

where,  $\bar{\Xi}$  is an unknown actual value of the system parameter. The operating rule for the hypothesis test is to accept  $H_0$  if  $\bar{x} \geq c$  with a significance level  $\mu$ . Here,  $\bar{x}$  is the estimated average of the system parameter for the current structure from the perturbed measurements. The critical value  $c$ , used to determine the acceptance region of  $H_0$  in the base-



line distribution, can be obtained by solving the following equation for  $c$ .

$$P[\bar{x} \geq c | H_0] = 1 - \mu \quad (3.31)$$

The one-sided probability statement of Eq.(3.31) can be modified into the standardized form.

$$P[z \geq z_\mu | H_0] = \Phi(-z_\mu) = 1 - \mu \quad (3.32)$$

where,  $z = (\bar{x} - x_0) / \sigma$ ,  $z_\mu = (c - x_0) / \sigma$  and  $\Phi$  is the CDF of the standardized normal distribution. The critical value  $c$  is obtained by inverting the CDF for  $z_\alpha$  in Eq.(3.32) and using the definition of  $z_\alpha$

$$c = x_0 + z_\mu \sigma \quad (3.33)$$

If the estimated mean value of a member is less than the critical value  $c$ , then the null hypothesis  $H_0$  is rejected. Subsequently, the member is regarded as a damaged member. A member that has passed the hypothesis test is defined as undamaged with  $100 \times (1 - \alpha)$  % confidence. The damage index  $I_D$ , which represents the damage status of a member with the significance level of  $\alpha$ , is defined as the following equation.

$$I_D = \begin{cases} 0 & \text{if } H_0 \text{ accepted : } (\bar{x} \geq c) \\ 1 & \text{if } H_0 \text{ rejected : } (\bar{x} < c) \end{cases} \quad (3.34)$$

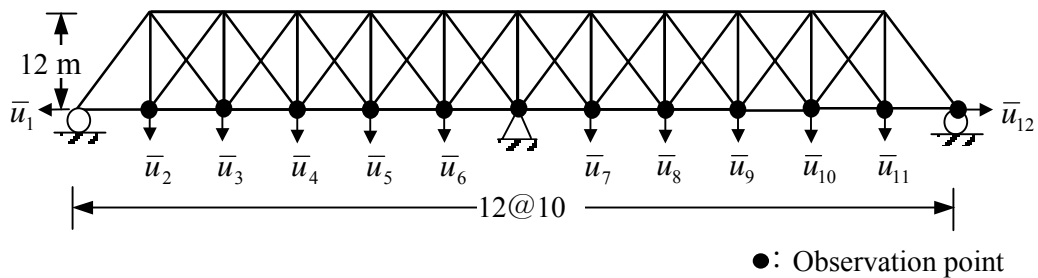
The severity of damage  $S_D$ , which indicates how seriously a member is damaged with the significance level of  $\mu$ , is defined as a relative distance of the computed mean from the baseline value.

$$S_D = \frac{x_0 - \bar{x}}{x_0} \times I_D \times 100(\%) \quad (3.35)$$

### 3.4. Numerical Examples – Damage Assessment of a two-Span Continuous Truss

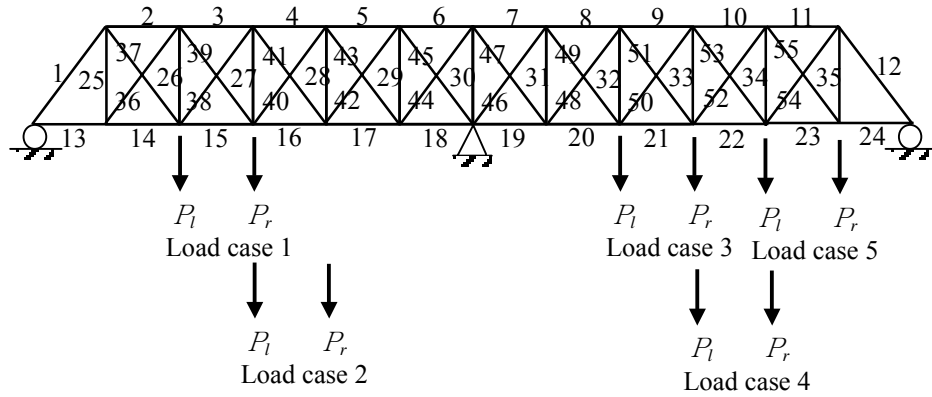
Numerical simulation studies are performed for three damage cases with the proposed method to determine the damage status of the two-span continuous truss presented by Yeo et. al. [Yeo00]. Damage cases I and II contain rather easy damage patterns to be identified, while the damage in case III is relatively difficult to identify for a large noise level. Detailed discussions are presented for damage case III. Fig. 3.4 shows the geometry, support conditions and the locations of 12 observation points, which are depicted as solid circles in the figure. Horizontal displacements are measured at the roller supports and vertical displacements are measured at the other observation points independently for each load case shown in Fig. 3.5.

Proportional random noise generated by a uniform probability function between  $\pm$  noise amplitude ( $A_N$ ) is added to the displacement obtained by a mathematical model to simulate real measurements. Unless otherwise stated, the noise amplitude of 5% is used



Member	Area (cm <sup>2</sup> )	Member	Area (cm <sup>2</sup> )
Top	250	Vertical	200
Bottom	300	Diagonal	220

Figure 3.4 Geometry, cross sectional areas and measured dofs of the two-span continuous truss



$$P_l : 80\text{KN} , \quad P_r = 136 \text{ KN}$$

Figure 3.5 Member ID numbers and load cases of a two-span continuous truss

in all examples. The significance level  $\mu$  is selected as 0.1 for the statistical damage assessment (Yeo et al. 2000). For the data perturbation, 30 Monte-Carlo trials are performed. Since more than 90% of the samples for system parameters in the intermediate class are deterministic for all examples, no additional perturbation is needed. The truncation number is determined by the discrepancy principle for the original, unperturbed data, and is fixed throughout all Monte-Carlo trials. The identification results by the proposed method are compared with those by the  $L_2$ -regularization scheme, in which all the algorithms are exactly the same as the proposed method except that the  $L_2$ -norm is used as the discrete regularization function.

The rank-deficiency and ill-posedness of SI of the truss are demonstrated by investigating the distribution of singular values of the sensitivity matrix. Since the system characteristics at the first iteration are solely determined by the baseline values of the system parameters and the locations of measurements, the distribution of the singular values at the

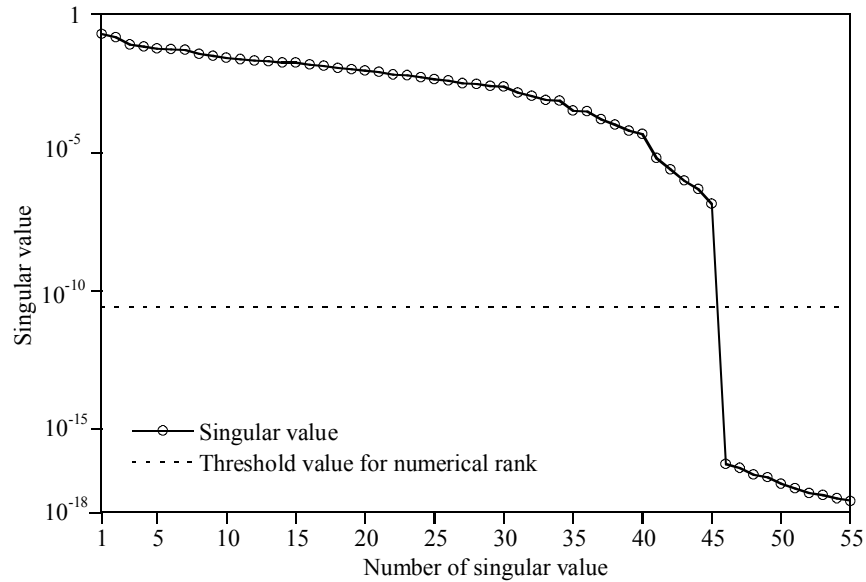


Fig. 3.6. Distribution of singular values for the two-span continuous truss

first iteration is a good indicator of the rank-deficiency and ill-posedness of all damage cases. As shown in Fig. 3.6, 10 singular values are smaller than the threshold value  $\epsilon$  for the numerical rank of the sensitivity matrix. Therefore, the sensitivity matrix of the truss for the given measurements is rank-deficient by 10 even though the number of independently measured data (60) is larger than those of the members (55). Moreover, the sensitivity matrix is severely ill-posed after truncating those 10 small singular values because the ratio of the largest singular value to the smallest retained singular value is  $1.33 \times 10^6$ . This fact implies that noise components in measurements may be amplified by a million times in the solution space, which results in a meaningless solution of SI even for very small noise levels.

### 3.4.1 Damage Case I

Damage is simulated with 70% and 30% reduction in the sectional areas of two bottom members (member 16 and member 21) as shown in Fig. 3.7. The error function evaluated by the converged solutions for each truncation number is presented in Fig. 3.8 together with estimated noise levels. The noise levels for the  $L_1$ - and the  $L_2$ -regularization scheme are estimated as 2.6 % by the cross validation, and the truncation numbers are selected as 4 and 7, respectively.

Fig. 3.9 shows the averages and the standard deviations of the system parameters normalized by the baseline values for 30 Monte-Carlo trials. The  $L_1$ -regularization scheme yields sharp drops of the system parameters only at the damaged members, while the system parameters of undamaged members in the vicinity of the damaged members are reduced in the  $L_2$ -regularization scheme. In particular, most of the damage information of member 21 is smeared out to members 20 and 22 in the  $L_2$ -regularization scheme. Since the standard deviations of the system parameters are very small, it seems that both  $L_2$ - and  $L_1$ -regularization scheme effectively control the ill-posedness of SI. The damage severity of each member assessed by the statistical approach is given in Fig. 3.10. The damaged members are identified exactly, and the damage severity is accurately estimated by the  $L_1$ -regularization scheme. Some of the undamaged members are identified as damaged me-

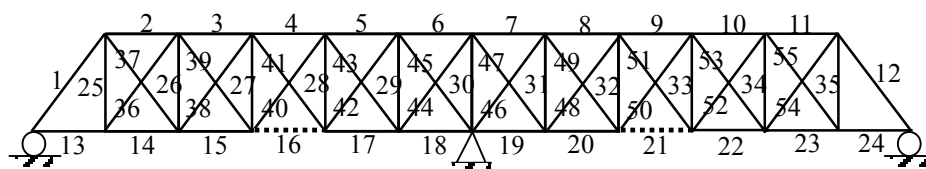


Fig. 3.7 Case I – the 16<sup>th</sup> bottom member and the 21<sup>st</sup> bottom member are damaged

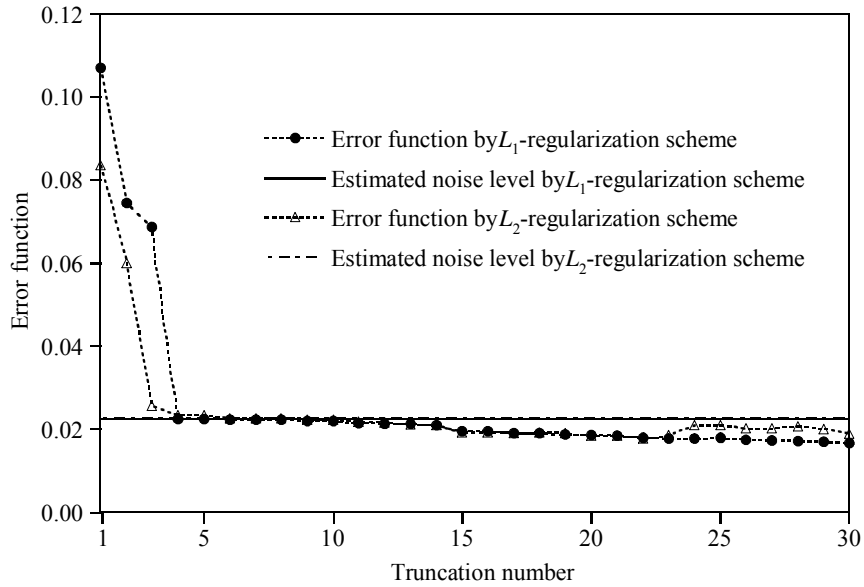


Fig. 3.8 Variation of the error function with truncation numbers and estimated noise level for damage case I

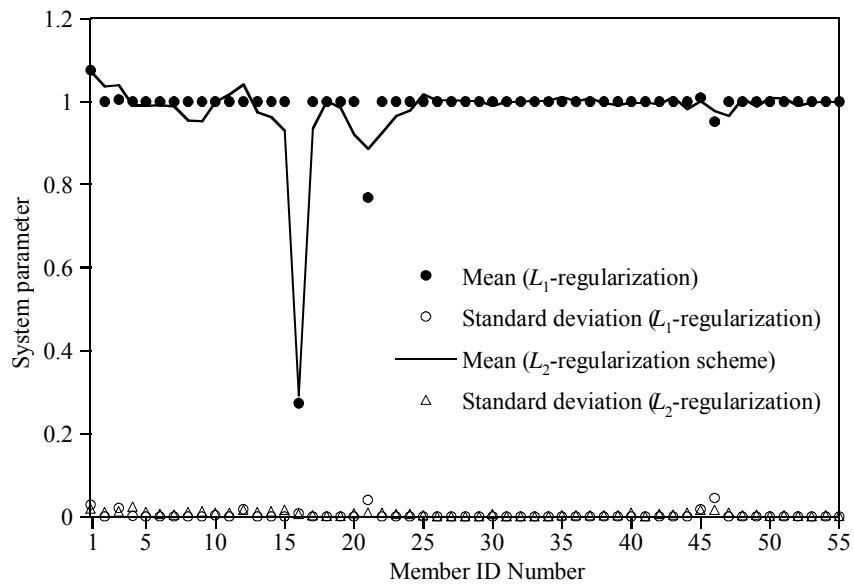


Fig. 3.9 Mean values and standard deviations of estimated system parameters for damage case I

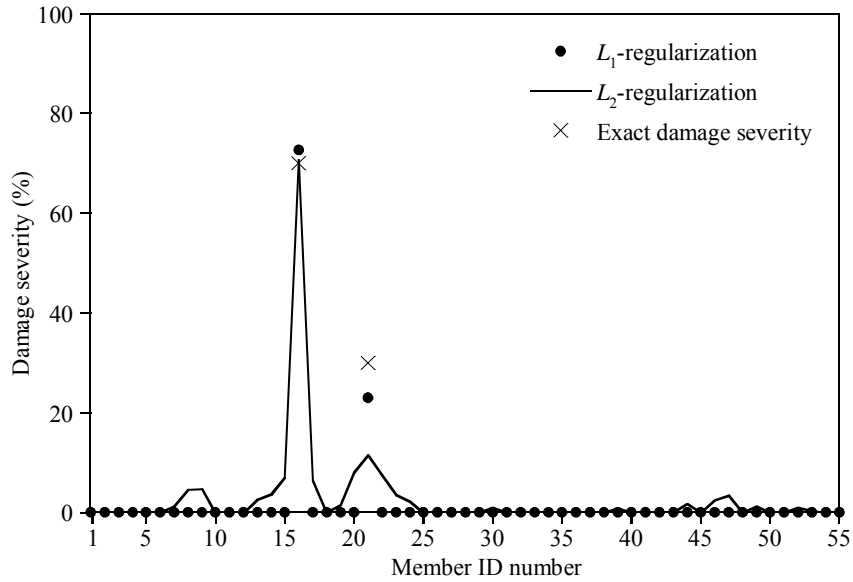


Fig. 3.10. Identified damage severity for damage case I

members, and the damage severity of member 21 is rather underestimated by the  $L_2$ -regularization scheme.

### 3.4.2 Damage Case II

It is assumed that diagonal member 48 and bottom member 22 are damaged by 30% in this damage case as shown in Fig. 3.11. The error function evaluated by the converged solutions for each truncation number is presented in Fig. 3.12 together with estimated noise

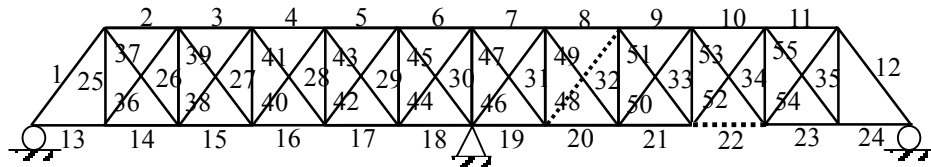


Fig. 3.11 Case II – the 22<sup>nd</sup> bottom member and the 48<sup>th</sup> diagonal member are damaged

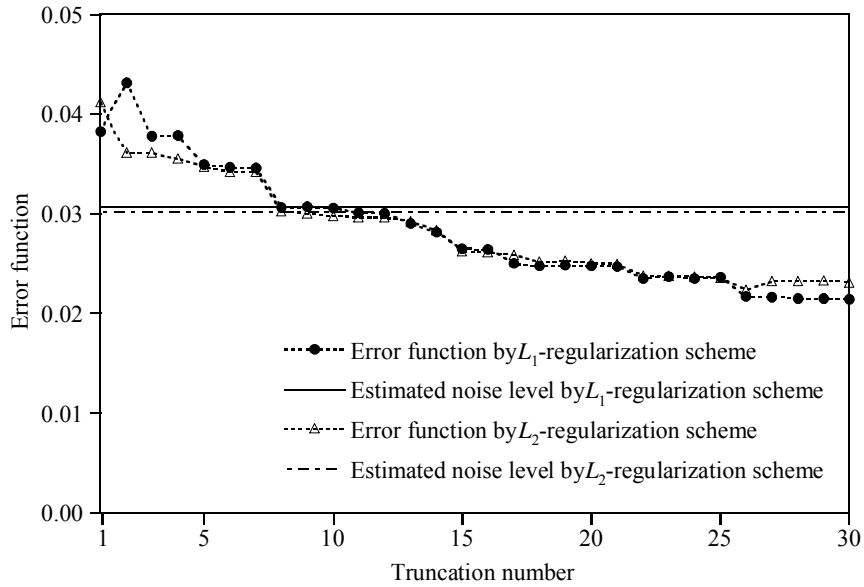


Fig. 3.12 Variation of the error function with truncation numbers and estimated noise level for damage case II

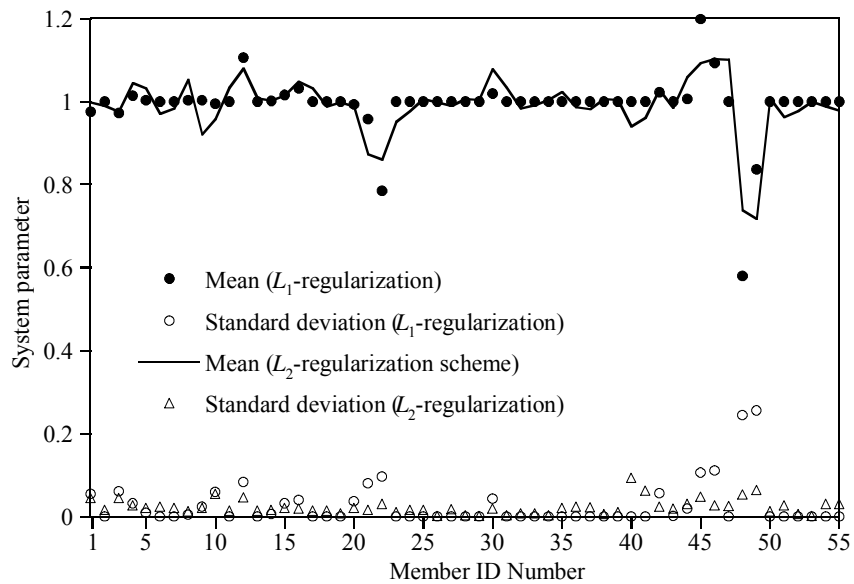


Fig. 3.13 Mean values and standard deviations of estimated system parameter for damage case II



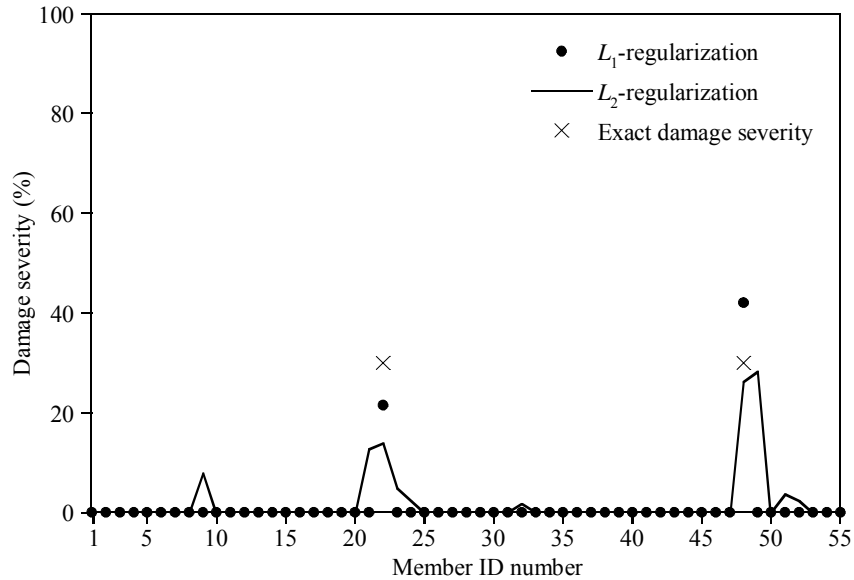


Fig. 3.14 Identified damage severity for damage case II

levels. The estimated noise levels for the  $L_1$ - and  $L_2$ -regularization schemes are 3.1% and 3.0%, respectively, while the actual noise level is 3.3%. The truncation number is selected as 8 for  $L_1$ -regularization scheme, and 9 for the  $L_2$ -regularization scheme. Fig. 3.13 shows the averages and the standard deviations of the system parameters normalized by the baseline values for 30 Monte-Carlo trials. Fig. 3.14 shows the identified damage severity of this damage case. As in the previous damage case, the damaged members are identified exactly, and none of undamaged members are falsely identified as damaged by the  $L_1$  regularization scheme. However, the damage severity of member 22 is a little bit underestimated, while that of member 48 is overestimated a little bit. It is believed that an underestimated noise level in this damage case causes inaccuracy in the damage severity. Meanwhile, the  $L_2$ -regularization scheme identifies several undamaged members as damaged ones, which represents the smearing characteristics of the  $L_2$ -norm of system param-

ters (Hansen and Mosegaard 1996).

### 3.4.3 Damage Case III

This damage case contains 60%, 70% and 30% damage in member 17, 33 and 38, respectively as shown in Fig. 3.15. The error function evaluated by the converged solutions for each truncation number is presented in Fig. 3.16 together with estimated noise levels. The truncation number is selected as 5 for  $L_1$ -regularization scheme, and 7 for the  $L_2$ -regularization scheme. Fig. 3.17 shows the averages and the standard deviations of the system parameters normalized by the baseline values for 30 Monte-Carlo trials. Fig. 3.18 shows the identified damage status of the truss. Both the  $L_1$ - and  $L_2$ -regularization scheme fail to identify the damage of the truss correctly. The  $L_1$ -regularization scheme identifies members 16 and 21, which are bottom members connected to the actually damaged members 17 and 33, as damaged members. The damage in member 38 is not detected at all. The  $L_2$ -regularization detects the damage in member 17, but member 16 is estimated as more severely damaged than member 17. Several undamaged members in the vicinity of members 33 and 38 are identified as damaged members, which is caused by the smearing characteristics of the  $L_2$ -regularity condition.

To investigate characteristics of this damage case systematically, several numerical

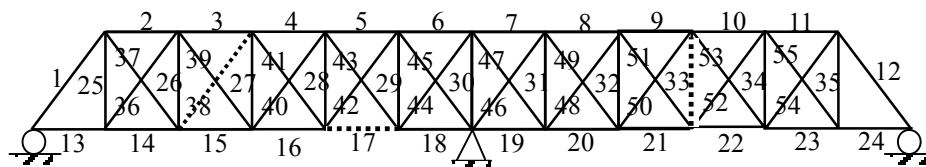


Fig. 3.15 Case III – the 17<sup>th</sup> bottom member, the 33<sup>rd</sup> vertical member, and the 39<sup>th</sup> diagonal member are damaged

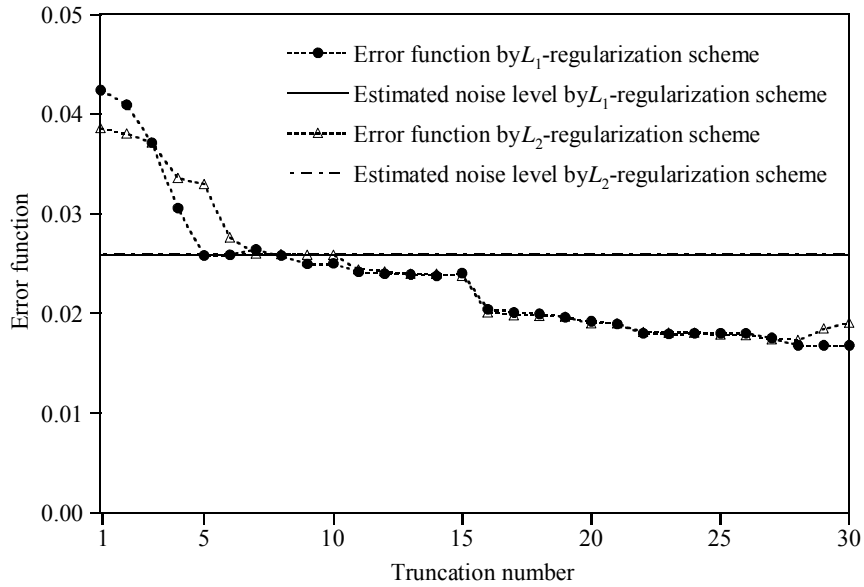


Fig. 3.16 Variation of the error function with truncation numbers and estimated noise level for damage case III

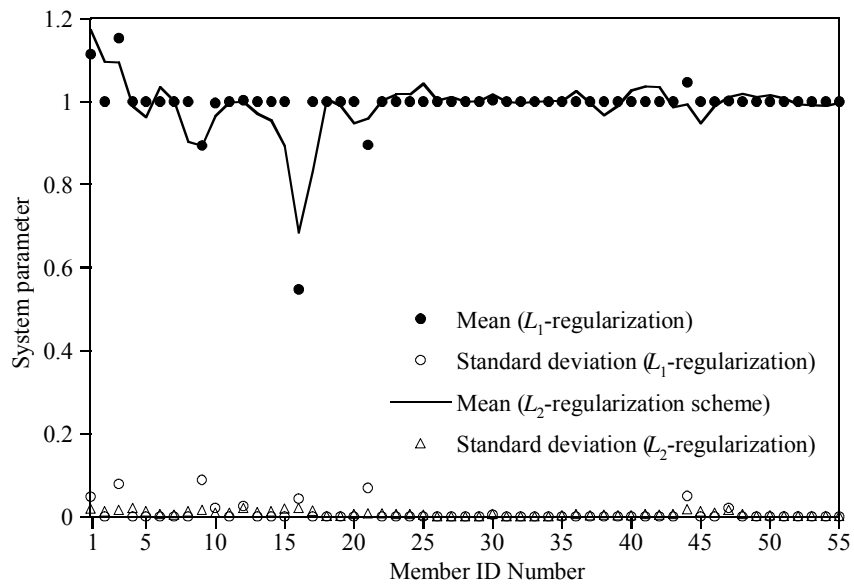


Fig. 3.17 Mean values and standard deviations of estimated system parameter for damage case III

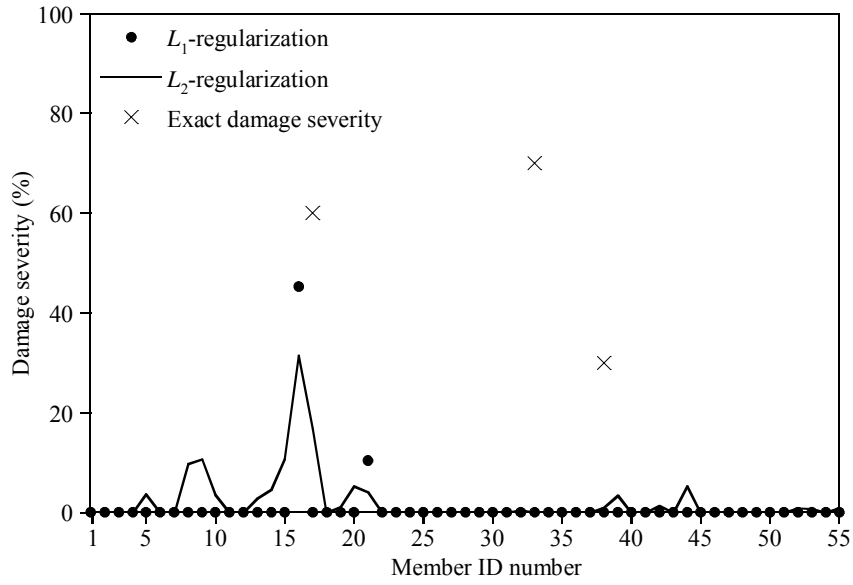


Fig. 3.18 Identified damage severity for damage case III

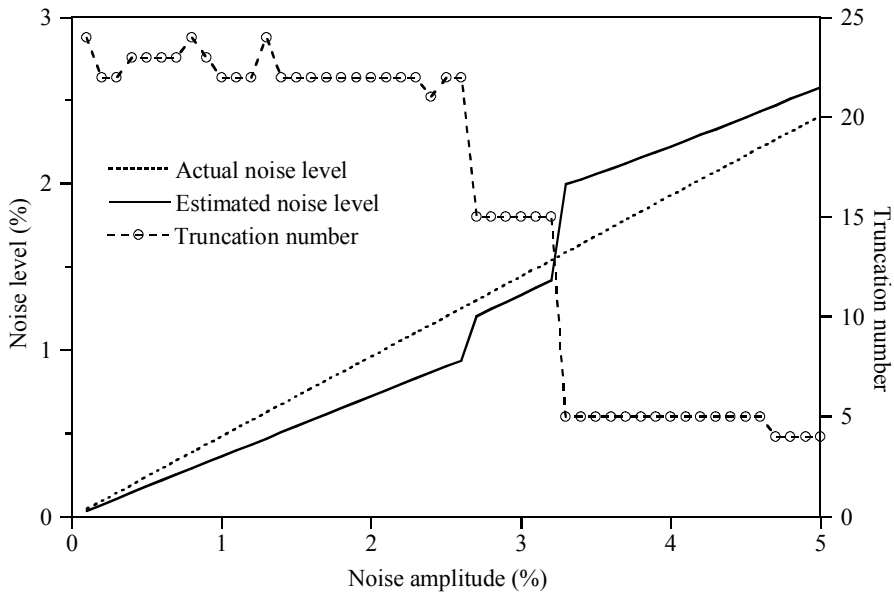


Fig. 3.19 Variations of estimated noise level and truncation number for damage case III with the noise amplitude

studies are performed. Fig. 3.19 shows the variation of the estimated and the actual noise levels and the truncation numbers with actual noise amplitudes. In the figure, the truncation numbers determined by the discrepancy principle are plotted for the right vertical axis while the estimated noise levels determined by the cross validation are plotted for the left vertical axis. The estimated noise level is smaller than the actual noise level up to 3.2 % noise amplitude, and becomes larger than the actual noise level after 3.2% noise amplitude. As the noise amplitude increases, the truncation number becomes smaller because more solution components are polluted for larger noise amplitudes. Fig. 3.19 illustrates that the truncation number varies with the noise amplitude in a stepwise fashion. There are three distinct regions in the variation of the truncation number with the noise amplitude, that is, truncation numbers for the noise amplitudes of  $A_N \leq 2.6\%$ ,  $2.6\% < A_N \leq 3.2\%$  and

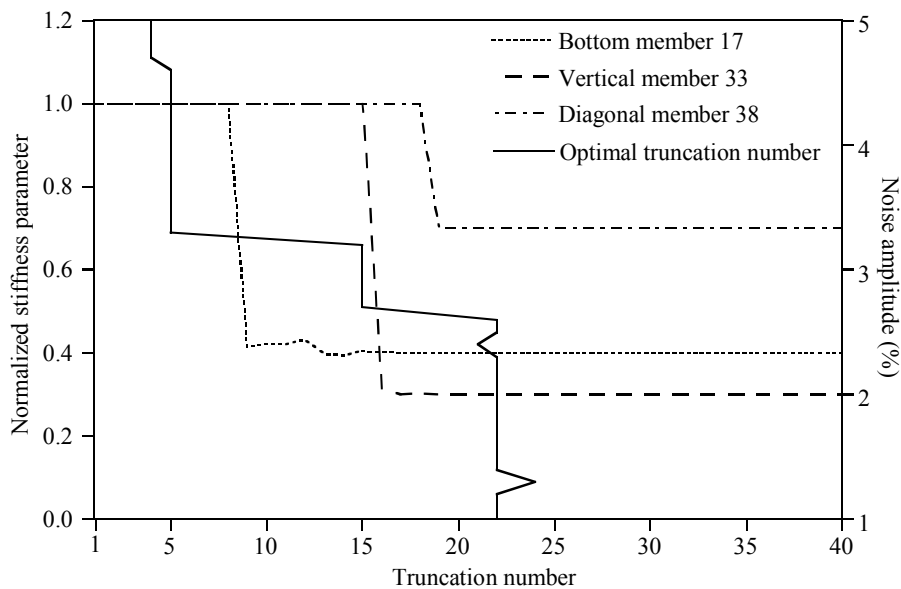


Fig. 3.20 Identified normalized stiffness parameters for noise-free data versus the truncation number

$3.2\% < A_N$  are 22, 15 and 5, respectively.

Fig. 3.20. shows the variations of the normalized system parameters of the damaged members with truncation numbers for noise-free measurements. It is clearly seen that the cross section area of each damaged member suddenly drops to exact damage severity at a certain truncation number. This is because the RSV corresponding to the truncation number that causes the sudden drop is associated with the damage information of the member. Therefore, to identify damage in a member, the RSV that contains damage information of the member should be included in the TSVD solution, (18). For damage case III the damage information of members 17, 33 and 38 is associated with the 9<sup>th</sup>, 16<sup>th</sup> and 19<sup>th</sup> RSV, respectively. The truncation number determined by the estimated noise level shown in Fig. 3.19 is also drawn in Fig. 3.20 by using the right vertical axis as the noise amplitude. As shown in the figure, all damaged members can be identified for noise level smaller than 2.6% since the truncation number for the noise level is 22, and all damage information is included in the TSVD solution. In case the noise amplitude is larger than 2.6 % but smaller than 3.2 %, the truncation number becomes 15, and the damage information of members 33 and 39 is lost. In this case only the damage of member 17 can be identified. For noise amplitude larger than 3.2 %, none of the damage information is included in the TSVD solution since the truncation number becomes 5. Therefore, none of the damaged members can be identified in damage case III by the  $L_1$ -TSVD. It is believed that member 17 is identified as a damaged member in the  $L_2$  regularization scheme not by the exact information but by just smearing effect of the  $L_2$ -norm. To identify the damaged members correctly, the noise amplitude should be kept smaller than 2.6%.

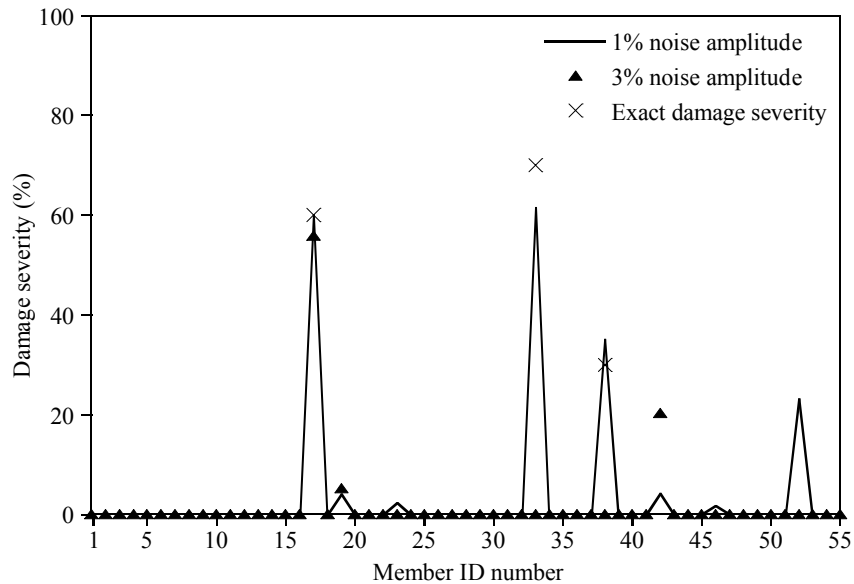


Fig. 3.21 Identified damage severity of damage case III for 1% and 3 % noise amplitude

The damage severity of the damaged members is shown in Fig. 3.21 for 1 % and 3 % noise amplitude. As explained above, all damaged members are identified for 1% noise amplitude, and only one damaged member, member 17, is identified for 3% noise amplitude. Member 52 and member 42 are falsely identified as damaged members for 1 % and 3% noise amplitudes, respectively. The damage severity of the other undamaged members that are falsely assessed as damaged members is small compared with that of the damaged members for both cases.

The aforementioned points give very important insights in planning the damage detection procedures. Since the RSV that contains the damage information of a member is determined by structural information, load cases and measurement locations, the target noise amplitude is rigorously estimated to identify certain damage patterns, and experimental setups are designed accordingly.

## Chapter 4

### Conclusions and Recommendations for Further Study

#### *Conclusions*

Regularization techniques in System Identification (SI) for the damage assessment of structures were proposed. SI used in this study is based on the minimization of the least squared error between measured and calculated responses, which is nonlinear inverse problem. SI based on the minimization of the least squared error between measured and calculated responses suffers from inherent instabilities caused by the ill-posedness of inverse problems, such as non-existence, non-uniqueness, and discontinuity unlike the forward problem.

In the chapter 2, a general concept of regularity condition with respect to the system property for SI was presented. By imposing a proper regularity condition, the inherent ill-posedness of SI can be relieved satisfactorily. A regularity condition of the system property for elastic continua was presented. Based on the proposed regularity condition, a regularization function based on the  $L_2$  norm with respect to the system properties was proposed. A regularity condition of system properties is discretized in terms of system parameters. Two different approaches to impose the discretized regularity condition on minimization of error function were presented; the truncated singular value decomposition (TSVD) and the Tikhonov regularization.

In the TSVD, the truncation number determines degree of regularity while the regularization factor does in the Tikhonov regularization. In the Tikhonov regularization, the most important issue is to keep consistent regularization effect on the parameter estimation,



which is controlled by a regularization factor. Therefore, it is crucial to determine a well-balanced regularization factor in order to obtain a physically meaningful and numerically stable solution of an inverse problem with the regularization technique.

This study illustrated that the error function with the Tikhonov regularization function results in a solution of a generalized average between the a priori estimates and the a posteriori solution. Here, the a priori estimates represent known baseline properties of system parameters, and the a posteriori solution denotes the solution obtained by given measured data. A new idea of the geometric mean scheme (GMS) was presented to select optimal regularization factors in nonlinear inverse problems. In the GMS, the optimal regularization factor is defined as the geometric mean between the maximum and minimum singular value for balancing the maximum and minimum effect of the a priori estimates and the a posteriori solution in a generalized average sense.

Numerical simulation studies are performed to demonstrate the validity and effectiveness of the GMS, and numerical behaviors of other schemes. The GMS yields the most accurate and reliable results regardless of random error and modeling error in measurements among the three schemes.

In chapter 3, it was shown that the regularity condition defined by the  $L_2$ -norm of the system property is too stringent for framed structures. To establish SI adequate for framed structures, a regularity condition of system properties for framed structures was proposed. Based on the proposed regularity condition, a regularization function based on the  $L_1$  norm with respect to the system properties was proposed. The  $L_1$ -regularity condition is imposed as an additional minimization problem to the minimization of the error function. The TSVD is utilized to filter out noise components in a solution, and the trun-

cated solution components are restored by the optimization of the  $L_1$ -regularity condition, in which the simplex method is adopted. The cross validation method is applied to determine an optimal truncation number in the TSVD. Damage status of each member is assessed statistically using a hypothesis test for the interval estimation of the mean value.

The validity of the  $L_1$ -regularity condition in SI for framed structures was presented by finding damages of a two-span continuous bridge with three damage scenarios for different noise amplitudes in measurements. SI with  $L_1$ -regularity condition could estimate the actual material properties of each member in the framed structure successfully to the maximum resolution limits of the error function regardless of the serious sparseness of measurements and the measurement noise.

### ***Recommendations for further study***

#### *Damage detectability with respect to damage severity and measurement noise*

It is very important to evaluate possible detectability or identifiability of each structural member in the current SI for damage assessment. This study mainly investigates system characteristics affecting the identification results under the fixed measurement locations and loading conditions. Even though the structural characteristics cannot be altered, the load case and measurement locations can be selected so as to improve the resolution of the damage detection.

Detectability of each member can be evaluated through numerical simulations with various damage severity and measurement noise by using SI with regularization technique. After detectability of all the members with respect to damage severity and measurement noise is calculated from numerical simulations, it is possible to evaluate which members up

to how much damage severity can be identified when real responses of a structure are measured. Based on the evaluation, loading condition, precision of sensors, locations of sensors can be rearranged to increase the detectability of members which are classified as undetectable. Continuous researches on these fields should be intensively performed to apply SI-based damage detection schemes to actual problems.

#### *Investigation of relationships between probabilistic SI and SI with regularization*

The joint probability density function between the system parameters and measurements can be obtained by probabilistic SI such as Bayesian approach [Tar87]. It is known that the Bayesian approach is closely connected with the SI with the Tikhonov regularization [Neu79, Tar87]. For example, if both a priori distribution and posteriori distribution are assumed to be gaussian, the probability of the joint distribution with respect to the system parameters is known to become maximal at the average of system parameters which is equivalent to the solution to the minimization problem of the  $L_2$ -regularized error function [Tar87]. As far as damage assessment of structures is concerned, a damage detection algorithm of structures based on a Bayesian approach was proposed by Sohn (1997). Further research on relationships between the regularized error function and the Bayesian approach is suggested since it can give strong backgrounds of probabilistic theory to the current study.

#### *Improvement of signal to noise ratio*

There are two ways to increase the signal to noise ratio in SI for damage assessment. One is reduce the noise amplitude by using more precise sensors and filtering the noise components in signal. The current study is focused on filtering the noise component ef-

fectively. The other is to amplify the signal by arranging the loading condition and sensor locations so that measurements can include sufficient information of damaged members. This is closely related with optimal loading conditions and optimal sensor locations. Therefore, further researches combining the regularized SI with optimal loading conditions and optimal sensor locations are strongly recommended because they may increase the resolution limit of the current SI up to in-situ noise magnitude.

#### *Application to Dynamic Responses*

Most measured responses of civil structures are dynamic responses such as acceleration, natural frequencies and mode shapes. The SI with regularization technique proposed in this study can be applied to these dynamic responses easily. Moreover, the amount of measurements is tremendously larger than that of static responses used in this study, the SI with regularization may results in more meaningful and reliable results. However, real-time SI is very time-consuming since the calculation of sensitivity of dynamic responses in the time domain with respect to system parameters costs a lot of computational time. Research on the direct differentiation of frequency response function in frequency domain incorporated with fast Fourier transform technique will be very interesting since computational time of sensitivity of dynamic response in time domain may be reduced considerably, which is crucial to real-time SI.

## REFERENCES

Ali75

Alifanov, O. M. and Artyukhin, E. A., "Regularized numerical solution of non-linear heat conduction problems" *Journal of Engineering Physics*, **29**, 934-938 (1975)

Alt87

Altman, J., *Smoothing data with correlated errors* Technical Report 280, Department of Statistics, Stanford University (1987)

Akt00

Aktan, A. E., Catbas, F. N., Grimmelsman, K. A., and Tsikos, C. J., "Issues in infrastructure health monitoring for management" *Journal of Engineering Mechanics*, ASCE, **126**(7), 711-724 (2000)

Bar73

Barrondale, I., and Roberts, F.D.K., "An improved algorithm for discrete  $l_1$  linear approximation" *SIAM J. Numer. Anal.* **10**(5), 839-848, (1973)

Bec84

Becks J. V. and Murio, D. A., "Combined function specification – regularization procedure for the solution of inverse heat conduction problem" *AIAA Journal*, **24** 180-185 (1984)

Bec85

Becks, J. V., Blackwell, B., and St. Clair, C. R., *Inverse Heat Conduction : Ill-Posed Problems*, (Wiley, New York, 1985)

Bez93

Bezerra, L. M. and Saigal, S., "A boundary element formulation for the inverse elastostatics problem (IESP) of flaw detection", *International Journal for Numerical Methods in Engineering*, **36**, 2189-2202 (1993)

Bis94

Bishop, C.M., "Neural networks and their applications", *Review of Scientific Instruments*, **65**(6), 1803-1832 (1994)

Bra89

Bray, D. E. and Stanley, R. K., *Nondestructive Evaluation: A Tool for Design, Manufacturing, and Service*, McGraw-Hill Co. (1989)

- Bui94  
Bui, H. D., *Inverse Problems in the Mechanics of Materials: An Introduction*, CRC Press, Boca Raton (1994)
- Car94  
Carasso, A. L., "Overcoming Holder continuity in ill-posed continuation problems" *SIAM J. Numer. Anal.* 31(6), 1535-1557 (1994)
- Dev90  
DeVito, C. L., *Functional Analysis and Linear Operator Theory*, (Addison-Wesley, Redwood City, CA, 1990)
- Doe99  
Doebling, S. W., Farrar, C. R., Prime, M. B., and Shevitz, D. W., *Damage Identification and Health Monitoring of Structural and Mechanical Systems From Changes in Their Vibration Characteristics: A Literature Review*, Los Alamos National Laboratory Report LA-13070-MS (1996)
- Doe96  
Doebling, S. W. and Farrar, C. R., *The State of the Art in Structural Identification of Constructed Facilities*, (A Report by the ASCE Committee on Structural Identification of Constructed Facilities, 1999)  
PDF format is available in [http://ext.lanl.gov/projects/damage\\_id](http://ext.lanl.gov/projects/damage_id)
- Eri96  
Eriksson, J., *Optimization and Regularization of Nonlinear Least Squares Problems*, Ph.D. Thesis, Department of Computing Science, Umeå University, Sweden (1996)
- Fes94  
Fessler, J. A., "Penalized weighted least-squares image reconstruction for positron emission tomography" *IEEE Transactions on medical imaging*, **13**(2), (1994)
- Fra00  
Frazin, R. A., "Tomography of the solar corona. I. A robust regularized, positive estimation method" *The Astrophysical Journal*, **530**, 1026-1035, (2000)
- Gio80  
Gioda, G. and Maie, Giulio, "Direct search solution of an inverse problem in elasto-plasticity: Identification of cohesion, friction angle and in situ stress by pressure tunnel test" *International Journal for Numerical Methods in Engineering*, **15**, 1823-1848 (1980)
- Ge98a  
Ge, L. and Soong, T. T., "Damage identification through regularization method. I: Theory" *Journal of Engineering Mechanics*, ASCE, 124(1) 103-108, 1998

Ge98b

Ge, L. and Soong, T. T., "Damage identification through regularization method. II: Applications" *Journal of Engineering Mechanics*, ASCE, 124(1) 109-116, 1998

Gol78

Golub, G. H., Heath, M., and Wahba, G., "Generalized cross-validation as a method for choosing a good ridge parameter" *Technometrics*, **21**, 215-223 (1978)

Gol89

Goldberg, D.E., *Genetic algorithms in search, optimization, and machine learning*, Addison-Wesley (1989)

Gol96

Golub, G. H. and Van Loan, C.F., *Matrix Computations*, 3<sup>rd</sup> ed., The Johns Hopkins University Press, London (1996)

Gon95

Gondzio, J. and Terlasky, T., A computational view of interior-point methods for linear programming. In J. Beasley, editor, *Advances in Linear and Integer Programming*, (Oxford University Press, Oxford, 1995)

Gro84

Groetsch, C. W., *The theory of Tikhonov Regularization for Fredholm Equations of the First Kind*, Pitman Advanced Publishing, Boston (1984)

Hab00

Haber, E., and Oldenburg, D.W., "A GCV based method for nonlinear ill-posed problems," *Computational Geosciences*, **4**(1), 41-63 (2000)

Han92a

Hansen, P. C., "Analysis of discrete ill-posed problems by means of the L-curve" *SIAM review*, **34**(4), 561-580 (1992)

Han92b

Hansen, P. C., Sekii, T., Shibahashi, H., "The modified truncated SVD method for regularization in general form" *SIAM J. Sci. Stat. Comput.*, **13**, 1142-1150 (1992)

Han96a

Hanke, M. and Nagy, J. G., "Restoration of atmospherically blurred images by symmetric indefinite conjugate gradient techniques" *Inverse Problems*, **12**, 157-173 (1996)

- Han96b  
Hansen, P. C. and Mosegaard, K., "Piecewise polynomial solutions without a priori break points" *Numer. Linear Algebra Appl.*, **3** 513-524 (1996)
- Han98  
Hansen, P. C., *Rank-deficient and Discrete Ill-Posed Problems : Numerical Aspects of Linear Inversion*, (SIAM, Philadelphia, 1998)
- Hje96a  
Hjelmstad, K. D. and Shin, S., "Damage Detection and Assessment of Structures from static response" *Journal of Engineering Mechanics*, ASCE, **123**(6), 568-576 (1996)
- Hje96b  
Hjelmstad, K. D., "On the uniqueness of modal parameter estimation" *Journal of Sound and Vibration*, **192**(2), 581-598 (1996)
- Hon94  
Honjo, Y., Wen-Tsung, L., and Guha, S., "Inverse analysis of an embankment on soft clay by extended Bayesian method", *International Journal for Numerical Methods in Engineering* **18**, 709-734 (1994)
- Hug87  
Hughes, T. J. R., *The Finite Element Method, Linear Static and Dynamic Finite Element Analysis*, (Prentice-Hall, Englewood Cliffs, NJ, 1987)
- Joh87  
Johnson, C., *Numerical Solution of Partial Differential Equations by the Finite Element Methods*, (Cambridge University Press, New York, 1987)
- Kal96  
Kaller, F. and Bertrant, M., "Tissue elasticity reconstruction using linear perturbation method" *IEEE transaction of medical imaging*, **15**(3), 299-313 (1996)
- Lee99  
Lee, H. S., Kim, Y. H., Park, C. J., and Park. H. W., "A new spatial regularization scheme for the identification of geometric shapes of inclusions in finite bodies" *International Journal for Numerical Methods in Engineering*, **46**(7), 973-992 (1999)
- Lee00  
Lee, H. S., Park, C. J., and Park. H. W., "Identification of geometric shapes and material properties of inclusions in two dimensional finite bodies by boundary parameterization" *Computer Methods in Applied Mechanics and Engineering*, **181**(1-3), 1-20 (2000)



Lju87

Ljung, L., *System Identification : Theory for the user*, (P T R Prentice Hall Inc., Englewood Cliffs, New Jersey 07632, 1987)

Lue89

Luenberger, D. G., *Linear and Nonlinear Programming* 2<sup>nd</sup> edn. (Addison-Wesley, Reading, 1989)

Mah96

Mahnken, R. and Stein, E., "Parameter identification for viscoplastic models based on analytical derivatives of a least-squares functional and stability investigations" *International Journal of Plasticity*, **12**(4) 451-479 (1996)

Man89

Maniatty, A., Zabarar, N., and Stelson, K., "Finite element analysis of some inverse elasticity problems", *Journal of Engineering Mechanics, ASCE* **115**, 1303-1317 (1989)

McC96

McCormac, J. C., and Nelson, J. K. *Structural analysis – a classical and matrix approach*, 2<sup>nd</sup> ed., (Addison-Wesley, Reading Massachusetts, 1996)

Me195

Mellings, S. C. and Aliabadi, M. H., 'Flaw identification using the boundary element method', *International Journal for Numerical Methods in Engineering*, **38**, 399-419 (1995)

Men89

Menke, W., *Geophysical Data Analysis: Discrete Inverse Theory*, (Academic Press, San Diego, 1989)

Mor84

Morozov, V.A., *Methods for Solving Incorrectly Posed Problems, English Ed.*(Springer-Verlag, New York, 1984)

Mor93

Morozov, V.A., *Regularization Methods for Ill-posed Problems, English Ed.*(CRC Press, 1993)

Neu73

Neuman, S. P., "Calibration of distributed parameter groundwater flow models viewed as a multiple-objective decision process under uncertainty," *Water Resources Research*, **9**(4), 1006-1021 (1973)

Neu75

Neuman, S. P., "Role of subjective value judgement in parameter identification," *Modeling and Simulation of Water Resources Systems*, edited by G. C. Vansteenkiste, North-Holland Amsterdam, 59-84 (1975)

Neu79

Neuman, S. P. and Yakowitz, S., "A statistical approach to the inverse problem of aquifer hydrology," *Water Resources Research*, **15**(4), 845-860 (1979)

Nor89

Norris, M. A. and Meirovitch, L., "On the problem of modeling for parameter identification in distributed structures" *International Journal for Numerical Methods in engineering*, **28**, 2451-2463 (1989)

Ode79

Oden, J. T., *Applied Functional Analysis : A First Course for Students of Mechanics and Engineering Science*, (Prentice-Hall, Englewood Cliffs, NJ, 1979)

Par01

Park, H.W., Shin, S.B., and Lee, H.S., "Determination of an optimal regularization factor in system identification with Tikhonov function for linear elastic continua" *International Journal for Numerical Methods in Engineering*, **51**(10), 1211-1230 (2001)

San91

Sanayei, M. and Onipede, O., "Damage assessment of structures using static test data", *AIAA Journal*, **29**(7), 1174-1179 (1991)

Sch90

Schnur, D. S. and Zabarar, N., "Finite element solution of two dimensional inverse elastic problems using spatial smoothing" *International Journal for Numerical methods in Engineering*, **30**, 57-75 (1990)

Sch92

Schnur, D. S. and Zabarar, N., "An inverse method for determining elastic material properties and a material interface", *International Journal for Numerical Methods in Engineering*, **33**, 2039-2057, (1992)

Shi94

Shin, S., *Damage Detection and Assessment of Structural Systems from Measured Response*, Ph.D. Thesis, Department of civil engineering, University of Illinois at Urbana-Champaign, 1994

Shi99

Shin, S. and Koh, H. M., "A numerical study on detecting defects in a plane stressed body by system identification", *Nuclear Engineering and Design*, **190**, 17-28 (1999)

Sim99

Simon, H., *Neural Networks : a Comprehensive Foundation*, 2<sup>nd</sup> ed., Prentice-Hall, London (1999)

Soh97

Sohn, H. and Law, K.H., "A Bayesian probabilistic approach for structure damage detection", *Earthquake Engineering and Structural Dynamics*, **26**, 1259-1281 (1997)

Str73

Strang, G. and Fi, G. J., *An Analysis of the Finite Element Method*, (Prentice-Hall, Englewood Cliffs, N.J., 1973)

Tan89

Tanaka, M. and Yamagiwa, K., "A boundary element method for some inverse problems in elastodynamics" *Applied Mathematical Modelling*, **13**, 307-312 (1989)

Tar87

Tarantola, A. *Inverse Problem Theory : Methods for Data Fitting and Model Parameter Estimation*, Elsevier, Amsterdam (1987)

Tik77

Tikhonov, A. and Arsenine, V., *Solutions to Ill-Posed Problems*, (Winston-Wiley, New York, 1977)

Vog86

Vogel, C. R., "Optimal choice of a truncation level for the truncated SVD solution of linear first kind integral equations when data are noisy," *SIAM J. of Numerical Analysis*, **23**(1), 109-117 (1986)

Vog96

Vogel, C. R. and Oman, M. E., "Iterative methods for total variation denoising" *SIAM Sci. Comput.*, **17**(1), 227-238 (1996)

Wat80

Watson, G. A., *Approximation Theory and Numerical Methods*, (Wiley, Chichester, 1980)

Yeo99

Yeo, I. H., *Statistical Damage Assessment of Structures from Static Responses Using System Identification with Tikhonov Regularization*, Ph.D. Thesis, Department of civil engineering, Seoul National University, 1999

Yeo00

Yeo, I. H., Shin, S., Lee, H. S., and Chang, S. P., "Statistical Damage Assessment of Framed Structures from Static Responses" *Journal of Engineering Mechanics, ASCE*, **126** (4), 414-421 (2000)

## 국문초록

구조물 손상진단을 위한 시스템확인 (SI) 에서의 정규화기법을 제안한다. 이 연구에서는 측정응답과 계산응답 간의 자승오차를 최소화해 근간한 SI기법을 사용하는데, 이 SI기법은 비선형 역해석문제이다.

시스템물성치에 대한 정규조건의 일반적인 개념을 제시한다. 적절한 정규조건을 부과함으로써 SI문제가 가지는 본래의 ill-posedness를 경감시킨다. 탄성체를 위한 정규조건이 시스템물성치의  $L_2$ -norm으로 정의됨을 보인다. 구조물의 응답의 민감도 행렬에 특이치분해법을 적용하여 비선형 역해석 문제의 특성과 정규화의 역할을 고찰한다. 이를 근간으로 기하평균법을 제안한다. 기하평균법에서는 최적정규화계수를 민감도행렬 특이치의 최대값과 최소값간의 기하평균으로 정의한다. 기하평균법의 타당성을 계측오차와 모델링오차를 가지는 수치예제들을 통해서 검증한다.

탄성체문제와는 다르게 시스템물성치의  $L_2$ -norm으로 정의되는 해의 공간이 뼈대구조물에는 적절하지 않음을 보인다. 시스템물성치에 대한  $L_1$ -norm으로 정의되는 새로운 정규화함수를 뼈대구조물을 위해서 도입한다. 오차함수의 이차종속문제에서 계측오차에 오염된 해의 성분을 제거하기 위해 TSVD방법을 사용한다. 시스템변수벡터의  $L_1$ -norm으로 정의되는 이산화된 정규조건을 각 이차종속문제에서 분리된 최적화문제로서 부과한다. 최적절단번호를 교차타당성에 의해 결정한다. 뼈대구조물의 최종손상상태는 자료교란법과 가설검정법에 근

거한 통계적접근법으로 진단한다. 제안된 정규조건의 타당성을 계측오차가 있는 이경간 연속 트리스의 세가지 손상사례에서 손상을 탐지하는 문제를 통해 검증한다.

Key Words: 시스템확인, 정규화기법, 손상진단, ill-posedness, 정규조건, 기하평균  
법

학번 : 97415-807

## 감사의 글

대학원생활을 시작한지 벌써 7년이란 시간이 흘렀습니다. 급변하는 세상물정으로 볼 때는 무척이나 긴 시간이지만, 연구라는 묘목을 심고 그 열매의 짧은 맛이나마 보기엔 그리 길지 않은 시간이었다는 생각이 듭니다. 그렇지만, 처음 연구를 시작했을 때 어떻게 해야 할 지 몰라서 갈팡질팡하던 모습과 지금의 나를 비교해 보면 정말 감회가 새롭습니다.

항상 부족한 저에게 끊임없는 가르침과 독려를 통해 이제 미약하나마 연구의 끝자락을 잡게 이끌어주신 이해성 선생님께 깊은 감사를 드립니다. 한편의 논문이라도 제대로 쓰려면 얼마만큼의 공을 들여야하는지 보여주신 것 잊지 않겠습니다. 제가 논문을 준비하는 과정 내내 항상 유익하고 발전적인 조언을 주신 동아대학교 신수봉교수님께도 깊이 감사드립니다. 그리고 바쁘신 와중에도 저의 졸고가 좀 더 나은 방향으로 나아갈 수 있게 조언해주신 장승필 교수님, 고현무 교수님, 그리고 카이스트의 윤정방 교수님께도 정말 감사드립니다. 대학원 과정에서 학문의 기초를 닦는데 도움을 주신 오병환교수님과 김재관교수님께도 감사드립니다.

연구실과 집을 오가는 단조로운 생활 속에서도 늘 활기와 웃음을 잃지 않게 도와준 실험실과 대학원의 동기, 선후배들께도 고마움을 전합니다. 제 연구주제에 대해 꾸준히 조언해 주고 특히 작년 제가 시카고학회에 갔을 때 편안하게 지낼 수 있도록 배려해준 여인호 박사님께 특히 고마움을 전합니다.

이제는 장가가서 예전처럼 얼굴을 보기 힘든 형이지만 항상 마음으로 보내주던 따뜻한 격려 고마웠습니다. 무엇보다 제가 아무런 걱정없이 오로지 연구에만 전념할 수 있도록 항상 뒷바라지 해주시고 지켜봐 주신 어머니, 아버지께 무한한 감사를 드리며 이 논문을 바칩니다.

## VITA

Hyun Woo Park was born on February 16, 1973 in Ulsan, Korea. He graduated from Haksung High School in Ulsan, Korea in February 1991. Then he enrolled in the department of Civil Engineering at the Seoul National University in Seoul, Korea in March 1991. He received a Bachelor of Science degree in Civil Engineering in February 1995 and a Master of Science degree in Civil Engineering in February 1997 from Seoul National University in Seoul, Korea. He continued his graduate studies up to now in the department of Civil Engineering at the Seoul National University. His graduate research involved inverse problems in the engineering mechanics and regularization techniques in system identification of structures. He is a coauthor with H. S. Lee and S. B. Shin of the publication, "Determination of an optimal regularization factor in system identification with Tikhonov regularization for linear elastic continua."